AD-A032 441 UNITED TECHNOLOGIES RESEARCH CENTER EAST HARTFORD CONN F/G 20/12
IMPROVEMENT OF ELECTRONICS RELIABILITY BY RF SPUTTERING TECHNIQ--ETC(U)
MAY 76 D H GRANTHAM, J L SWINDAL N00019-75-C-0465
UNCLASSIFIED UTRC-R76-922139-4 NL

1 OF 2
ADA032441

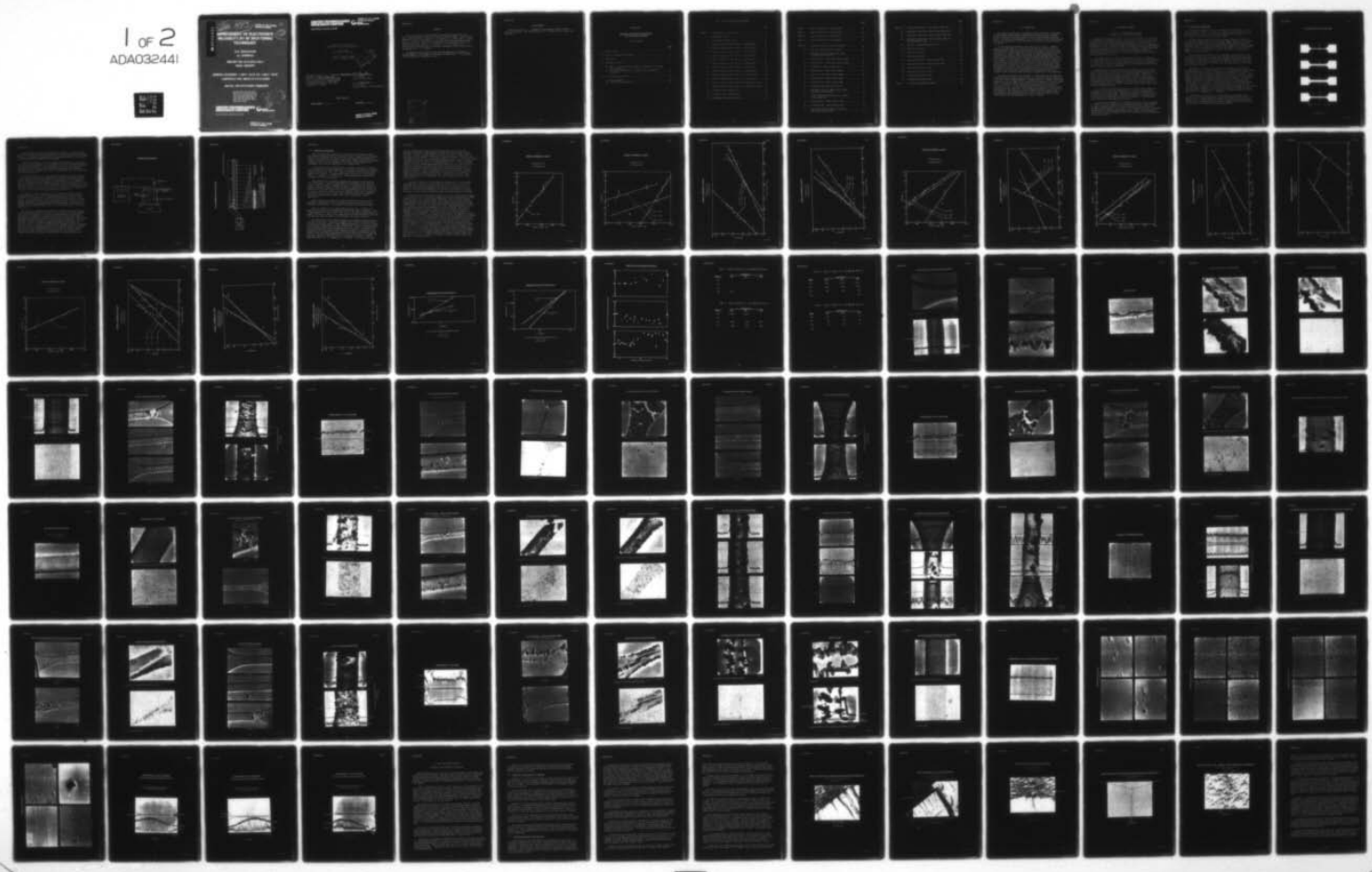

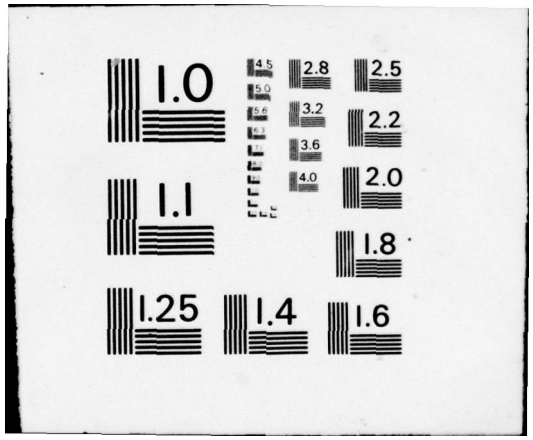
1.0
1.1
1.25
1.4
1.6
1.8
2.0
2.2
2.5
2.8
3.2
3.6
4.0
4.5
5.0
5.6

FC

12

IMPROVEMENT OF ELECTRONICS RELIABILITY BY RF SPUTTERING TECHNIQUES

D.H. GRANTHAM
J.L. SWINDAL

REPORT NO. R76-922139-4
FINAL REPORT

PERIOD COVERED: 1 MAY 1975 TO 1 MAY 1976
CONTRACT NO. N00019-75-C-0465

NAVAL AIR SYSTEMS COMMAND

UNITED TECHNOLOGIES RESEARCH CENTER

EAST HARTFORD, CONNECTICUT 06108

UNITED TECHNOLOGIES

76-03-247-3

UNITED TECHNOLOGIES RESEARCH CENTER

UNITED TECHNOLOGIES

East Hartford, Connecticut 06108

Improvement of Electronics
Reliability by rf Sputtering Techniques

FINAL REPORT
1 May 1975 to 1 May 1976

Naval Air Systems Command
Contract No. N00019-75-C-0465

REPORTED BY D. H. Grantham

D. H. Grantham
Chief, Microelectronics

J. L. Swindal
Research Scientist, Microelectronics

DATE May 1976

NO. OF PAGES _____

COPY NO. _____

APPROVED FOR PUBLIC RELEASE:
DISTRIBUTION UNLIMITED

FOREWORD

This report describes work performed from 1 May 1975 through 1 May 1976 under Contract N00019-75-C-0465 for the Naval Air Systems Command. NAVAIR program managers for this work were Messrs: C. D. Caposell, A. S. Glista, and S. M. Linder of code: AIR 52022. This report was prepared by the United Technologies Research Center, East Hartford, Connecticut, and describes work performed in the Electromagnetics Laboratory headed by A. J. DeMaria. Dr. D. H. Grantham, Chief, Microelectronics Technology was the principal investigator and technical assistance was provided by Mr. J. L. Swindal.

Publication of this report does not constitute approval by the Naval Air Systems Command of the findings or conclusions contained herein. It is published for the exchange and stimulation of ideas.

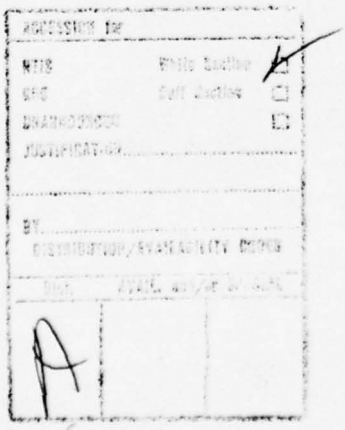

Acknowledgments

Thanks are due to Dr. A. J. Shuskus for encouragement and many fruitful technical discussions. The contributions of Mr. J. Figucia and Ms. S. Smith were invaluable.

Improvement of Electronics Reliability By rf Sputtering Techniques

TABLE OF CONTENTS

2.0 LIST OF ILLUSTRATIONS AND TABLES

3.0 INTRODUCTION

Solid-state electronics has increasingly become a technology of thin-films--of thin epitaxial layers, shallow diffusions, thin dielectrics for isolation and gate insulation, thin metal contacts to devices and interconnects between devices. The control and repeatability over the formation of these films determine the cost and reliability of solid state devices and circuits and of the systems they comprise.

Two film deposition problems are the subject of this report. Aluminum-copper alloy films formed by a variety of techniques have been observed to be less susceptible to mass motion--and opening of conductors--at very high current densities and at elevated temperatures. This electromigration behavior has been investigated for layered deposits of aluminum and copper subsequently inter-diffused before subjection to the high current density high temperature stress. Flash evaporated films--probably of variable composition through the layer--have been evaluated. Neither approach to deposition of alloy films can be said to be a well-controlled integrated circuit and solid state device production scheme. Sputtering affords the greatest flexibility of the various techniques and offers maintainence of virtually identical composition between sputtered alloy target and deposited alloy film, a goal not readily achieved by other film deposition techniques. One aspect of the program described was the evaluation of rf sputtered films of aluminum copper alloys for susceptibility to electromigration.

The second problem which was the subject of this program was the deposition of beryllium oxide in layers thick enough to be useful for integrated circuit and solid state device thermal management. Beryllium oxide has a thermal conductivity comparable to that of copper while its electrical resistivity is one of the highest known. RF sputtering offers a unique approach to the deposition of layers of the necessary 0.001" to 0.005" thickness for elimination of "hot spots" in integrated circuits. The goals of this phase of the program were to find deposition parameters for "thick" thin films of beryllium oxide low in stress and with good adhesion. These films would provide intimate void-free thermal contact to solid state electronics devices and circuits so that the effects of solder voids formed in the die mounting process would be vitiated.

4.0 EXPERIMENTAL APPROACH

4.1 Phase I. Electromigration Problem Statement of the Problem and Discussion

Aluminum has many properties which render it most attractive as a thin film interconnection in integrated circuits. It adheres well to clean silicon oxides and forms its own thin self-adhering protective oxide in contact with air. Aluminum can be etched by several chemical formulations which do not significantly attack silicon oxides. The metal has one of the higher electrical conductivities. The ductility is high so that the effects of the mismatch in thermal coefficients of expansion between aluminum and the substrate are somewhat ameliorated. Deposition techniques for the pure metal are vacuum evaporation and sputtering--both straightforward in practice.

Pure aluminum, however, suffers from one serious drawback. Significant electromigration sets in at current densities of the order of one million amperes/cm^2. High speed, fine geometry devices easily exceed this level in operation and failures of circuits and systems are observed where aluminum conductors have opened at points of vacancy accumulation.

Aluminum alloys with copper have been investigated for longer life under high current densities. These alloy films have been deposited in alternating layers of first aluminum then copper to produce an average composition of a few percent copper which is homogenized by annealing near 500°C. Others have flash evaporated mixtures of aluminum and copper. Neither approach produces a truly uniform composition throughout the film conductor. The high temperature interdiffusion of copper and aluminum layers is not a practical solution for production purposes nor is it flexible in allowing study of small grained films as well as large/grained ones.

On the other hand rf sputtering produces a much more uniform composition throughout the film from a starting material of virtually the same nominal composition as the desired film. Films adhering very well to silicon oxide can be deposited at room temperature to produce fine-grained or amorphous layers. These very small grained films are thought to be superior to intermediate size grained films under electromigration conditions.

Under a previous program, United Technologies Research Center investigated rf sputtered films of aluminum and of aluminum-copper alloys. Small additions of copper to aluminum were seen to produce superior interconnections under electromigration conditions. This phase of this program had the goal of extending the sputtering of aluminum-copper alloys to higher copper content films and to collect data on the electromigration behavior of these films at high temperatures and current densities.

4.1.1 Test Pattern Preparation

The masks for definition of the test patterns are shown in Fig. 1. Four widths of stripe--0.00025 in., 0.00050 in., 0.00075 in., and 0.001 in. all 0.010 in. in length--were made so that the current density could be changed over a wide range of values without changing power supplies.

The metal films were deposited from alloy targets supplied by Haselden and had the nominal compositions 1, 8 and 12 percent copper. Because of the unusual behavior of the films from the 12 percent copper target several analyses were made which showed the vendor had not supplied exact compositions. Targets supplied were 0.74, 8.36 and 10.6 respectively by atomic absorption. The vendor agreed to replace the 10.6 percent target but it arrived very late in the program and analyzed 12.6 percent copper.

The deposition of the films was by rf sputtering. The substrates on which the films were deposited were silicon wafers oxidized using standard procedures and introduced immediately with no further treatment into the sputtering chamber. In those cases where wafers were stored after oxidation, they were cleaned with hot chromic acid and rinsed in distilled water and dried just prior to mounting on the substrate holder.

The substrates were heat sunk to the holder with Apiezon N vacuum grease and maintained at 25°C during the deposition. The rf power into the holder during a three minute sputter cleaning of the substrates was 100 watts at 13.56 MHz while the target power for sputter cleaning was 500 watts for 15 minutes. During sputter cleaning of both target and substrates a water-cooled shutter interposed between them collected the material removed during the cleaning. After sputter cleaning the shutter was removed from between target and substrates and the spacing closed to $\sim$ 1.25 inches. The substrates were covered with approximately 0.8 micrometers of alloy film. Test pattern preparation is described in the next paragraph. A detailed description of the sputtering equipment has been reported. (See Final Report #N921820-4 for 1 January 1974 through 31 December 1974 under NASC Contract No. N00019-74-C-0256 "Sputtering Technology for Improved Electron Devices" by D. H. Grantham and J. L. Swindal.)

Test patterns were etched in the alloy films which were deposited as described in the previous paragraph. The patterns produced were as shown in the masks of Fig. 1. Standard spin-on procedures using Kodak Thin Film Resist and and the usual developing processes were used to produce the protective overlays of photoresist in the shape of the metal pattern desired.

FIG. 1

ELECTROMIGRATION TEST BAR MASK

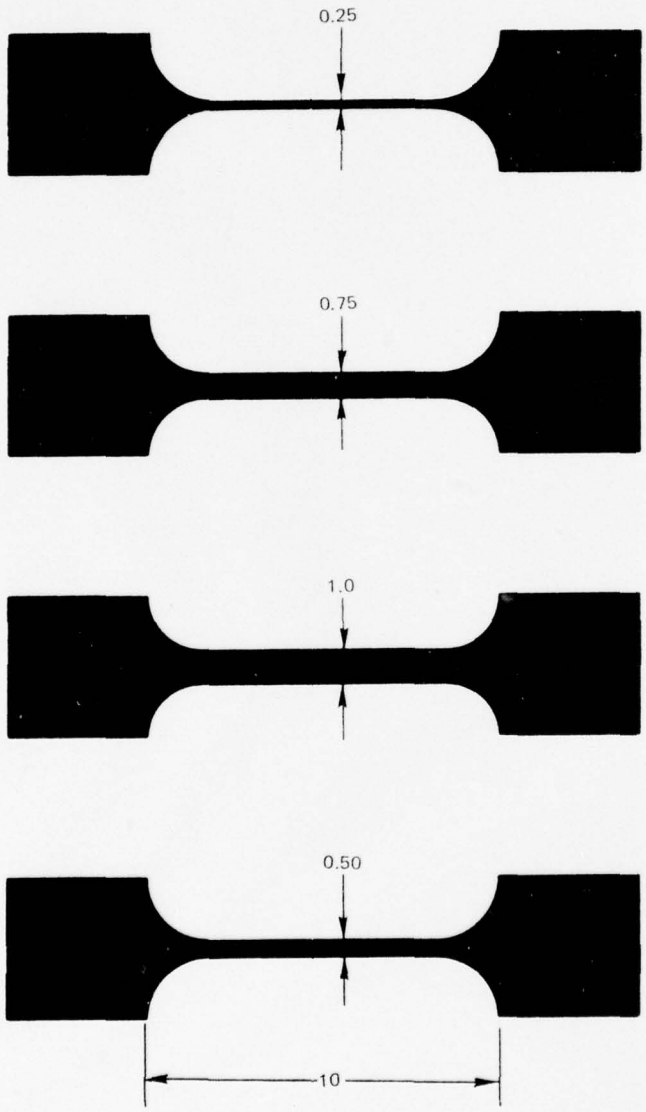

ALL DIMENSIONS IN mils

76–03–90–1

After etching in a nitric acid-phosphoric acid mixture to define the metal pattern the silicon wafer was scribed into 0.030 inch dice which were eutectically bonded in TO-5 packages. Aluminum wire was ultrasonically bonded to the dice and to the header posts to complete the test specimen.

Samples were maintained at the test temperature by immersion in one of five silicone oil baths controlled to ±1°C diagrammed in Fig. 2. Each bath temperature was adjusted to compensate for the temperature rise in the test specimens due to I^2R heating during the test so that the temperatures reported are true metal temperatures at the beginning of the tests. The metal film under test was always in contact with the oil.

Several test stripes of the same width and thickness were series connected and five constant current sources supplied the current levels required for four current densities--2.0×10^6 amps/cm^2, 3.0×10^6 amps/cm^2, 4.0×10^6 amps/cm^2 and 6×10^6 amps/cm^2--at four temperatures -200°C, 225°C, 250°C, and 275°C. The state of each series connected pattern--continuous or open--was monitored by a UTRC assembled data logger (Fig. 3). The opened stripe could be identified and replaced by a short circuit for continuation of the test. Resistance of all stripes as a function of time in each bath was also monitored and recorded.

In addition to time for failure of the test patterns, scanning electron microphotography and the electron beam microprobe were used for topographical inspection of test stripes and for compositional monitoring before and after stress. Two instruments were used for this portion of the evaluation--a CAMECA Scanning Electronic Microscope with Electron Beam Microprobe Attachment and the AMR-900 Scanning Electronic Microscope with EDAX attachment. Sample-detector alignment was a critical element in the use of these instruments as can be seen from Fig. 39.

Three kinds of information were obtained for typical test specimens--large depth-of-field photographs of the surface of the specimen, composition profiles of the specimen displayed in two ways and thickness profiles. Compositional information was displayed in arbitrary units as plots of quantity of copper or aluminum intercepted by the electron beam as a function of position on the stripe. No attempt was made to reduce this to concentration for this report. Even so, some care is required in sample alignment with respect to the detector as described below. A second mode of recording such information presents highlighted areas whose size and density are proportional to quantity present, in arbitrary units, over an area corresponding one to one with the test specimen geometry. This latter display technique is a straightforward way of identifying any nonuniformities which are present in any portion of the sample being scanned.

FIG. 2

TEMPERATURE CONTROL

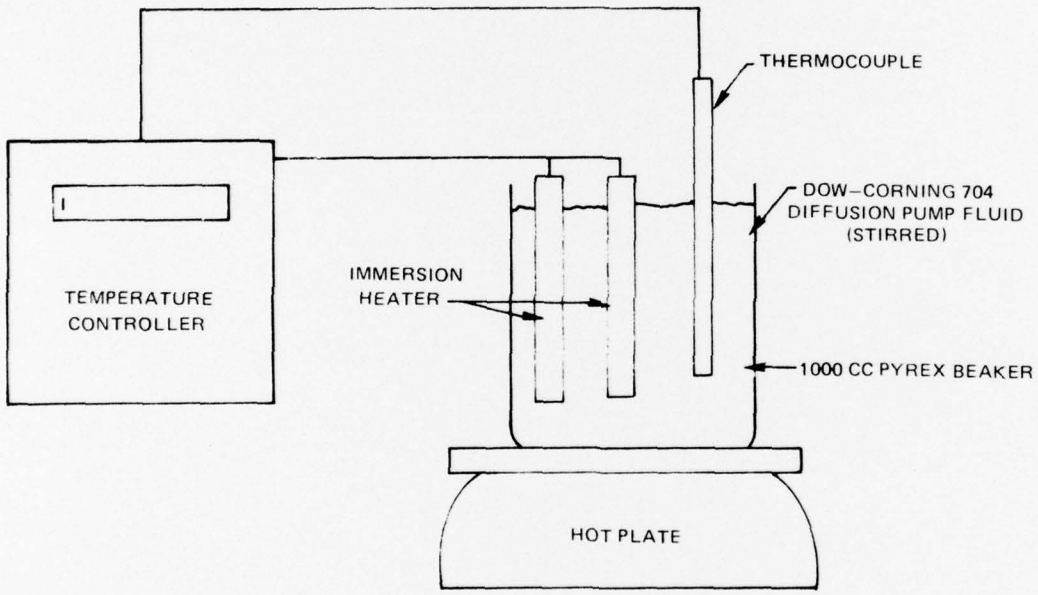

76–03–64–2

FIG. 3

ELECTROMIGRATION TEST CIRCUIT

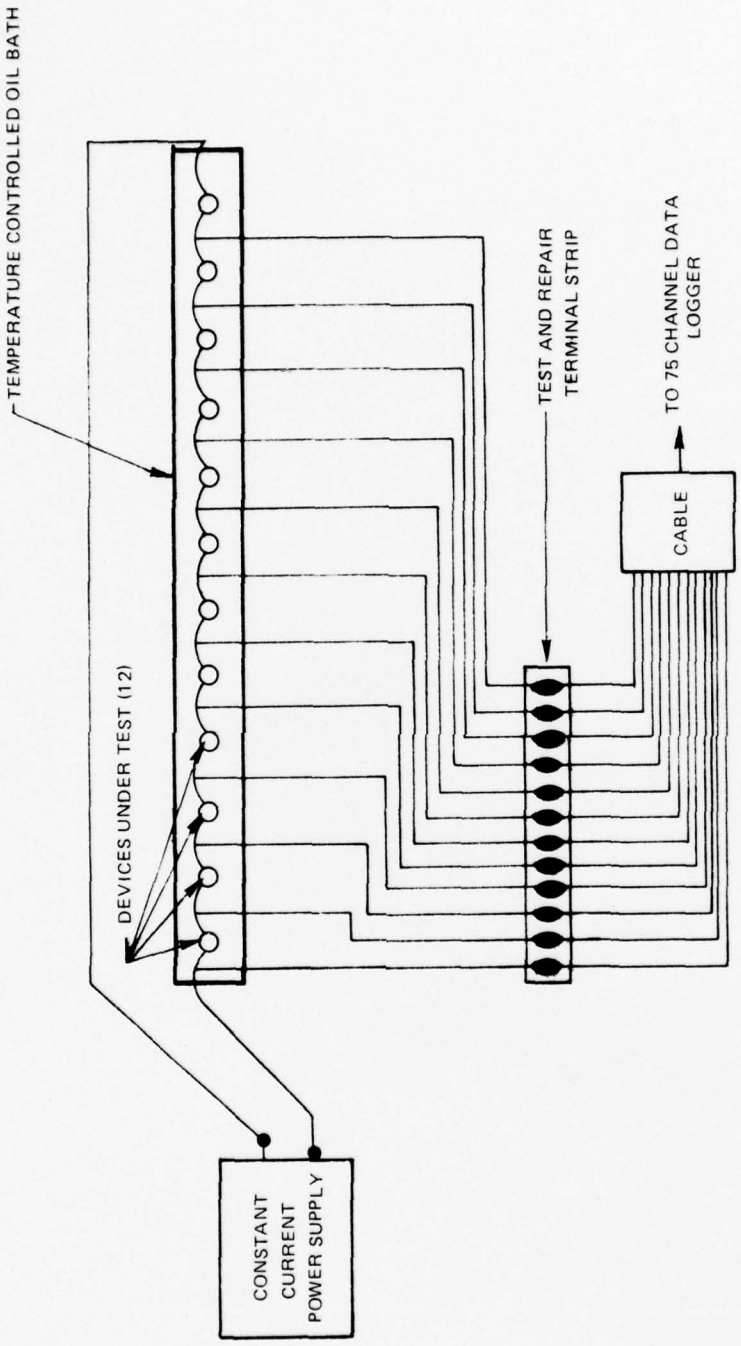

76-03-64-1

4.1.2 Results and Discussions

Time for failure data is presented as Weibull plots of cumulative median rank failed vs. logarithm of time for failure in Figs. 4 through 15. The estimator points are the "expected life" under the test conditions and are tabulated in Tables I through IV. For the sake of completeness, Weibull statistics is discussed in Appendix I including the significance of nonlinear Weibull plots and the reliability of such derived quantities as the "expected life."

The logarithms of the estimator points or estimated lifetimes were plotted vs. the reciprocal of absolute temperature for some cases and slopes were determined from these plots (Figs. 16 and 17). Using the Arrhenius equation an activation energy, E was inferred. Not surprisingly, values less than, as well as greater than, 1.0 eV resulted. In addition, Fig. 18 shows some typical variations of resistance with time during stress.

SEM photographs and accompanying compositional analyses are presented in Figs. 19 through 39. These are representative of the samples before and after stress. They are grouped by composition with each group showing the copper and aluminum distribution before and after stressing. Topographical photographs are shown of three unstressed metal films (for all compositions) in Figs. 19, 35, 36, 37 and 38. Progressive changes in surface topography toward larger crystallites are exhibited in all of these films. Three significant features are common to all of these specimens when examined after current stressing at elevated temperatures.

Massive migration of aluminum and copper takes place during high current stressing. Aluminum moves out of the stripe-pad transition region into the stripe at the cathode end. This thinning, of course, is the cause of failure.

The second feature is the copper motion along the bar. It follows the same pattern of motion as the aluminum except that some copper accumulation occurs in the neighborhood of the failure. Third, other local copper accumulations occur along the stripes in a more or less random fashion, in many cases almost completely depleting the stripe of copper at the detectable level (about 1 percent).

The Weibull plots do not exhibit straight line or smoothly changing nonlinear character in most cases. Rather, multisegment curves result from time-to-failure vs rank in the Weibull format. Several competing mechanisms for failure are likely to be operative simultaneously in these alloy systems. Surface and grain boundary related vacancy motions are two mechanisms which can be cited. In earlier work it has been shown that surface related failures in sputtered aluminum film interconnections can be inhibited by covering the metal stripes with sputtered silicon dioxide. (See Final Report #N921820-4 for 1 January 1974 through 31 December 1974 under NASC Contract No. N00019-74-C-0256, "Sputtering Technology for Improved Electron Devices" by D. H. Grantham and J. L. Swindal.) Introduction of copper

into the aluminum stripe adds two possible mechanisms to the already cited phenomena--the motion of copper along the surface and motion of copper through the bulk. Movement of copper atoms in the metal stripe is not simply related to temperature and the diffusion coefficient of copper in aluminum. Figure 26B shows the copper distribution in a stripe after annealing 350 hours at 250°C without current stressing while Fig. 27B depicts the copper distribution in a stripe of the same composition current stressed to 3×10^6 amperes/cm^2 at 200°C. In the absence of current stress only moderate agglomeration and diffusion of the copper took place while the introduction of current stress caused drastic departures from the relatively uniformly dispersed condition in the as-deposited stripe of the same nominal composition. Since atom diffusion processes are coupled with vacancy motions and depend on vacancy concentrations and mobilities, any enhancement of vacancy mobility must affect atom diffusion. Therefore, this enhanced copper diffusion result may not be surprising. We believe it has, however, not been reported before.

That there is migration of both copper and aluminum under the high current, high temperature stresses can be seen from Figs. 22C, 24C and 32C which show a microprobe plot of aluminum characteristic x-ray emission intensity along the length of a typical stressed specimen. The variation in intensity is a direct measure of the quantity of aluminum in the path of the microprobe electron beam and, thus, the trace shown is a thickness profile along the length of the stripe.

This change from a uniform film thickness to one which varies along the length of the stripe near the end is another complicating factor in interpreting the time-to-failure data. Once thinning becomes significant, current density increases and continually varies along the length of the stripe near the end and the local temperature also varies in this region, both parameters increasing with decreasing cross-section of the stripe. So, not only are there competing mechanisms but there are continually varying stress parameters. We have, therefore, chosen not to interpret the Arrhenius type fit of expected life as a function of reciprocal temperature. We have tabulated the expected life for the various alloys as a function of stress parameters. At the lower current and lower temperature levels it appears that the effects of increasing the concentration of copper in the aluminum beyond the 1 percent level probably is not effective in increasing conductor life and may even be detrimental to long life. This is consistent with the notion that accumulation of a second species at the grain boundaries in a metal will extend the electromigration life by pinning vacancies and that the bulk portions of the grains themselves are not the limiting factor. In these cases of sputtered films deposited at room temperature, the copper is uniformly dispersed throughout the aluminum on a scale resolvable by the electron microprobe but must have accumulated sufficiently in the grain boundaries during deposition to cause extension of life. This contrasts with the nonuniform distribution of copper one might expect from annealing layered films of copper on aluminum or from alloy films deposited from some type of evaporation source.

FIG. 4

WEIBULL PROBABILITY CHART

ALUMINUM PLUS 1% Cu

$J = 2 \times 10^6$ AMPS PER CM^2

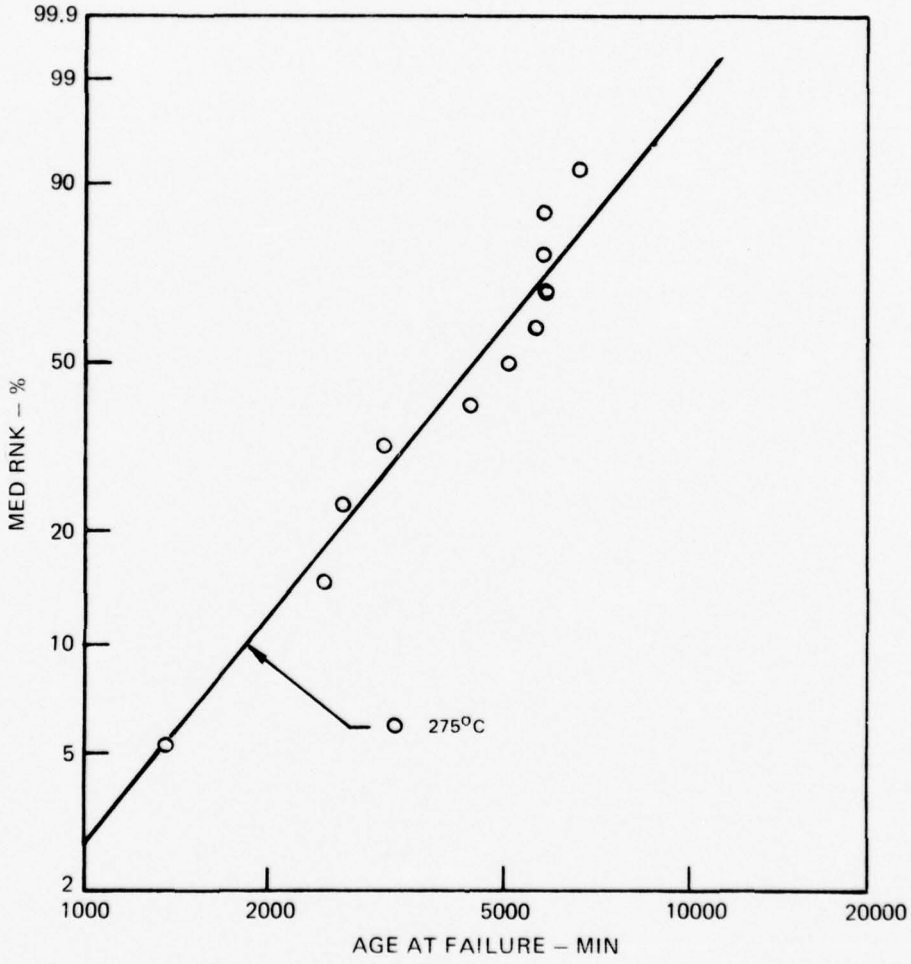

76–04–230–8

FIG. 5

WEIBULL PROBABILITY CHART

ALUMINUM PLUS 1% Cu

$J = 3 \times 10^6$ AMPS PER CM^2

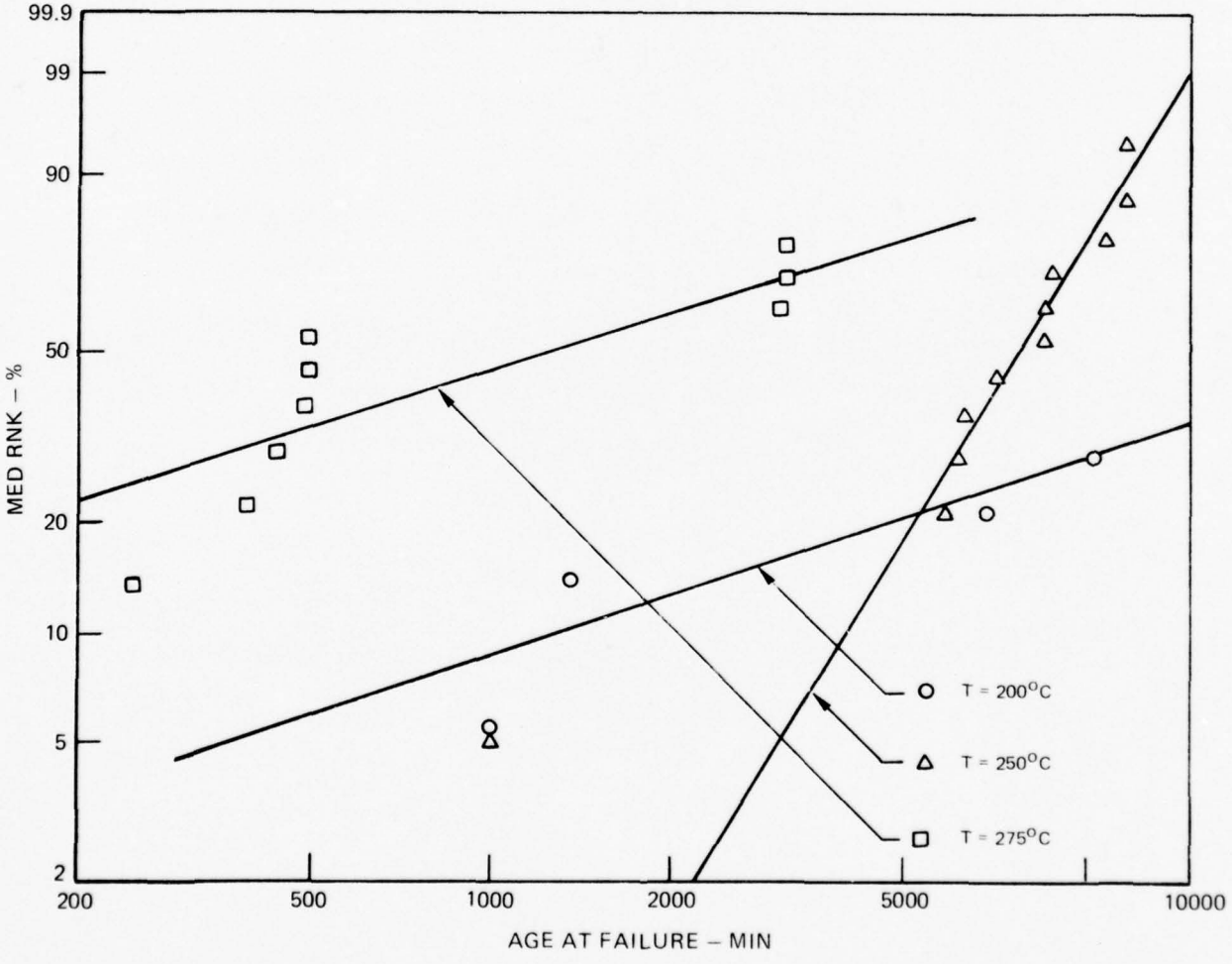

76-04-230-4

FIG. 6

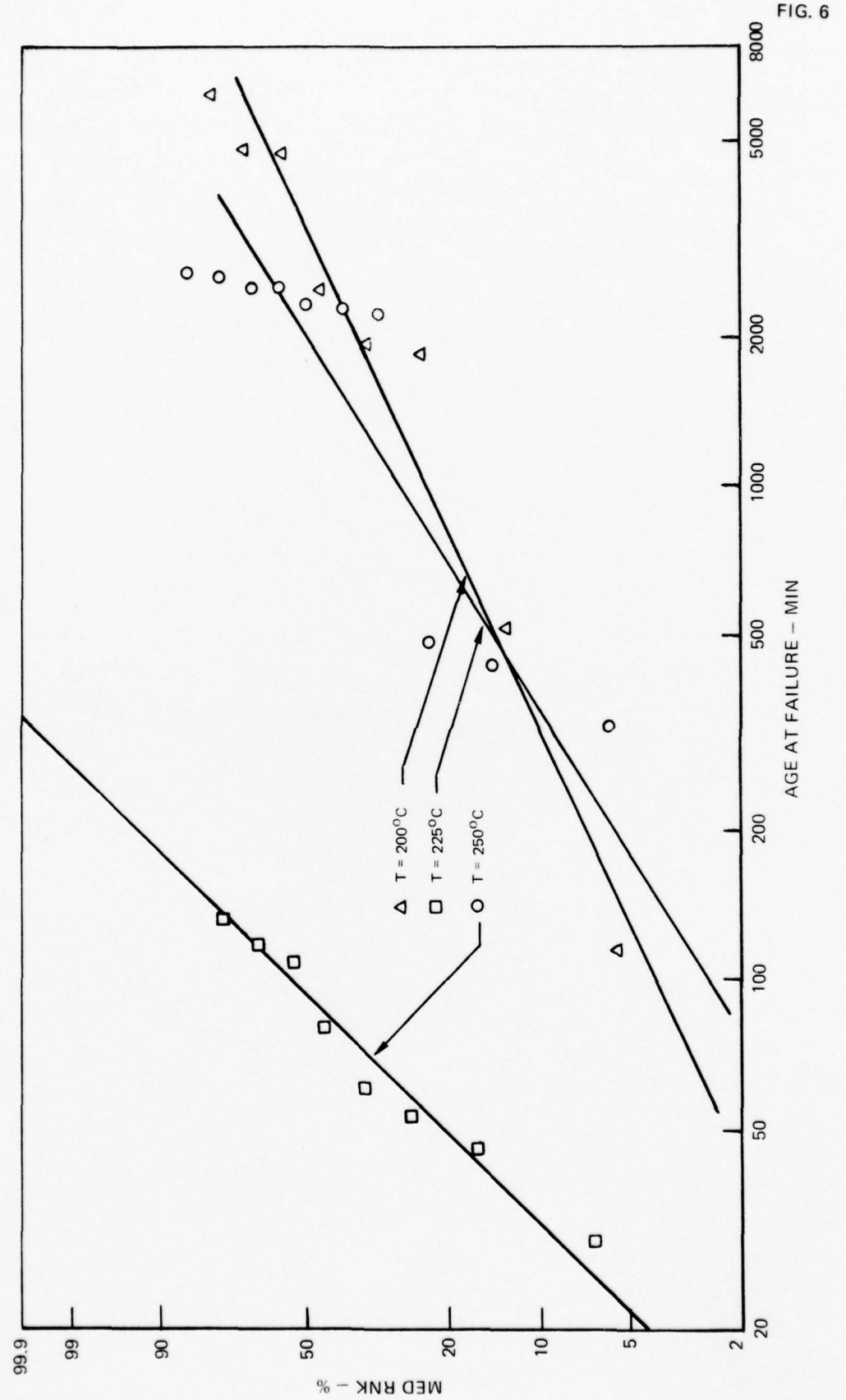
WEIBULL PROBABILITY CHART
ALUMINUM PLUS 1% Cu
J = 4x10^6 AMPS PER CM^2
MED RNK – %
99.9
99
90
50
20
10
5
2
AGE AT FAILURE – MIN
20
50
100
200
500
1000
2000
5000
8000
T = 200°C
T = 225°C
T = 250°C
76-04-230-9

FIG. 7

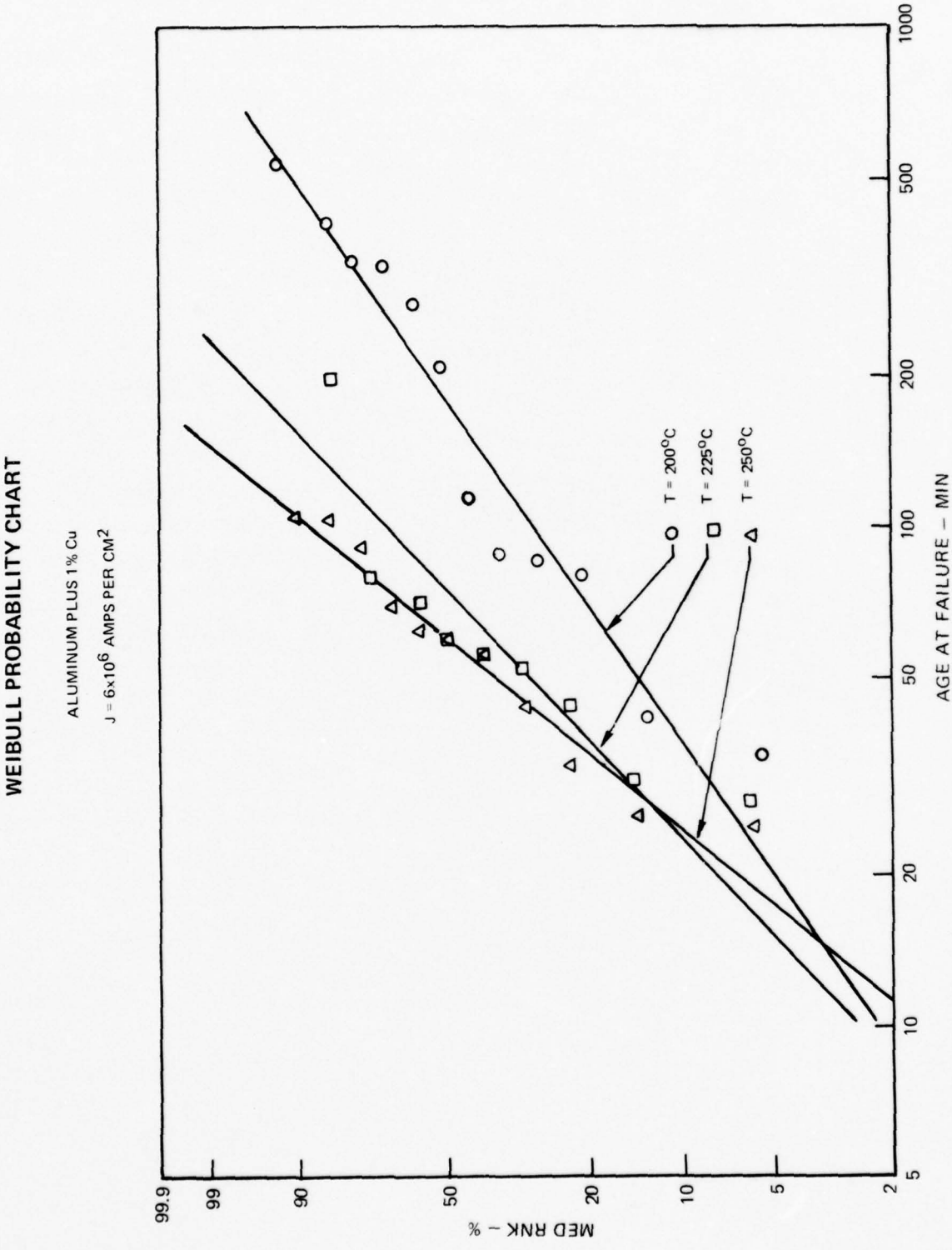
WEIBULL PROBABILITY CHART
ALUMINUM PLUS 1% Cu
J = 6x10^6 AMPS PER CM^2
MED RNK – %
99.9
99
90
50
20
10
5
2
AGE AT FAILURE – MIN
1000
500
200
100
50
20
10
5
T = 200°C
T = 225°C
T = 250°C
76-04-230-10

FIG. 8

WEIBULL PROBABILITY CHART

ALUMINUM PLUS 8% Cu

$J = 3 \times 10^6$ AMPS PER CM^2

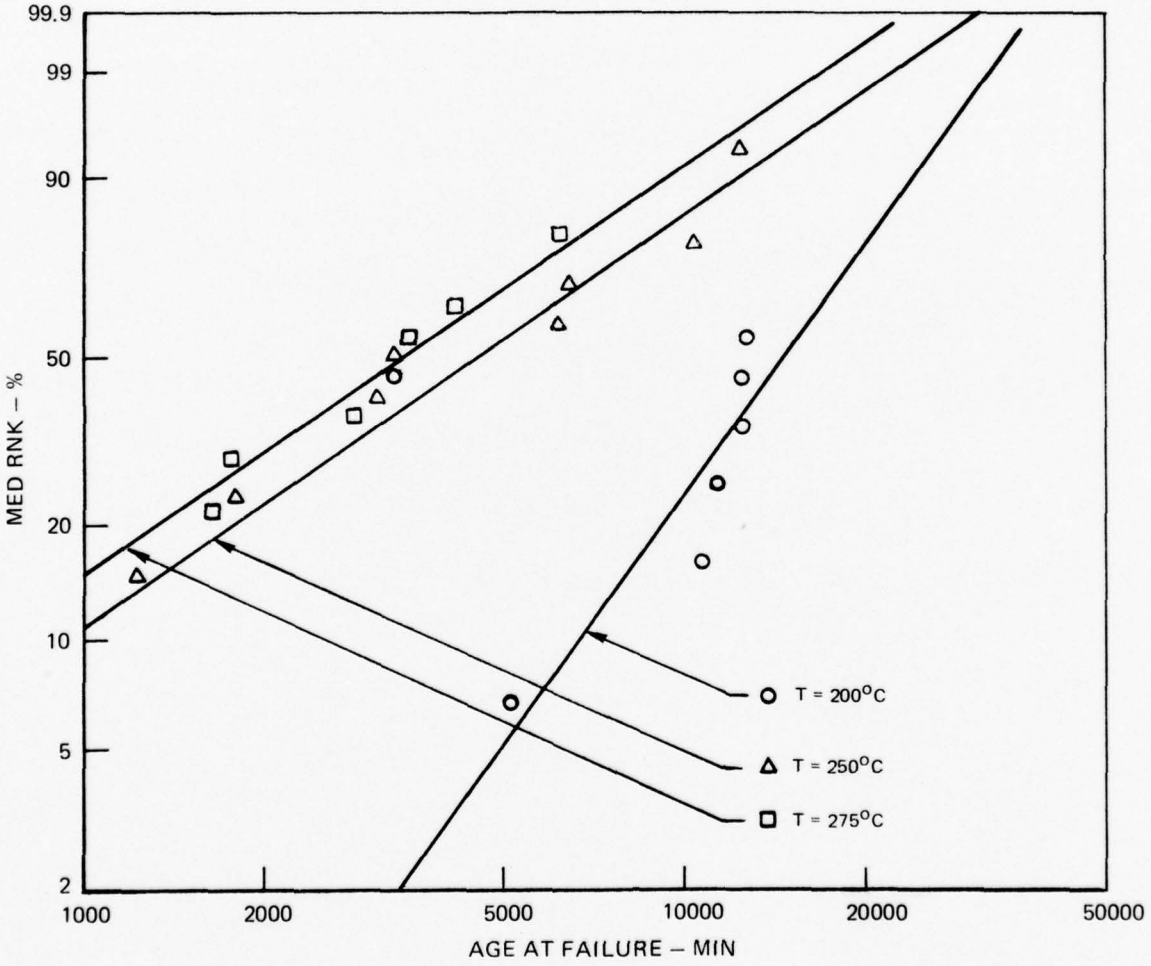

76–04–230–3

FIG. 9

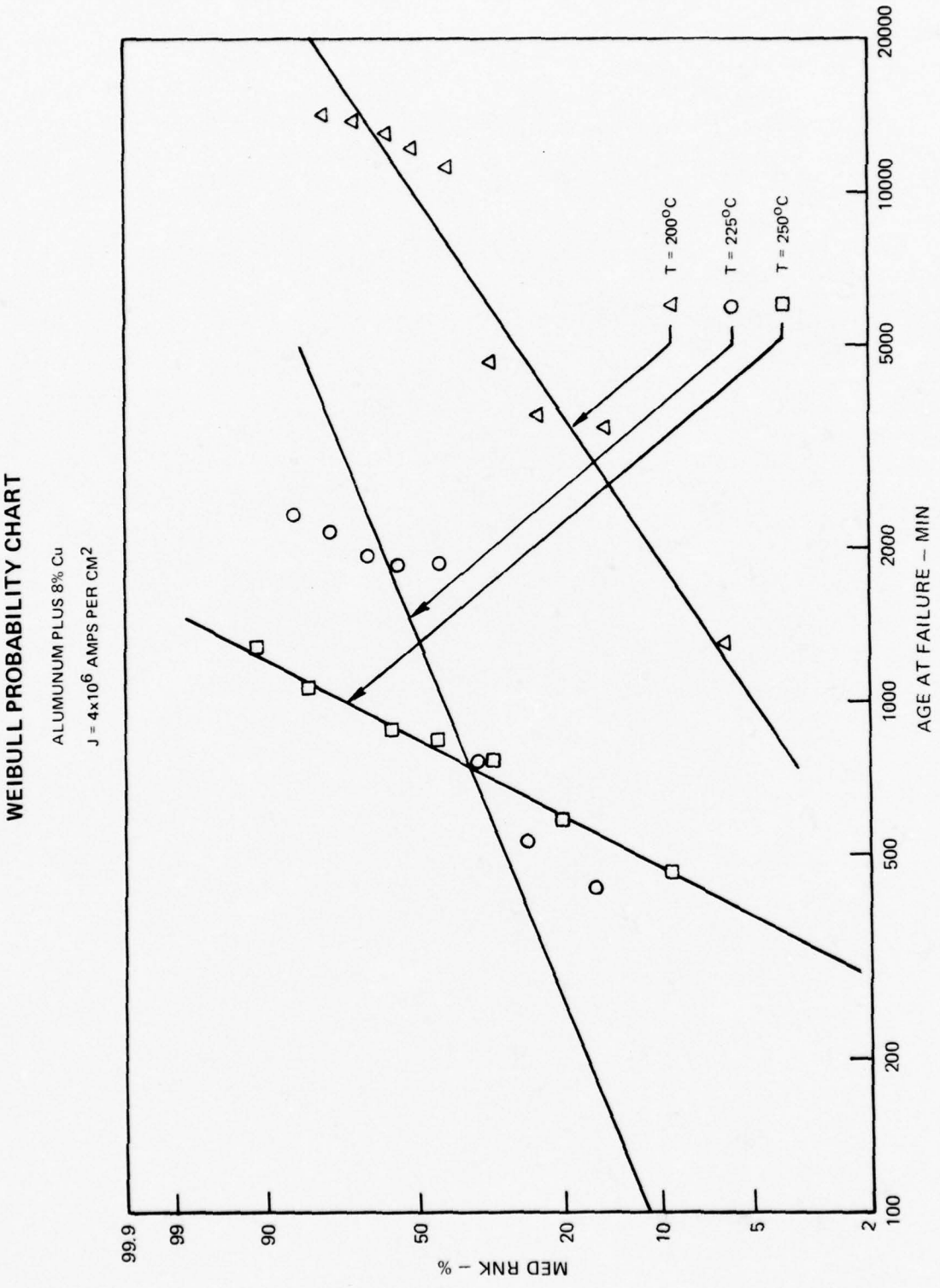

76-04-230-7

FIG. 10

WEIBULL PROBABILITY CHART

ALUMINUM PLUS 8% Cu

$J = 6 \times 10^6$ AMPS PER CM^2

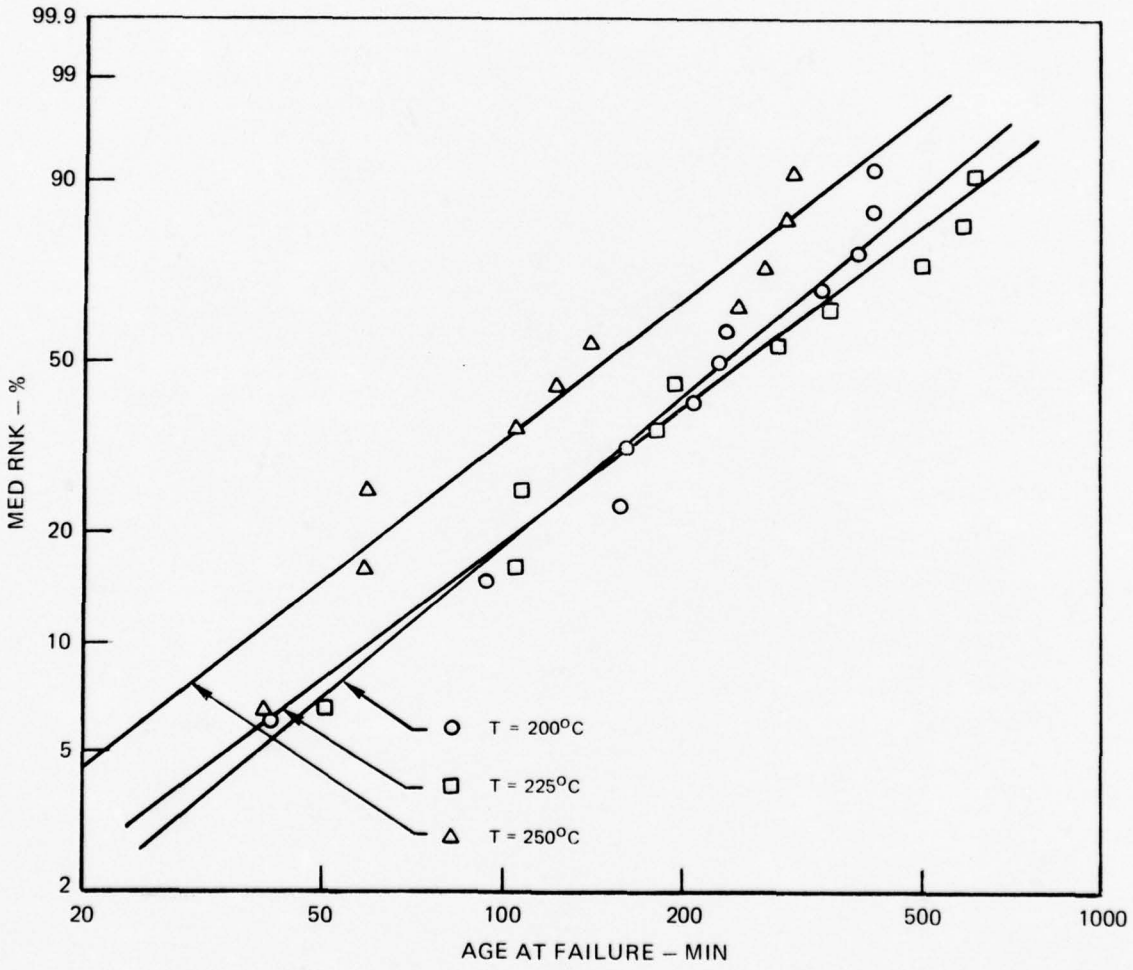

76–04–230–1

FIG. 11

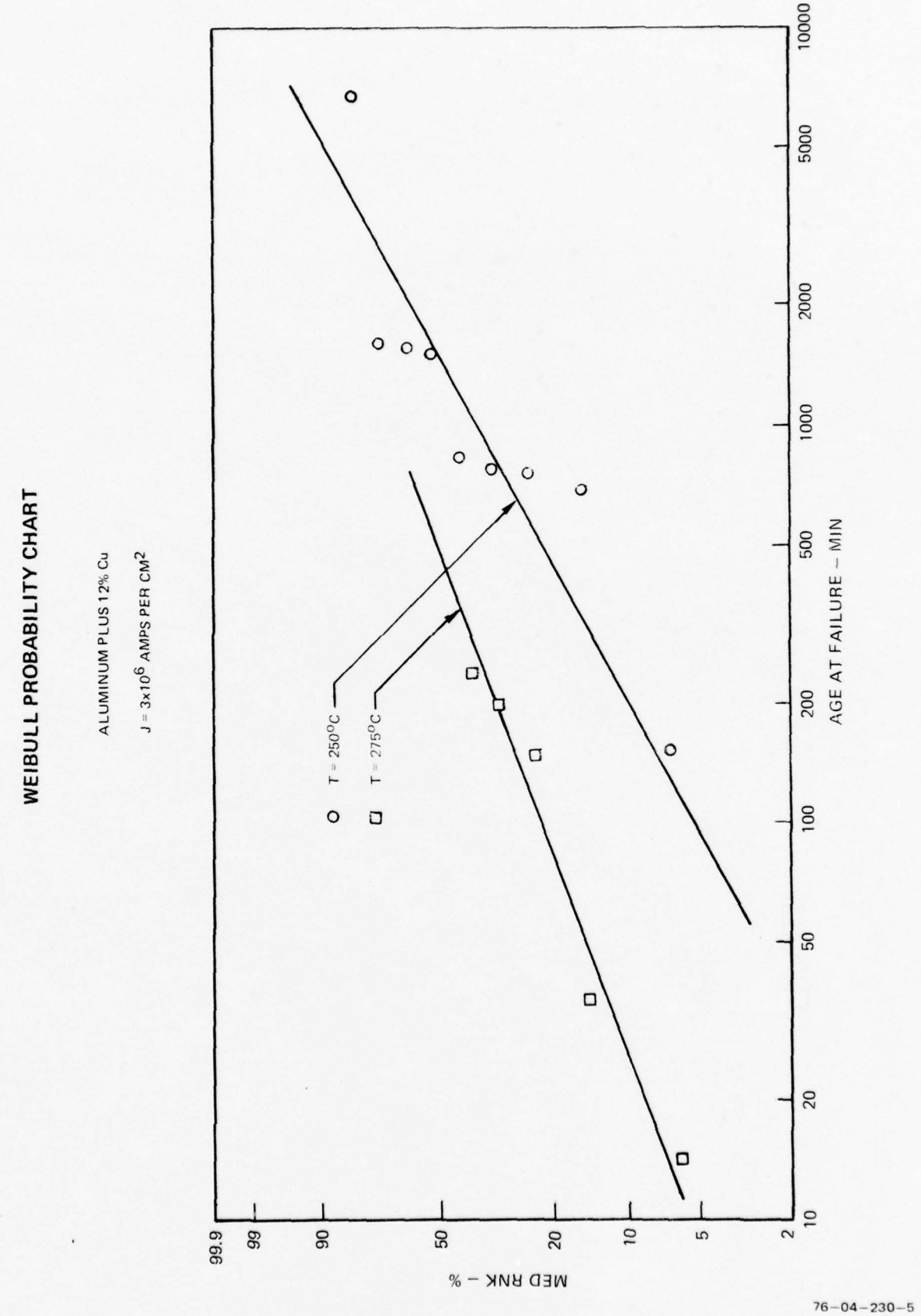
WEIBULL PROBABILITY CHART
ALUMINUM PLUS 12% Cu
J = 3x10^6 AMPS PER CM^2
T = 250°C
T = 275°C
MED RNK – %
99.9
99
90
50
20
10
5
2
10
20
50
100
200
500
1000
2000
5000
10000
AGE AT FAILURE – MIN
76–04–230–5

FIG. 12–A

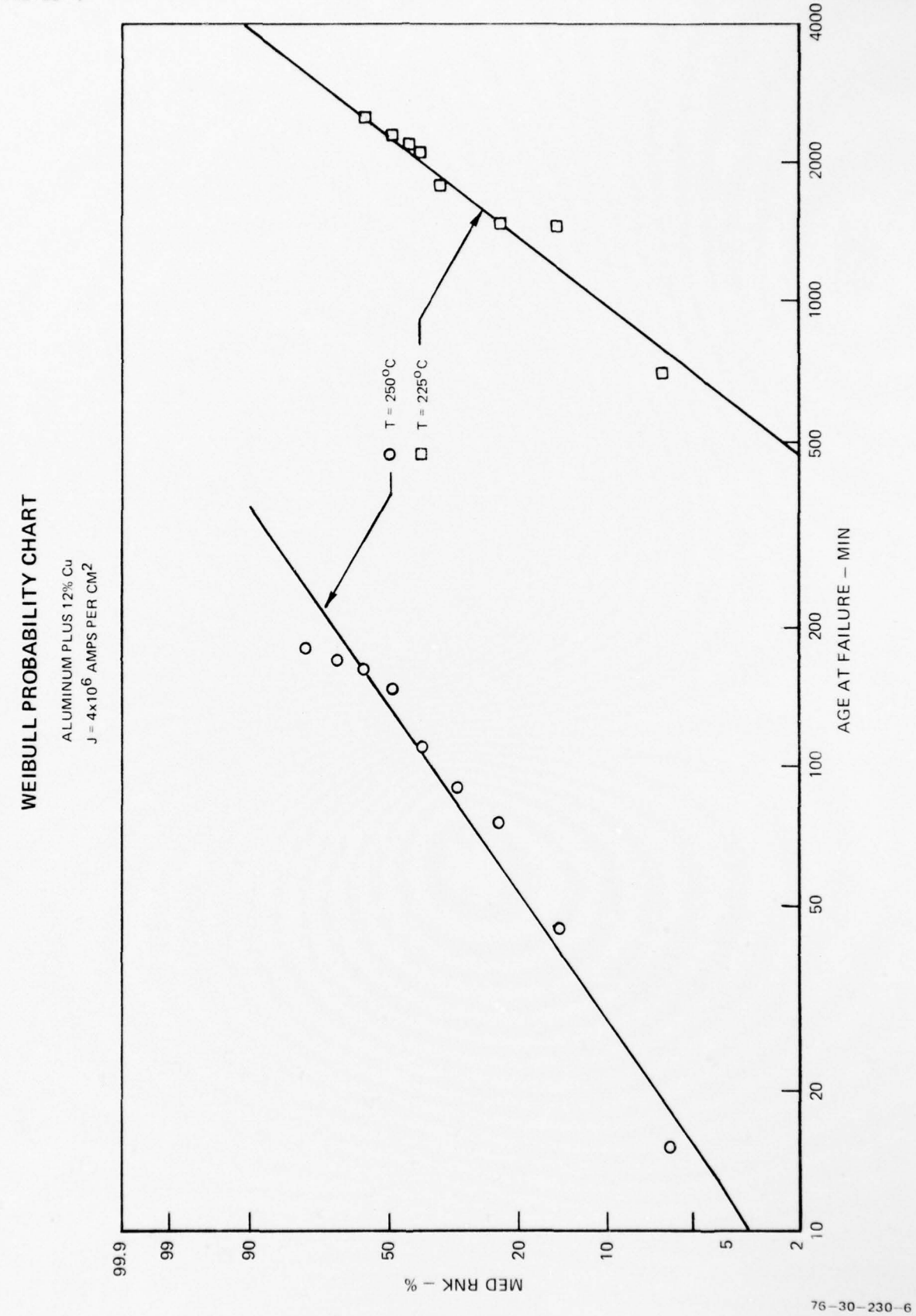
WEIBULL PROBABILITY CHART
ALUMINUM PLUS 12% Cu
J = 4x10^6 AMPS PER CM^2
T = 250°C
T = 225°C
MED RNK – %
99.9
99
90
50
20
10
5
2
AGE AT FAILURE – MIN
10
20
50
100
200
500
1000
2000
4000
76–30–230–6

WEIBULL PROBABILITY CHART

ALUMINUM PLUS 12% Cu

$J = 4 \times 10^6$ AMPS PER CM^2

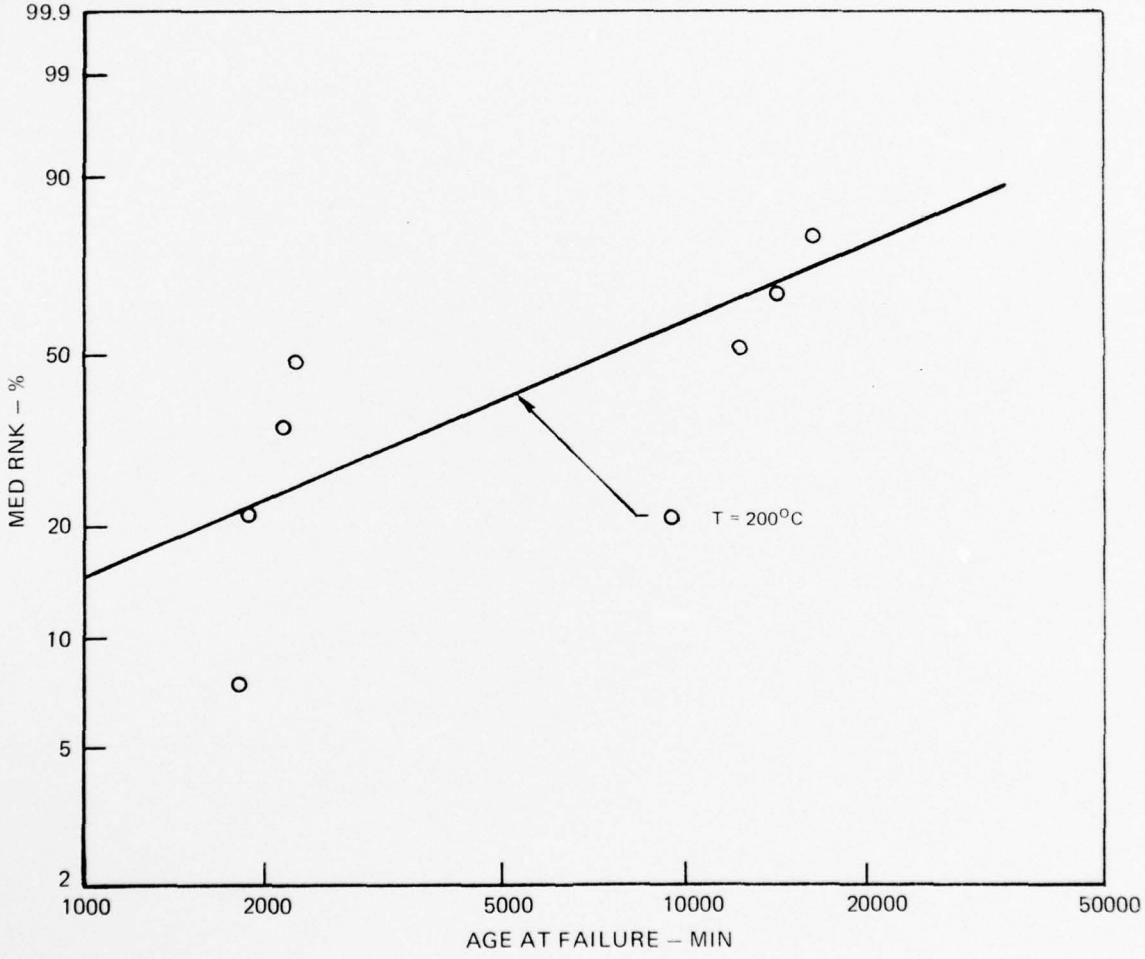

76-04-230-2

FIG. 13

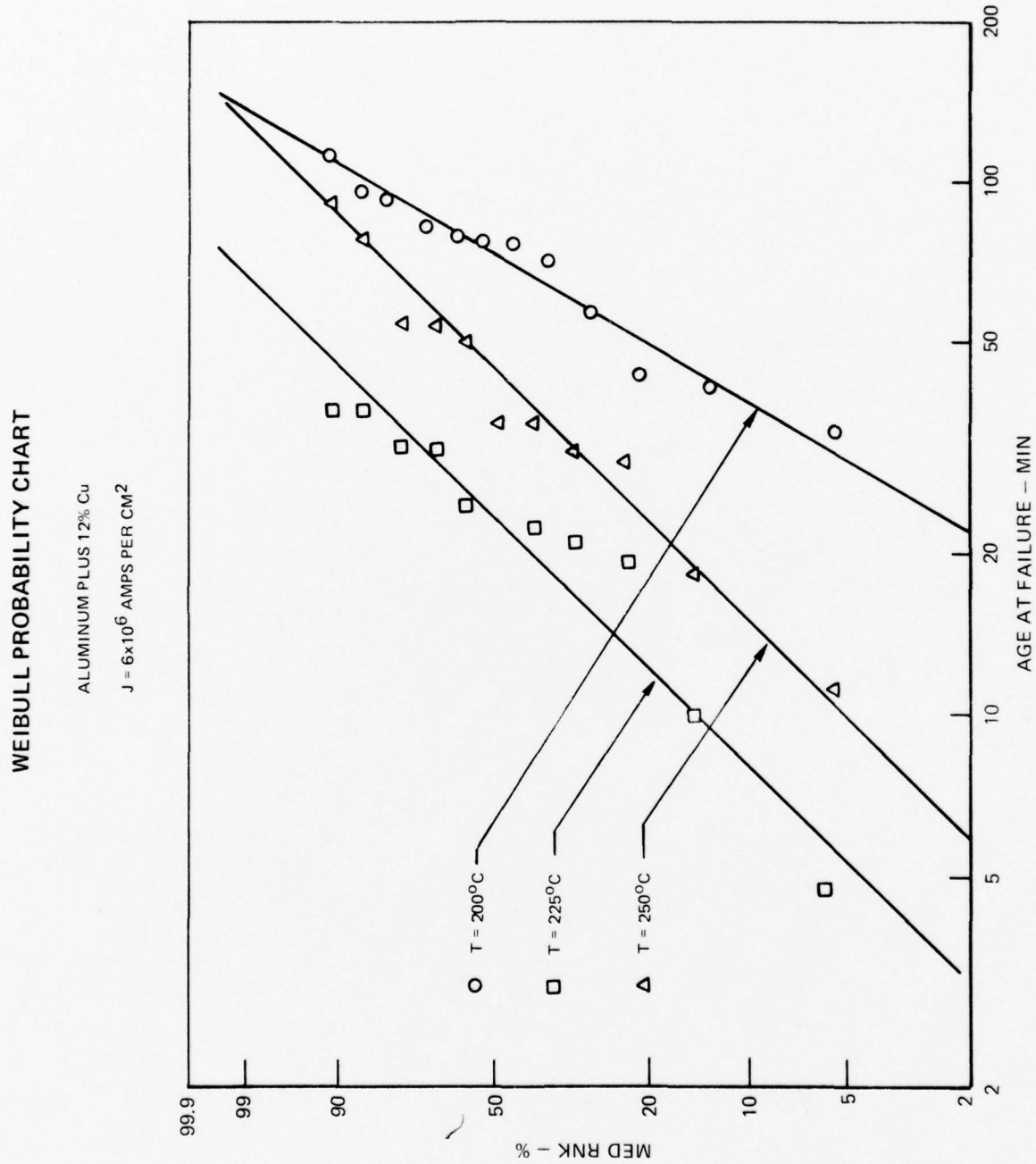

76-04-230-11

FIG. 14

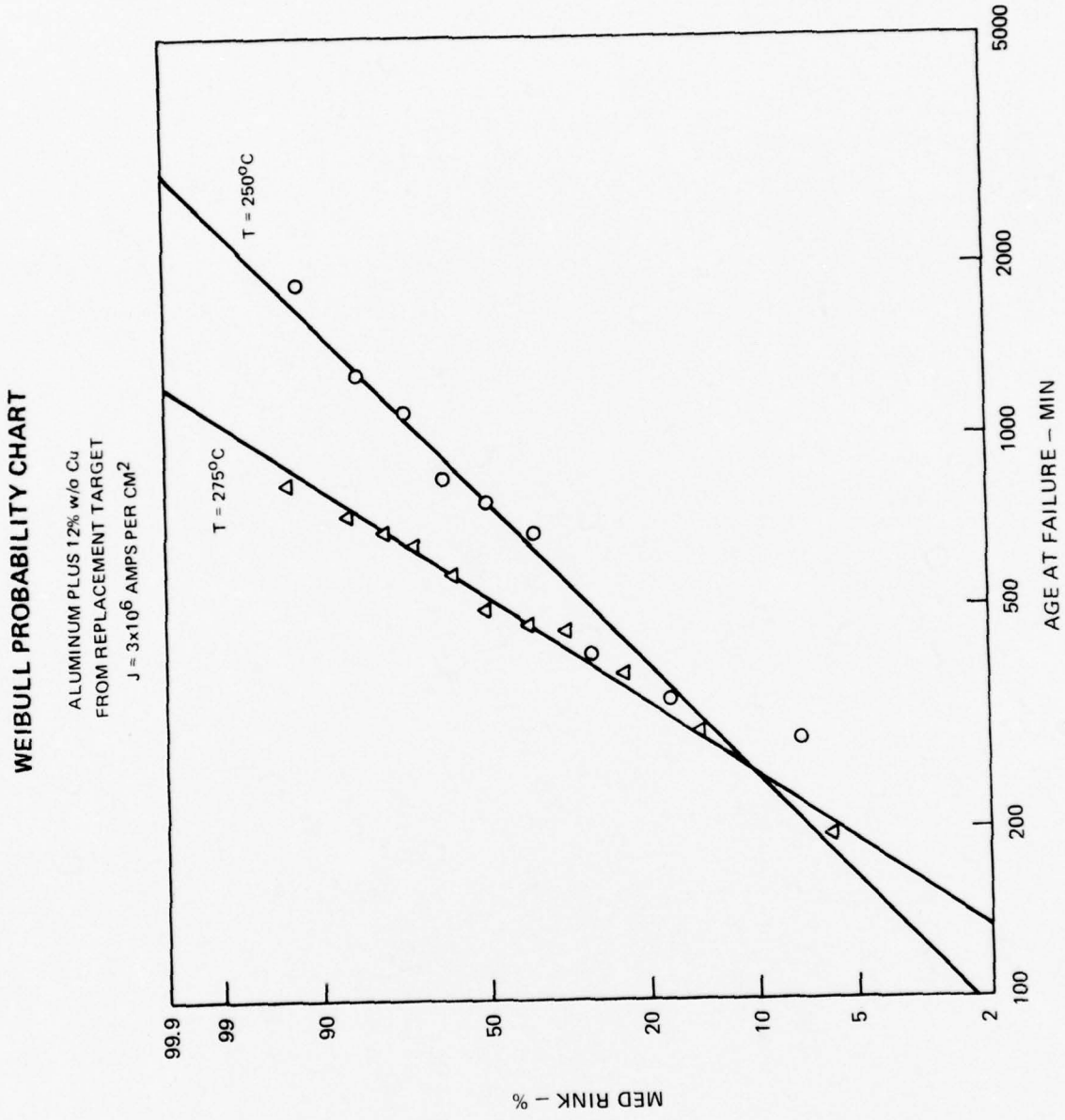

76–05–171–1

FIG. 15

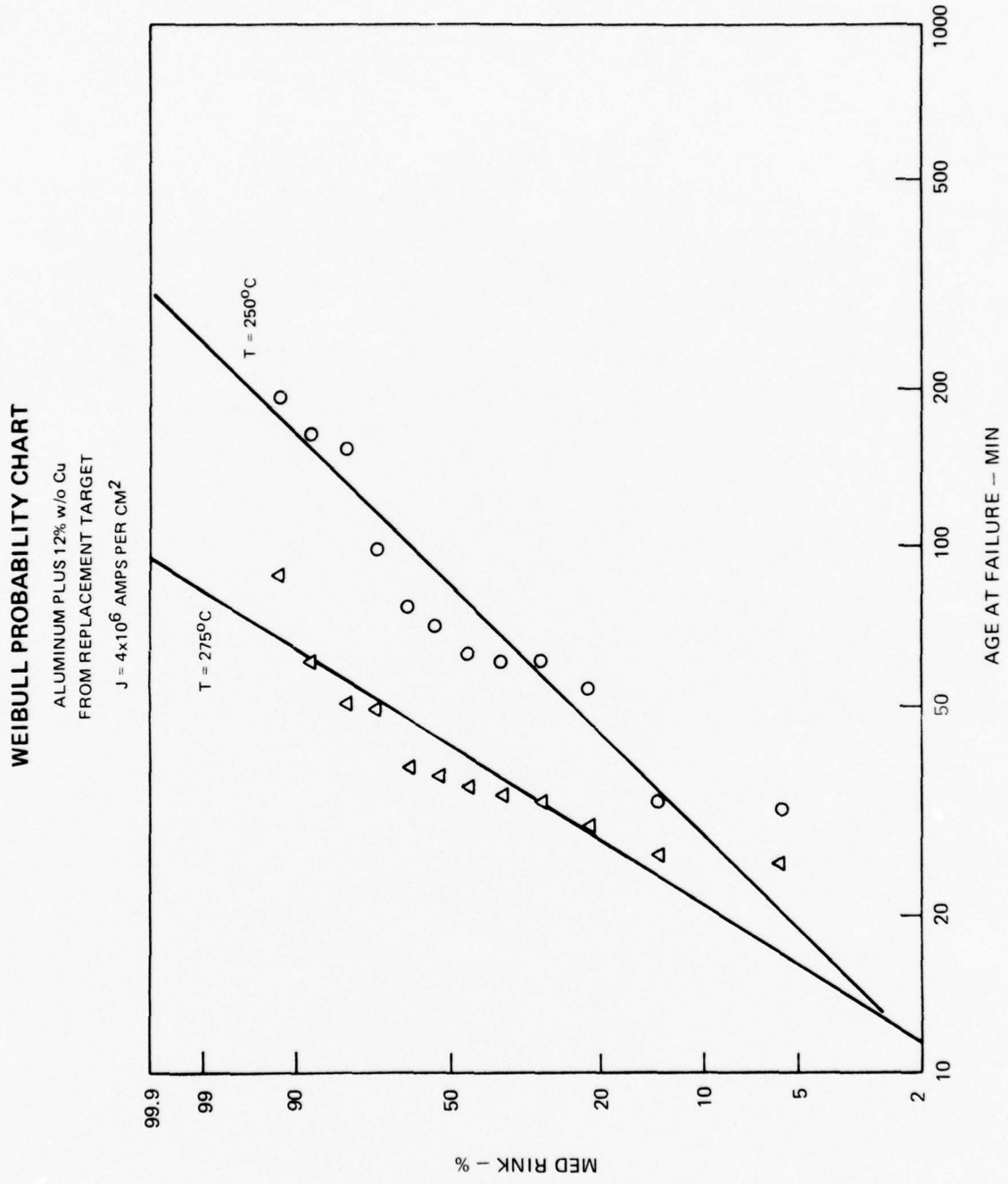

76-05-171-2

FIG. 16

ARRHENIUS PLOTS OF KINETIC DATA

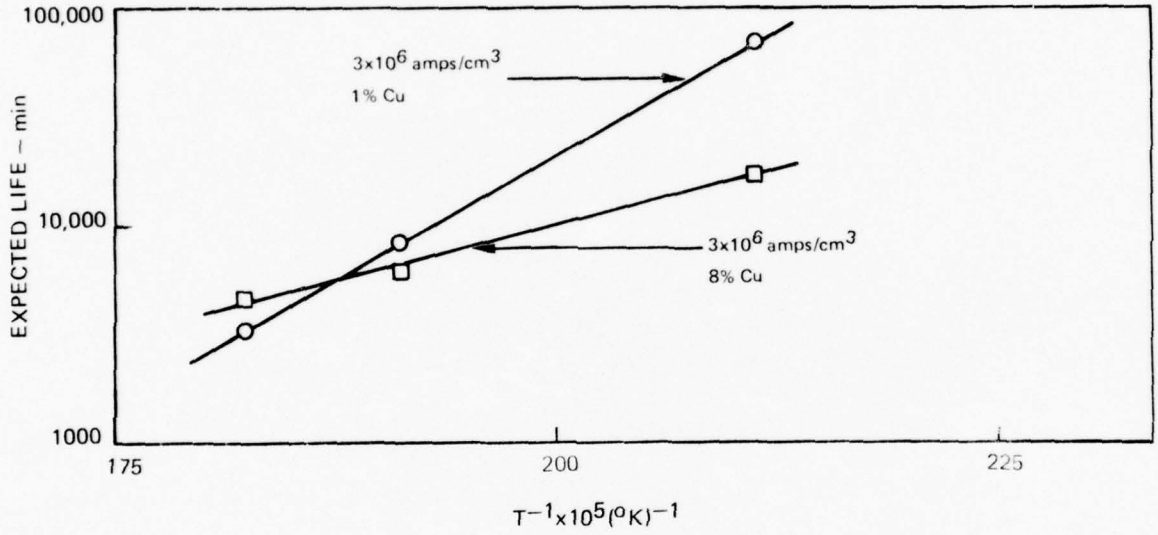

ACTIVATION ENERGIES DERIVED FROM ABOVE PLOTS:

1% Cu–E = 0.91 ev

8% Cu–E = 0.40 ev

76–03–255–4

FIG. 17

ARRHENIUS PLOTS OF KINETIC DATA

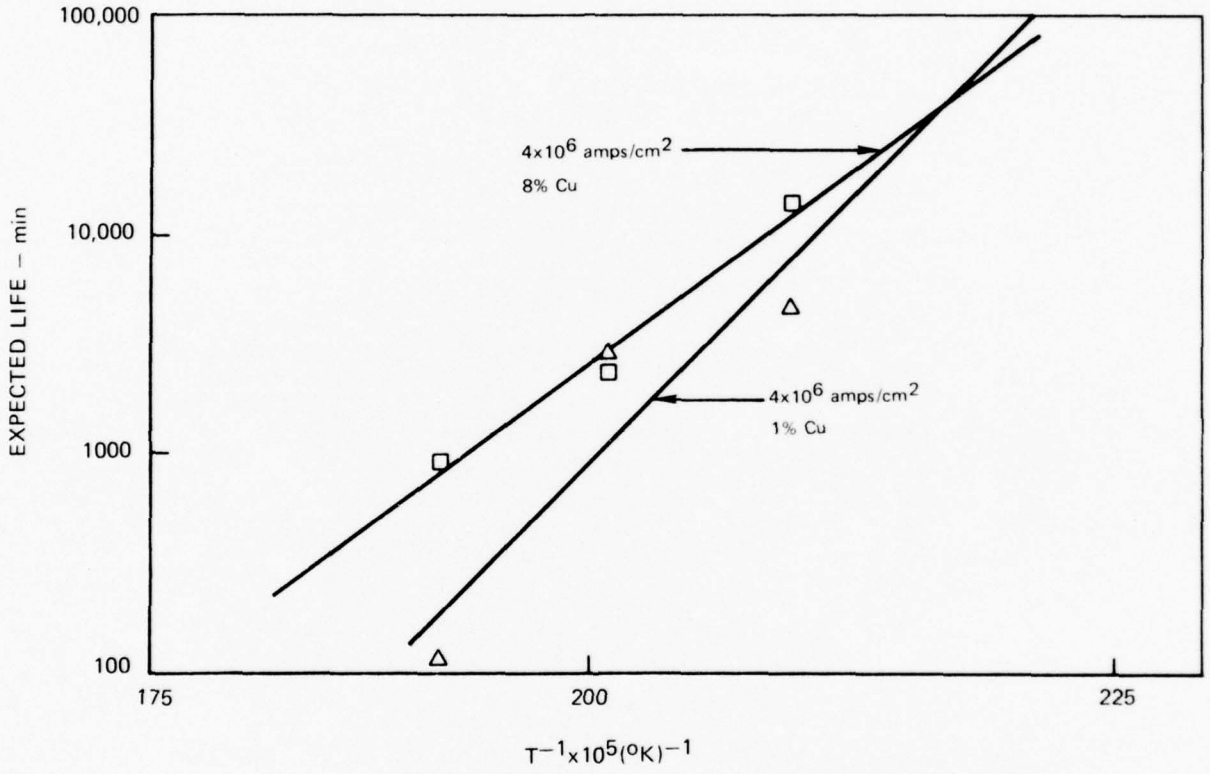

ACTIVATION ENERGIES DERIVED FROM ABOVE PLOTS:

1%Cu–E = 1.59 ev

8% Cu–E = 1.18 ev

76–04–271–1

FIG. 18

SOME TYPICAL RESISTANCE HISTORIES

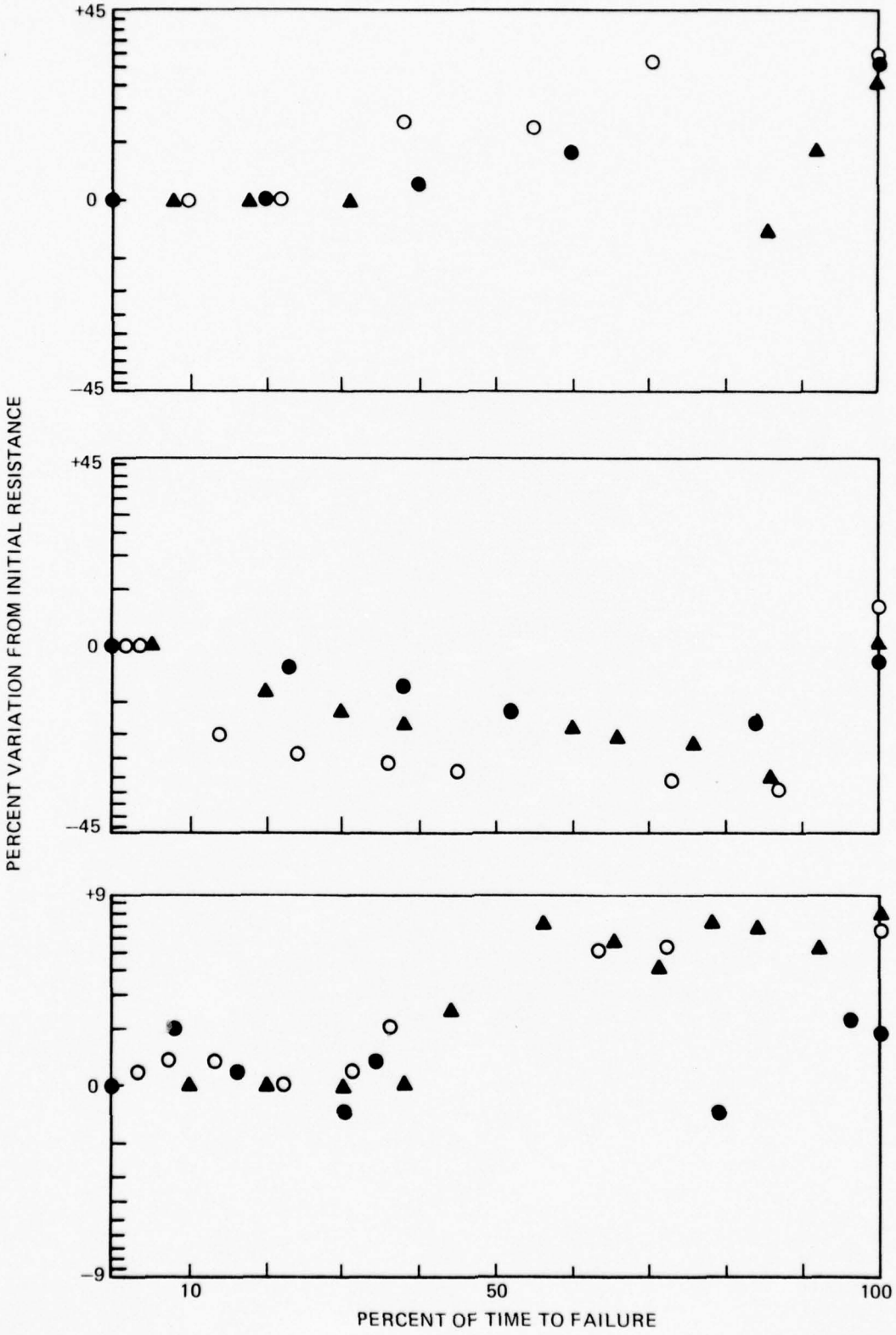

76–03–247–11

Table I. Time For Failure At 2 x 10^6 amps/cm^2 (Minutes)

Temp, °C	Composition 1%	8%	12%
200			
225			
250			
275	5200		

Table II. Time For Failure At 3 x 10^6 amps/cm^2 (Minutes)

Temp, °C	Composition 1%	8%	12%
200	70,000	17,500	
225			
250	8700	6200	2100
275	2300	4700	850

Table III. Time For Failure At 4×10^6 amps/cm^2 (Minutes)

Temp.	Composition 1%	8%	12%
200	5000	14,500	13,000
225	2800	2300	2700
250	120	950	175
275			190

Table IV. Time For Failure At 6×10^6 amps/cm^2 (Minutes)

Temp.	Composition 1%	8%	12%
200	240	300	80
225	95	340	28
250	70	200	52
275			

FIG. 19

UNSTRESSED TEST BAR–ONE PERCENT COPPER

(1) SURFACE TOPOGRAPHY

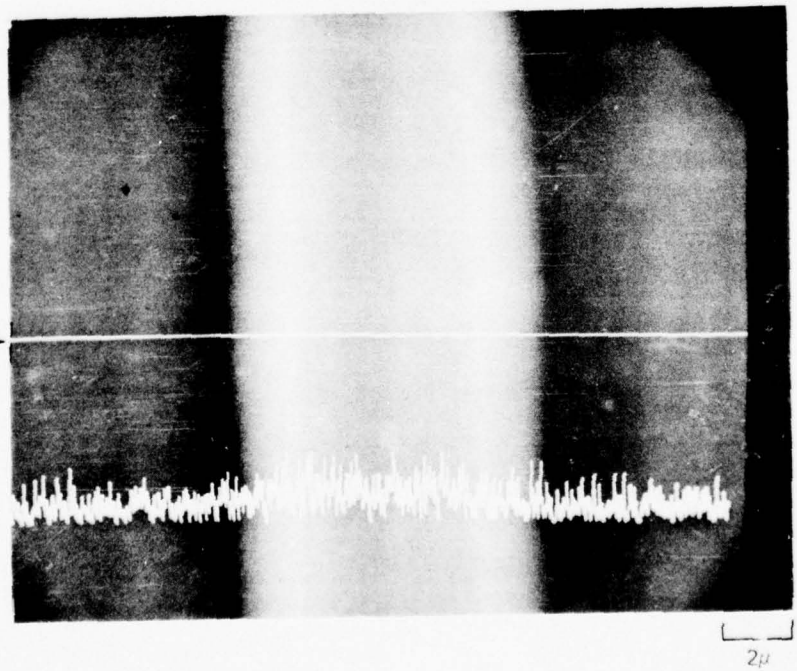

(2) X-RAY (COPPER) SCAN

76-03-33-14

FIG. 20–A

TEST BAR 1WT PERCENT COPPER

TEST TERMINATED AFTER 53 HRS (BAR STILL CONTINUOUS)

275°C, 3×10^6 amps/cm^2

5μ

CATHODE

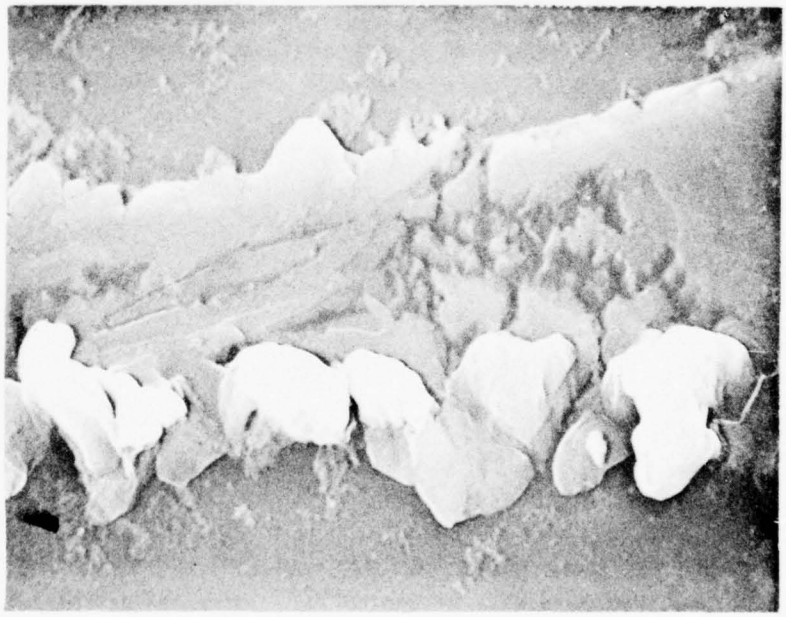

2μ

ANODE

76-03-21-10

FIG. 20-B

NEAR CATHODE

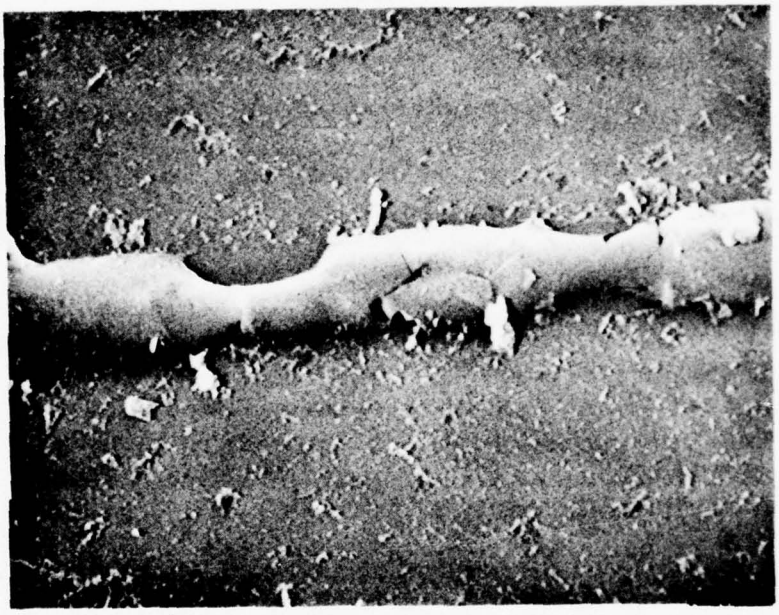

76 03 21 8

FIG. 20-C

ANODE DISTRIBUTION BY MICROPROBE

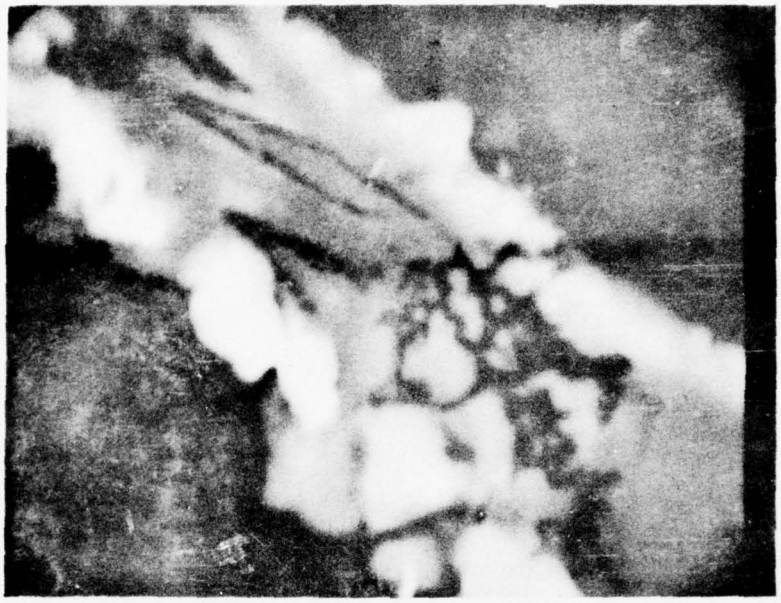

(1) BACKSCATTER MODE (ATOMIC NUMBER CONTRAST) 2.5μ

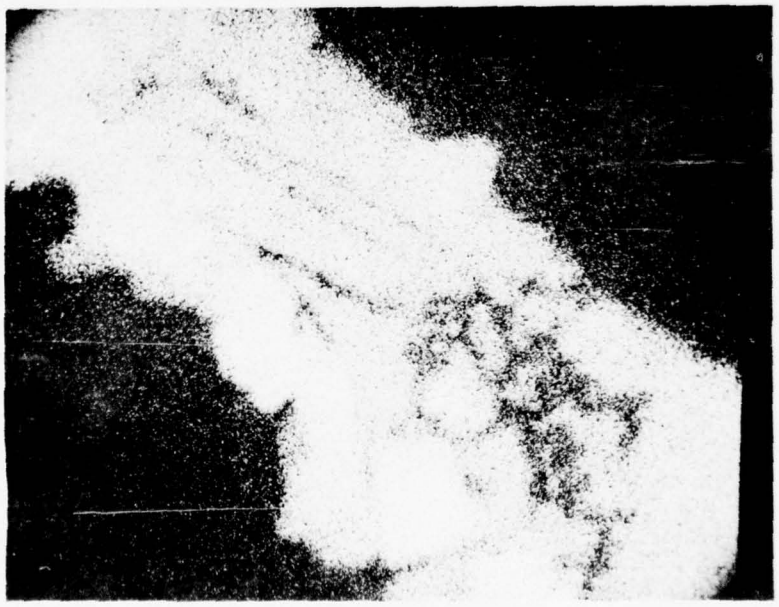

(2) X - RAY (ALUMINUM) SCAN 2.5μ

76 03 21 4

FIG. 20–D

ANODE DISTRIBUTION BY MICROPROBE

(1) MICROPROBE BACKSCATTER MODE (ATOMIC NUMBER CONTRAST)

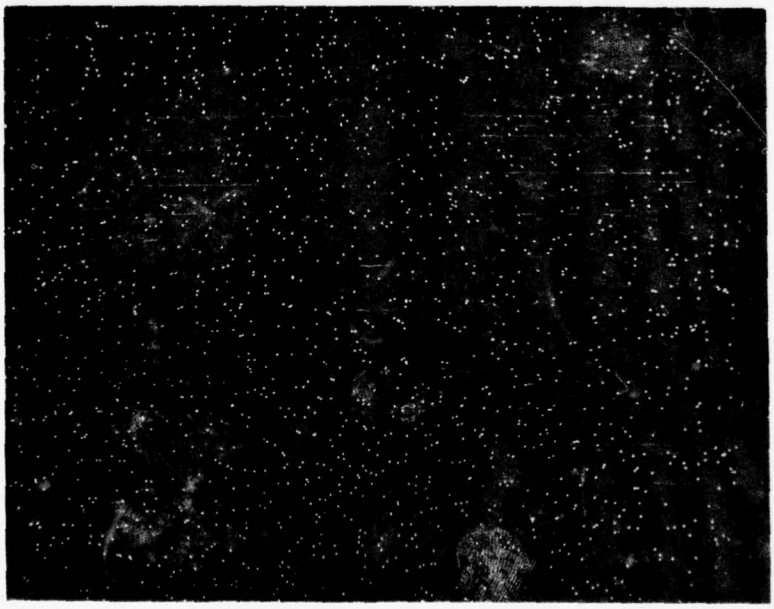

(2) MICROPROBE X - RAY (COPPER) SCAN

0.5μ

76-03-21-5

UNSTRESSED TEST BAR–EIGHT PERCENT COPPER–DISTRIBUTION BY MICROPROBE

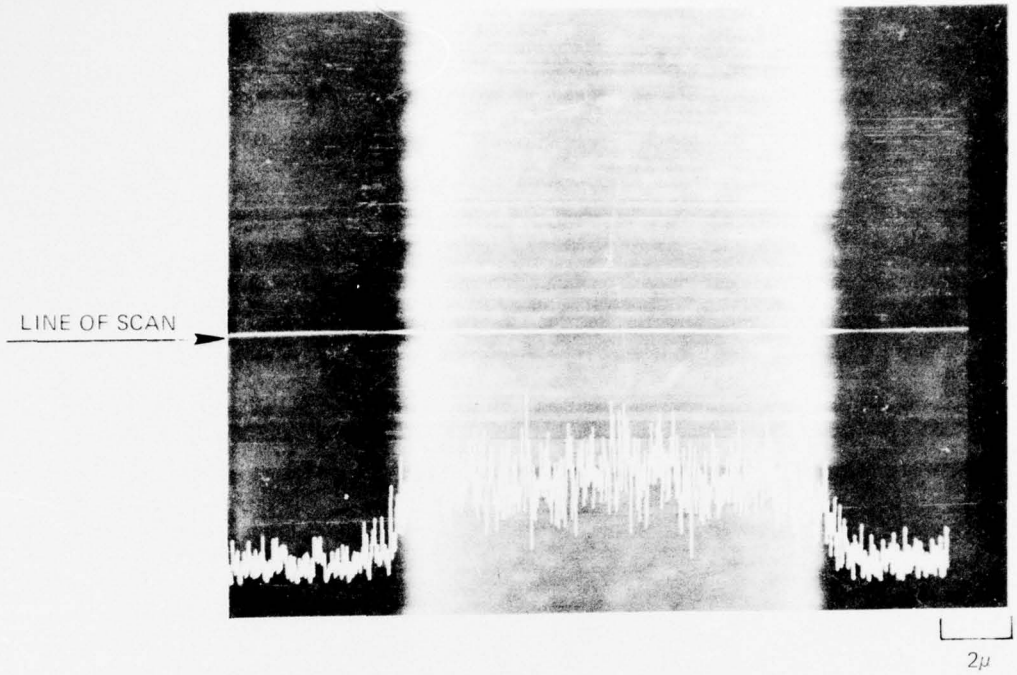

(1) BACKSCATTER PLUS X–RAY (COPPER) LINE SCAN

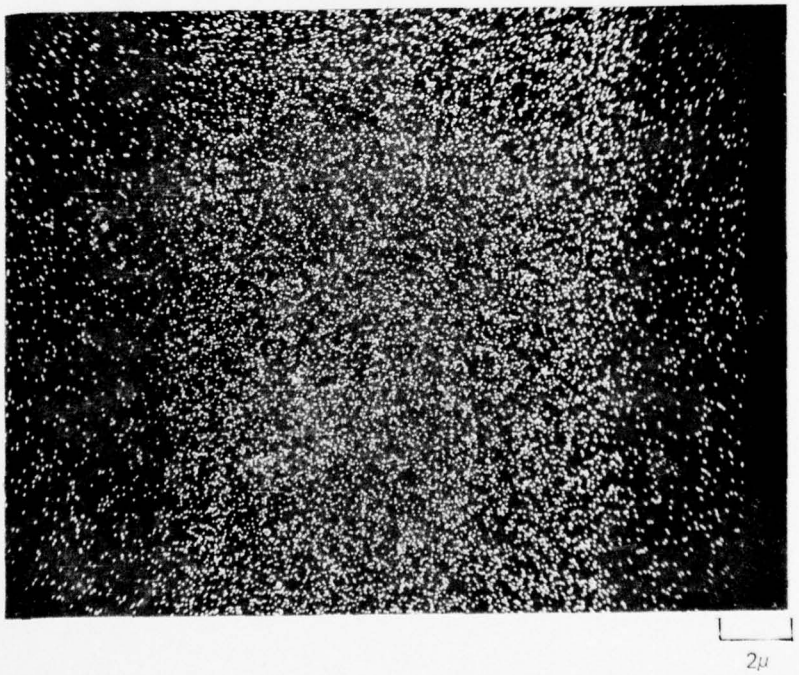

(2) X–RAY (COPPER) SCAN

76-03-33-15

FIG. 22–A

FAILED TEST BAR 8 WT PERCENT COPPER

120 MIN, 250°C, 6×10^6 AMPS/CM^2

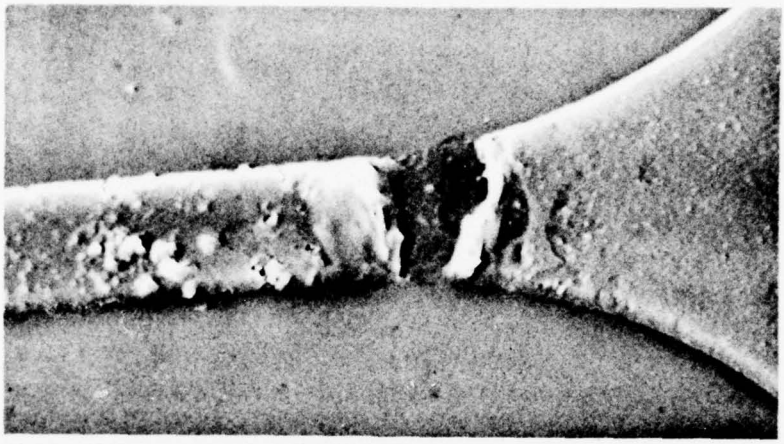

CATHODE

5μ

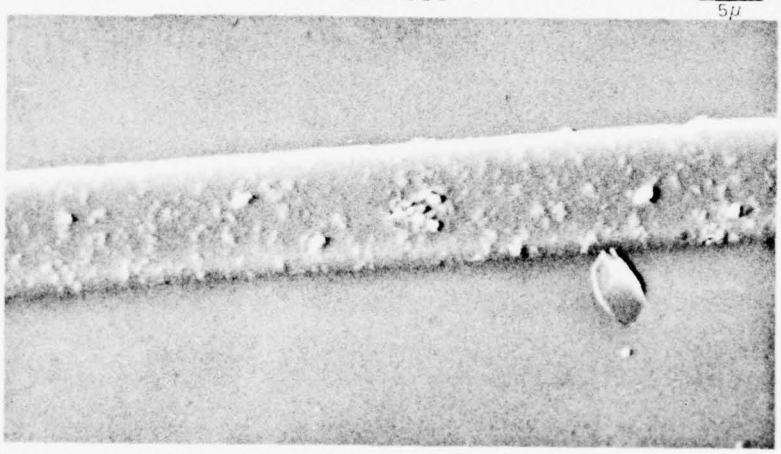

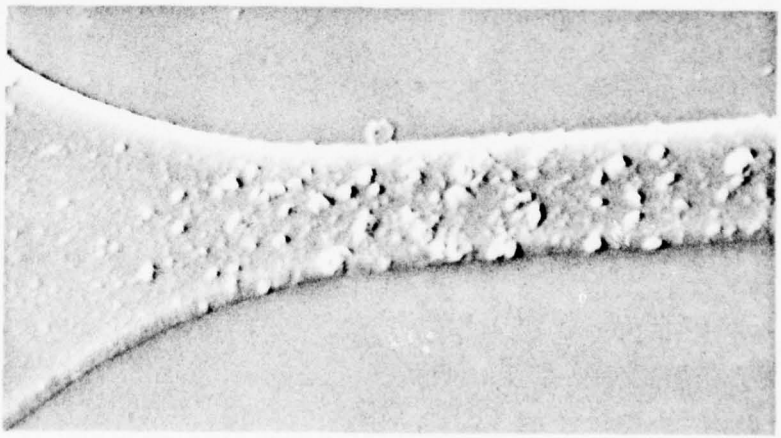

ANODE

76 03 111 4

FIG. 22–B

X–RAY LINE SCANS ACROSS ENDS

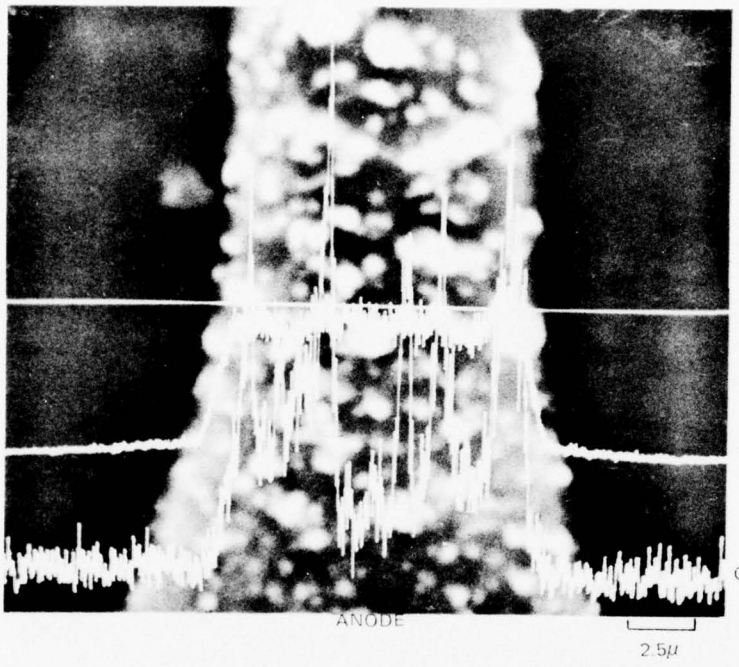

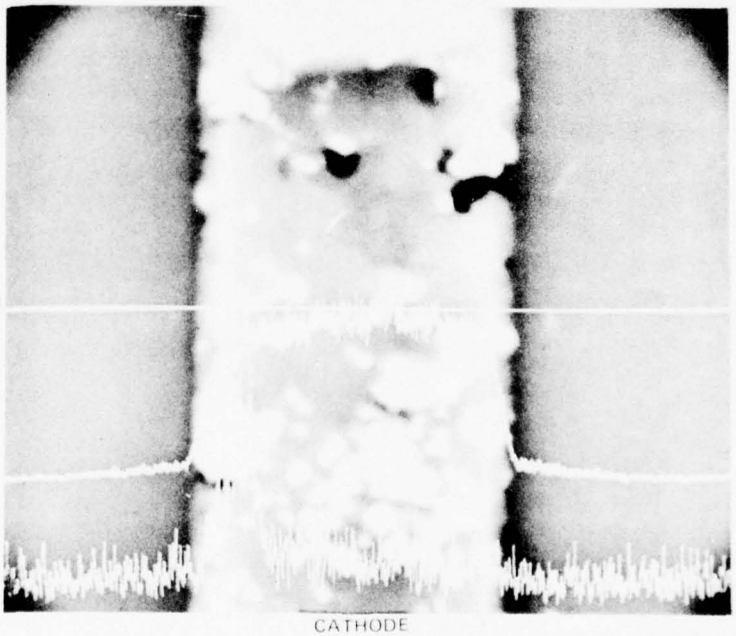

INCREASING METAL CONCENTRATION
ARB. UNITS

76 03 111 9

FIG. 22-C

LONGITUDINAL X-RAY LINE SCANS

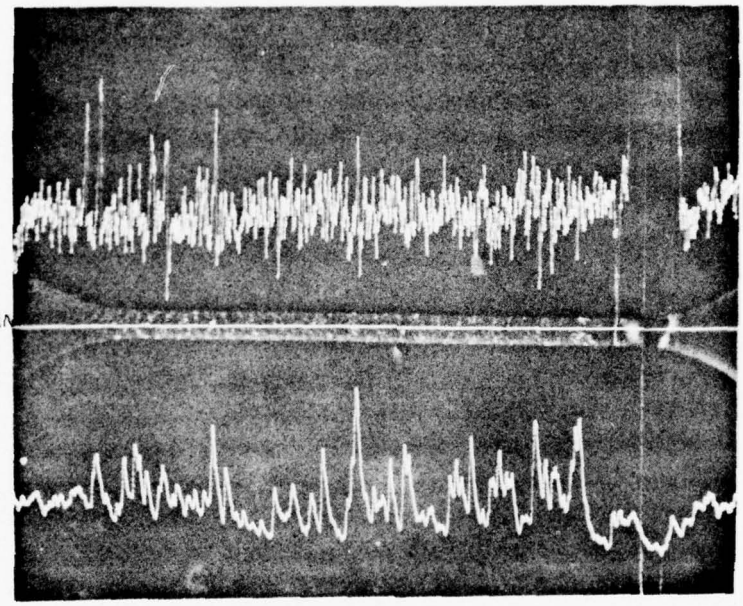

76-03-111-5

FIG. 23-A

FAILED TEST BAR 8 WT PERCENT COPPER

105 HRS, 250°C, 3×10^6 amps/cm^2

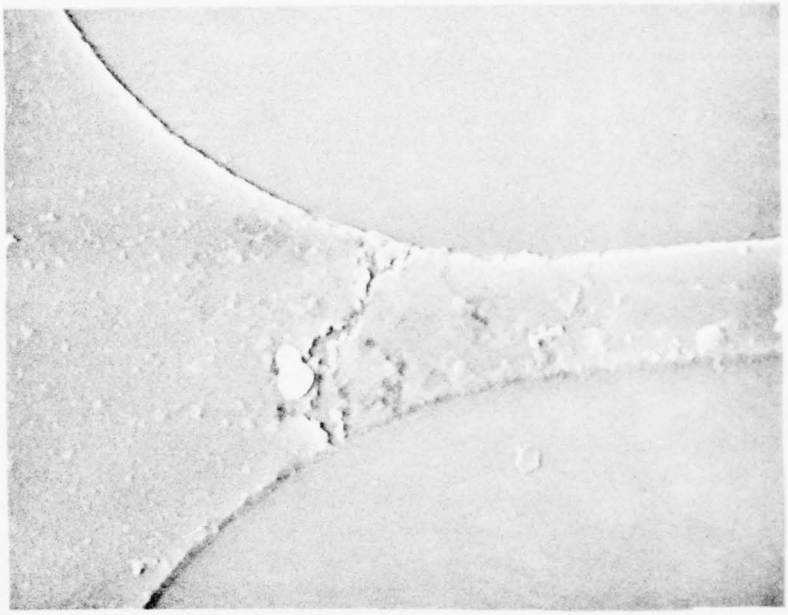

5μ

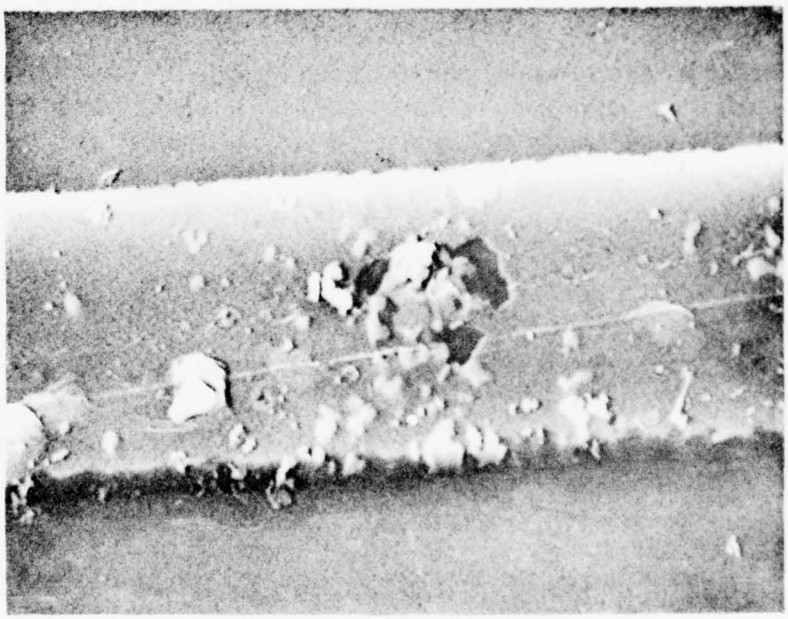

2μ

CATHODE DISTRIBUTION BY MICROPROBE

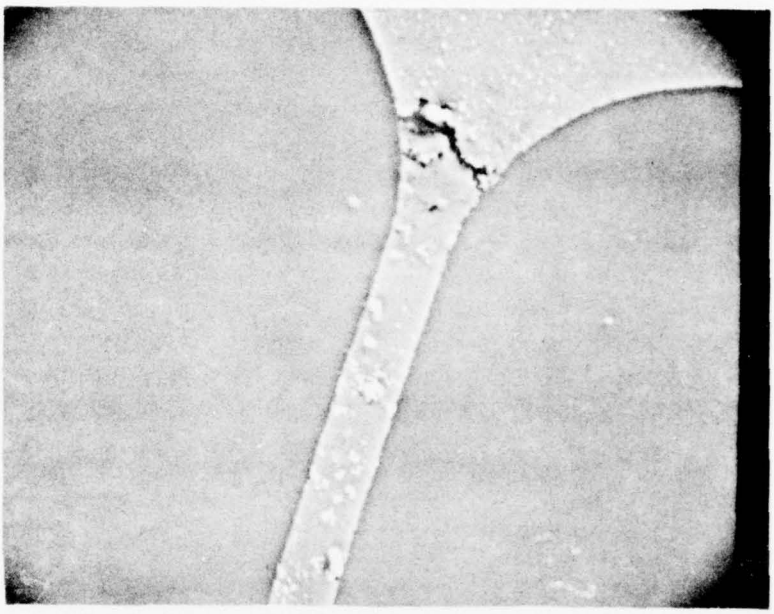

(1) BACKSCATTER MODE (ATONIC NUMBER CONTRAST) 12.5μ

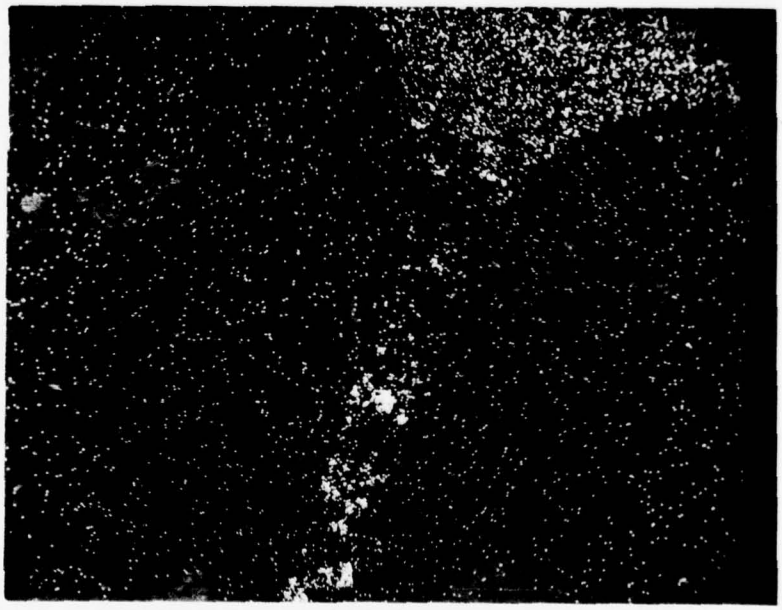

(2) X-RAY (COPPER) SCAN 12.5μ

76-03-21-2

CATHODE DISTRIBUTION BY MICROPROBE

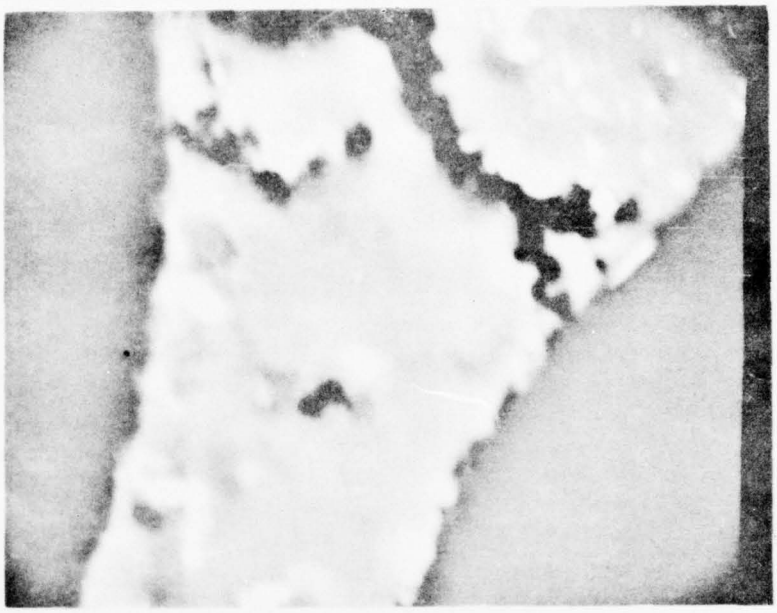

(1) BACKSCATTER MODE (ATOMIC NUMBER CONTRAST) 4μ

(2) X - RAY (COPPER) SCAN 4μ

76 03 21 1

FIG. 24–A

STRESSED BAR 8 WT PERCENT COPPER

300 MIN, 250°C, 6×10^6 AMPS/CM^2

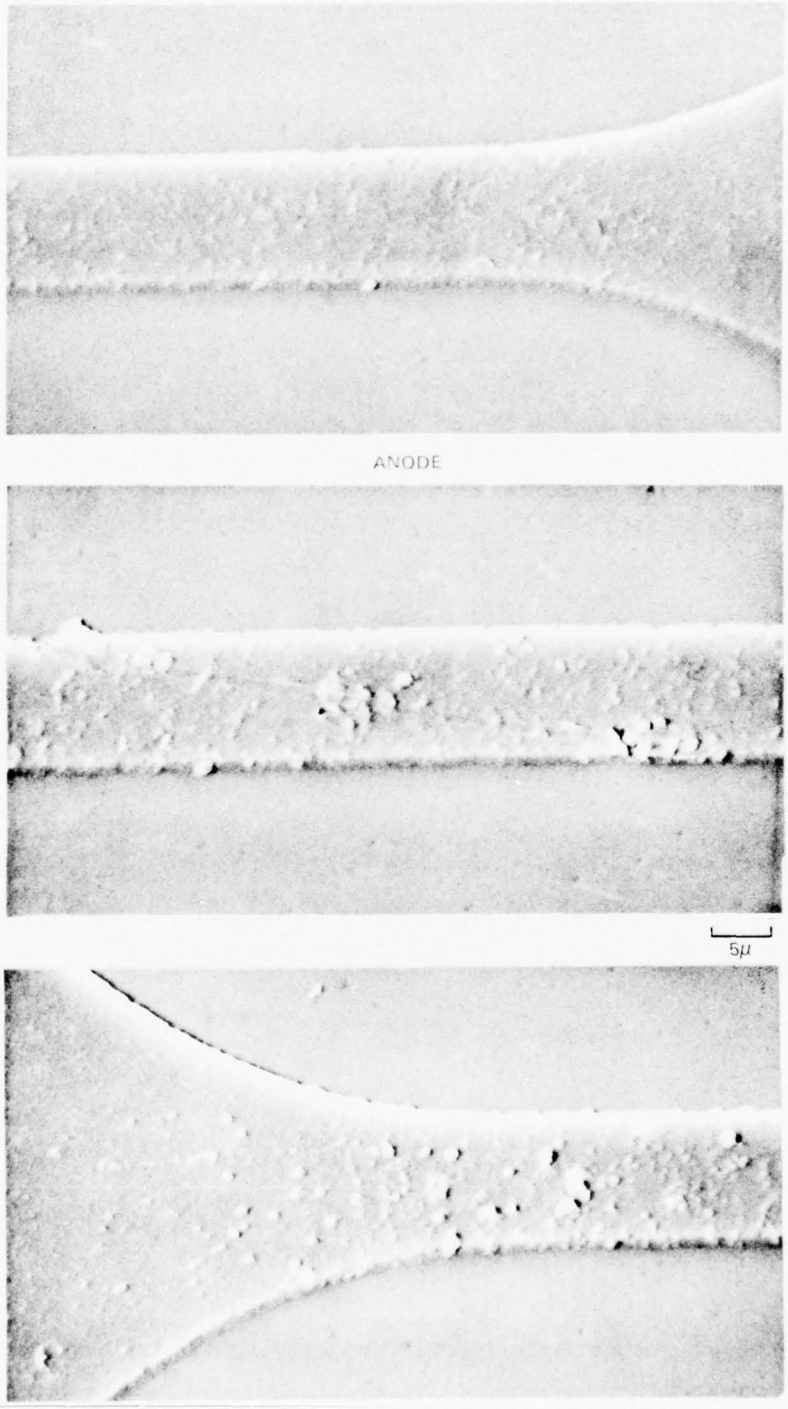

FIG. 24–B

X–RAY LINE SCANS ACROSS ENDS

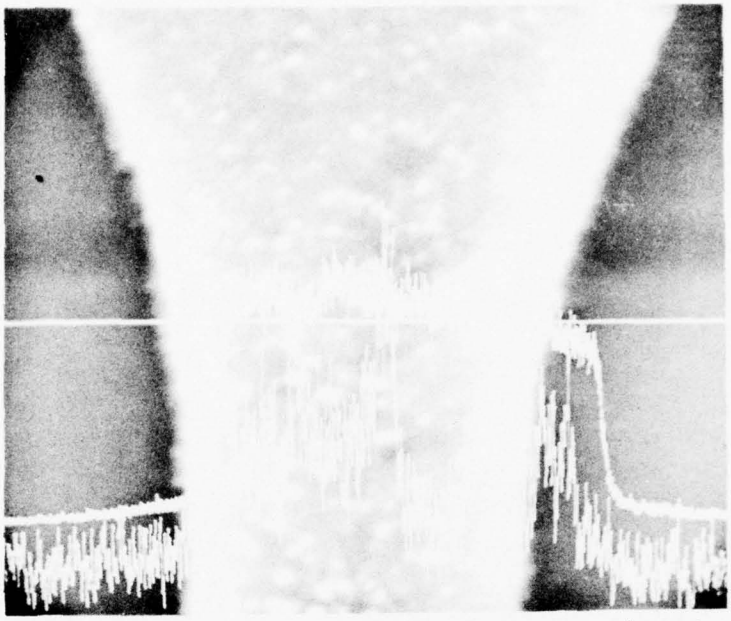

INCREASING METAL CONCENTRATION
ARB. UNITS

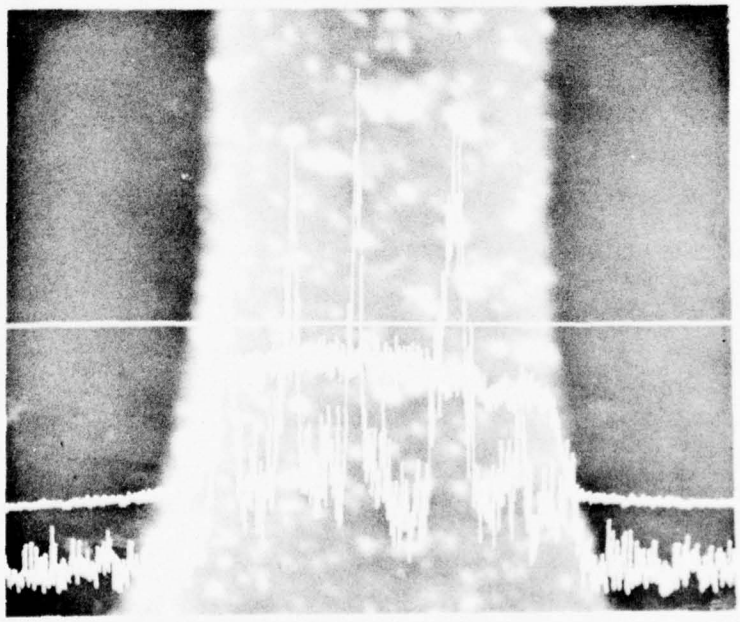

76-03-111-1

FIG. 24-C

LONGITUDINAL X-RAY LINE SCANS

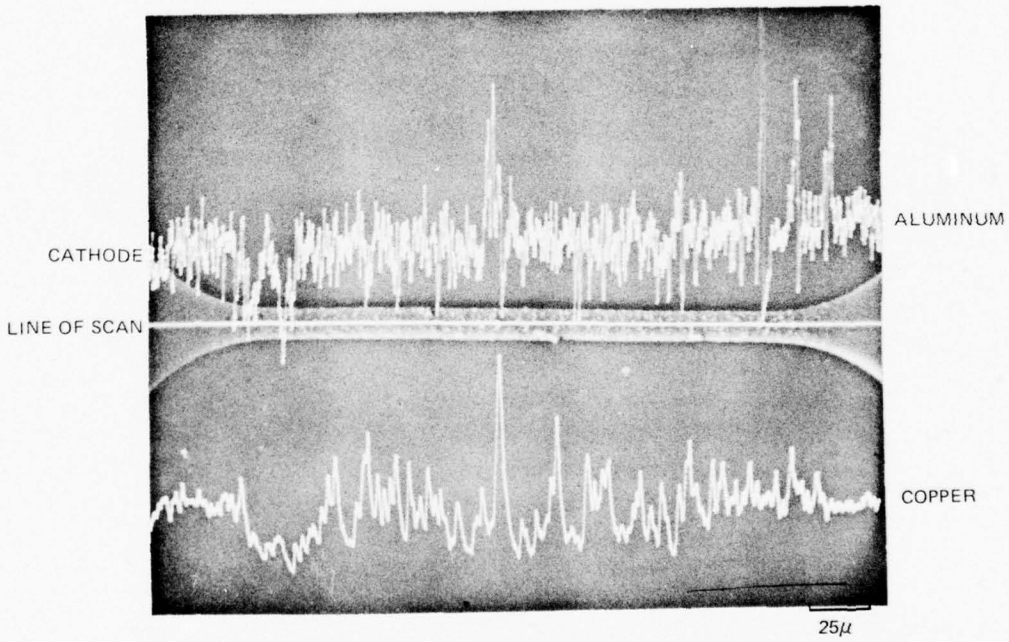

FIG. 25–A

CATHODE DISTRIBUTION BY MICROPROBE

(1) BACKSCATTER MODE (ATOMIC NUMBER CONTRAST) 4μ

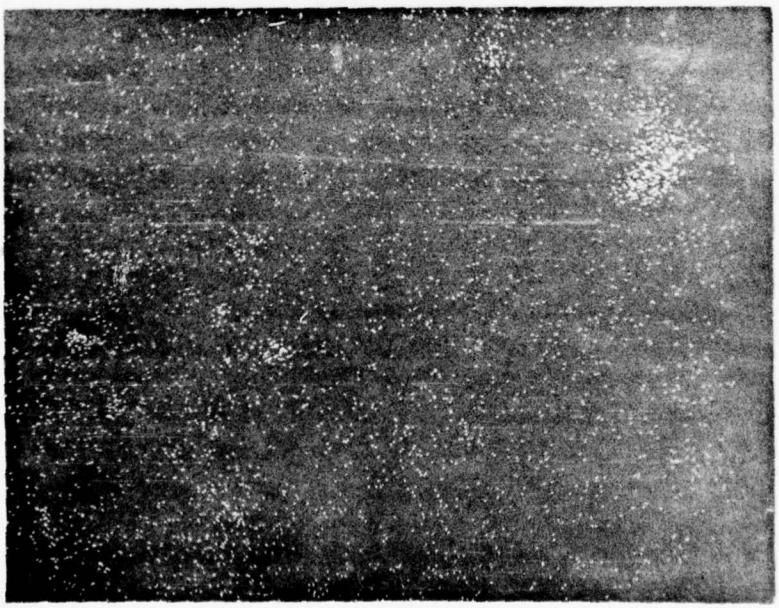

(2) X–RAY (COPPER) SCAN

76–03–21–7

FIG. 25-B

FAILED TEST BAR 8 WT PERCENT COPPER

28 HRS, 250°C, 3×10^6 amps/cm^2

CATHODE

ANODE

FIG. 25–C

ANODE DISTRIBUTION BY MICROPROBE

(1) BACKSCATTER MODE (ATOMIC NUMBER CONTRAST) 4μ

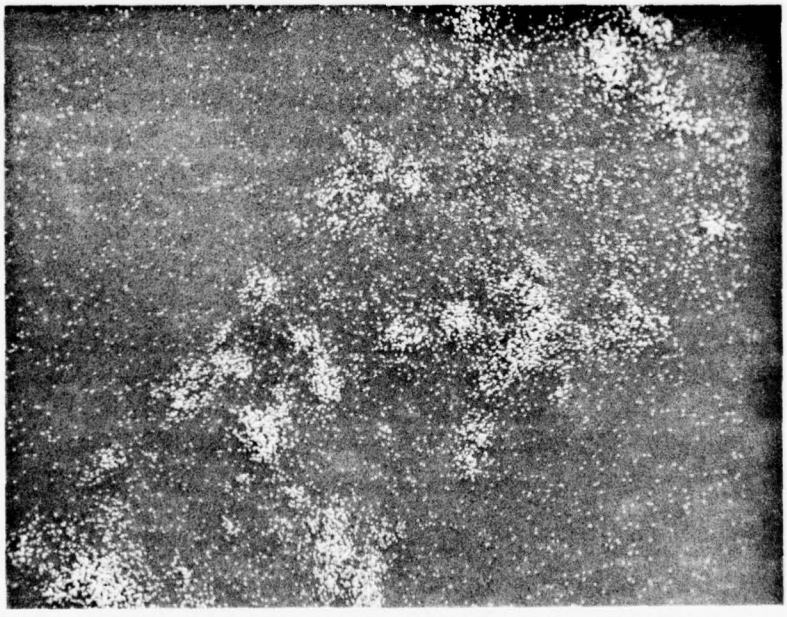

(2) X–RAY (COPPER) SCAN 4μ

76-03-21-3

FIG. 25-D

SUPERPOSITION OF BACKSCATTER MODE AND X-RAY (COPPER) LINE SCAN

NOTE POSITION OF LINE SCAN OF FIG. A&B

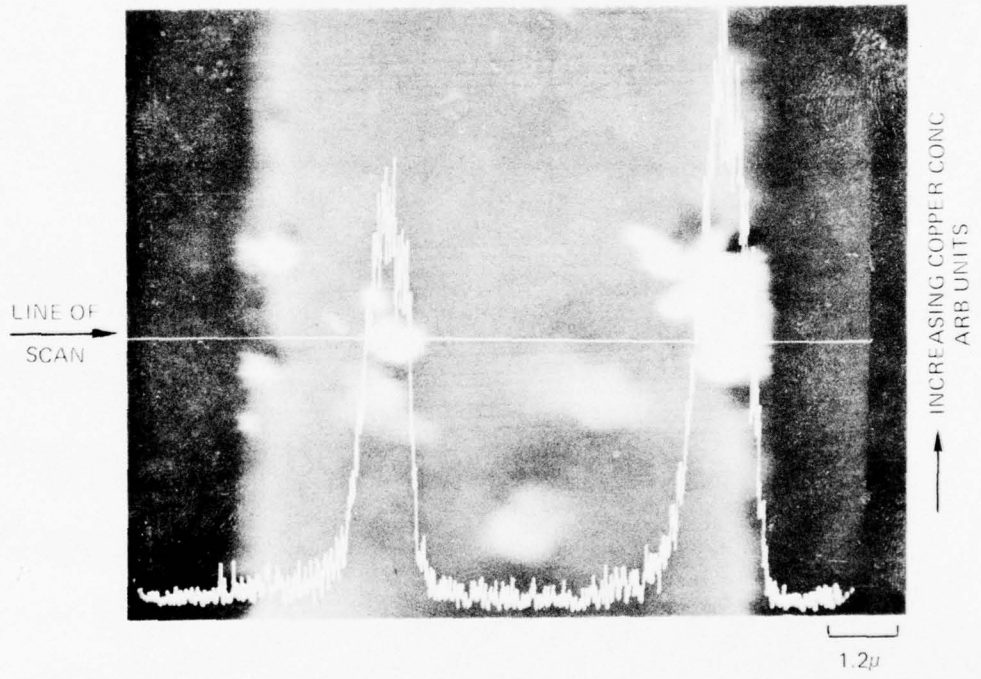

76-03-21-11

FIG. 26-A

TEST BAR 8 WT PERCENT COPPER

TEMPERATURE STRESS ONLY

T = 250°C, 350 HRS

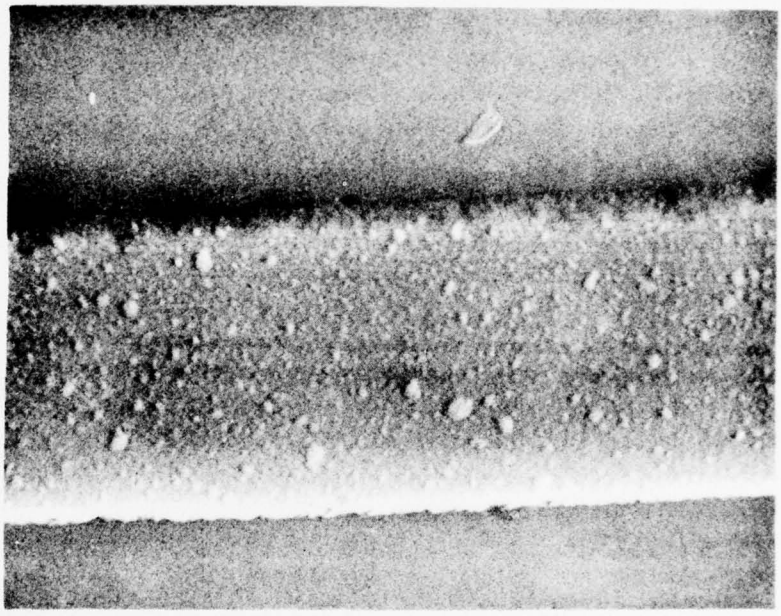

4 μ

76-03-21-13

FIG. 26–B

DISTRIBUTION BY MICROPROBE

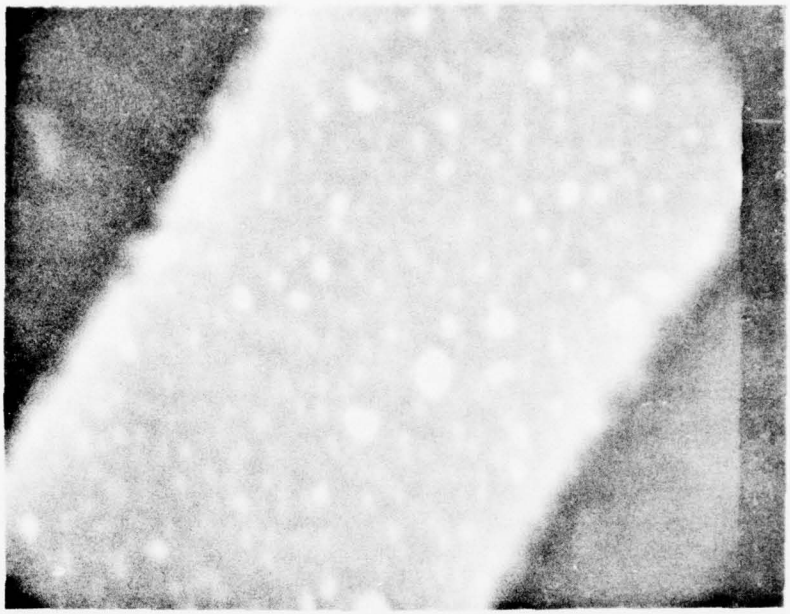

(1) BACKSCATTER MODE (ATOMIC NUMBER CONTRAST) 3 μ

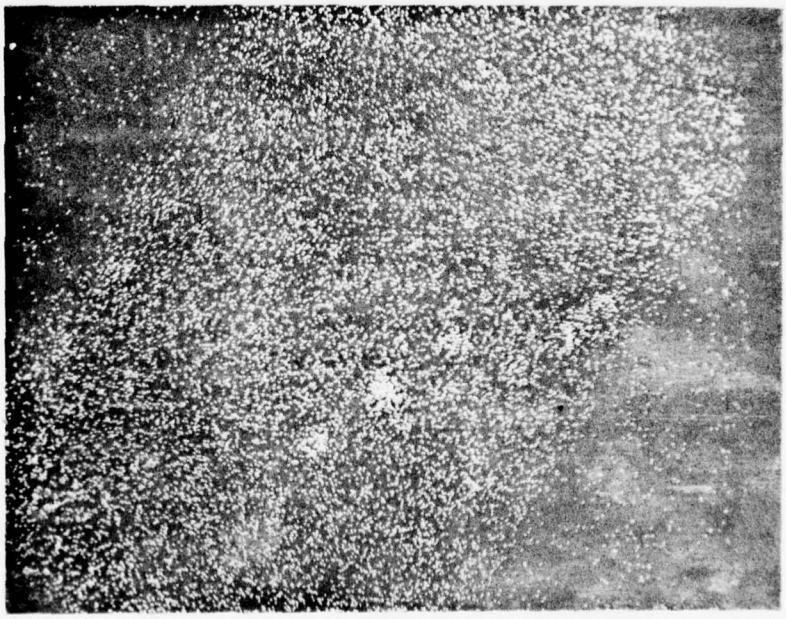

(2) X–RAY (COPPER) SCAN 3 μ

76–03–21–12

FIG. 27-A

FAILED TEST BAR – EIGHT PERCENT COPPER

266 HRS, 200°C, 3×10^6 amps/cm^2

CATHODE 2μ

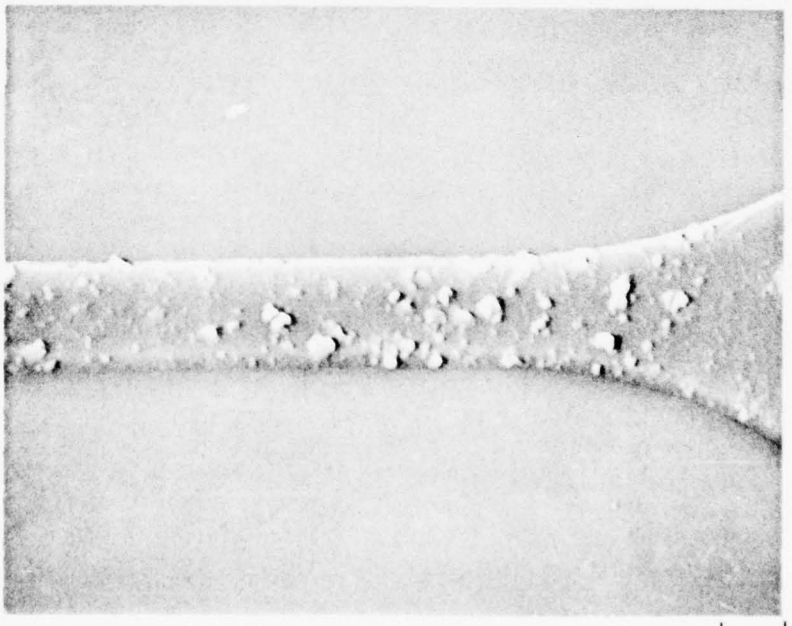

ANODE 5μ

76-03-33-10

FIG. 27-B

ANODE DISTRIBUTION BY MICROPROBE

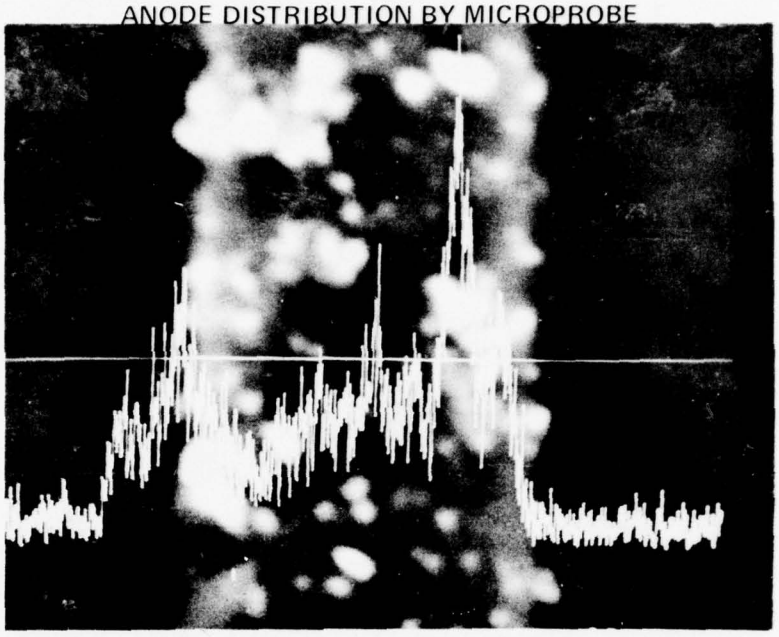

2μ

(1) BACKSCATTER PLUS X-RAY (COPPER) LINE SCAN

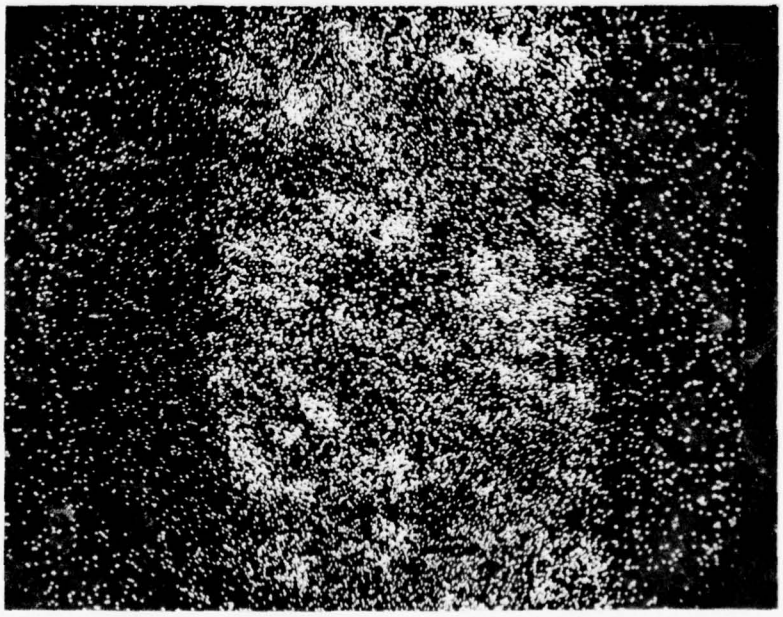

2μ

(2) X-RAY (COPPER) SCAN

76-03-33-11

FIG. 28–A

FAILED TEST BAR – EIGHT PERCENT COPPER

97 HRS, 200°C, 3×10^6 amps/cm^2

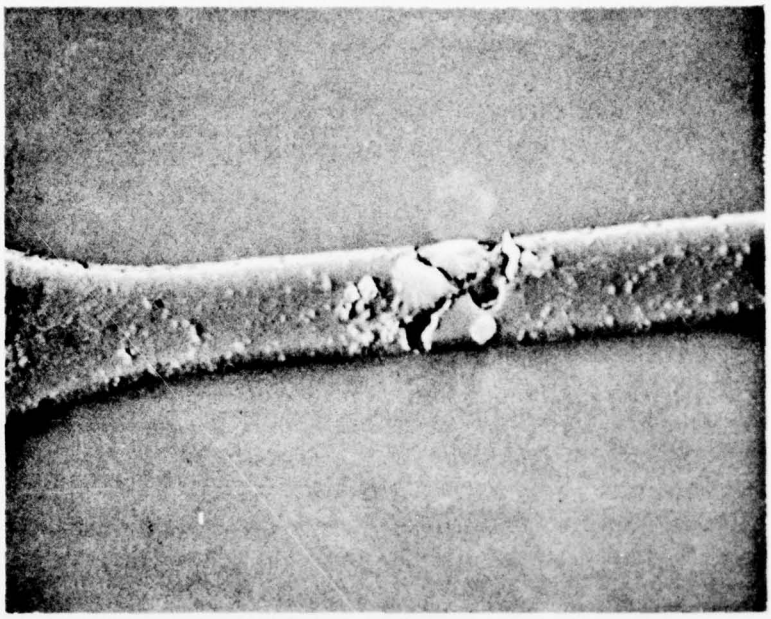

CATHODE

5μ

ANODE

2μ

76-03-33-1

FIG. 28–B

CATHODE DISTRIBUTION BY MICROPROBE

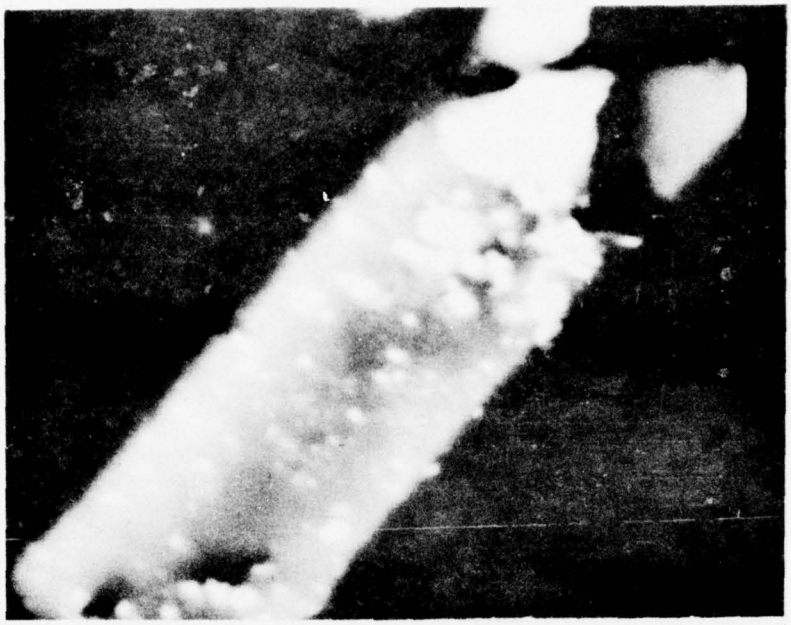

(1) BACKSCATTER (ATOMIC NUMBER CONTRAST)

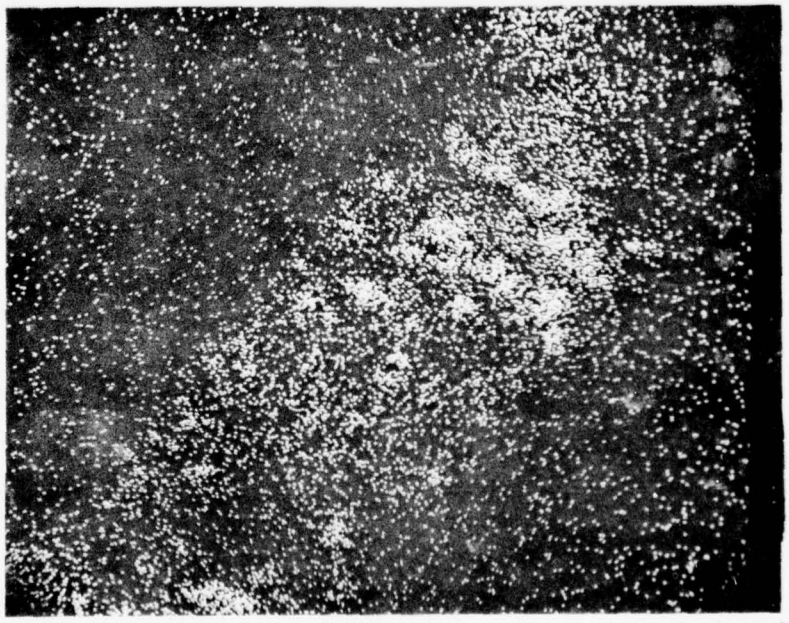

(2) X–RAY (COPPER) SCAN

76-03-33-2

FIG. 28–C

ANODE DISTRIBUTION BY MICROPROBE

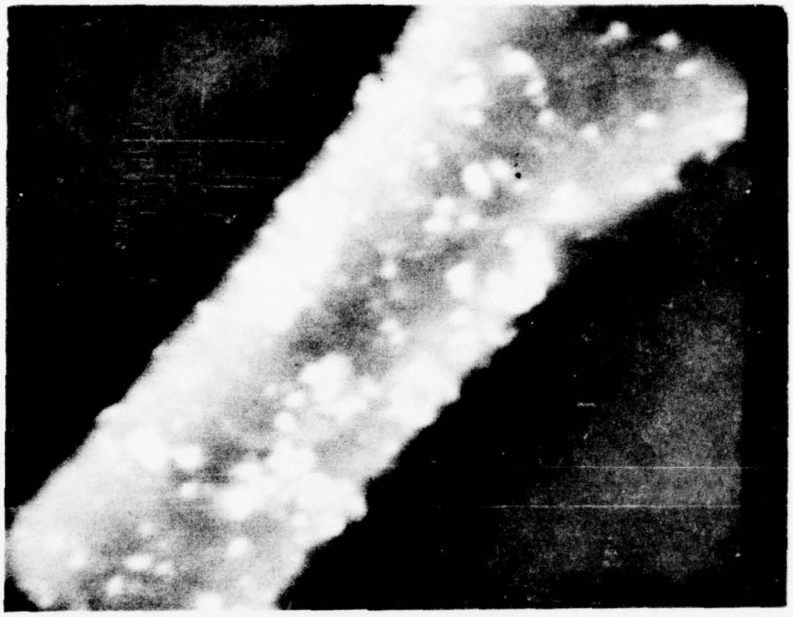

(1) BACKSCATTER (ATOMIC NUMBER CONTRAST)

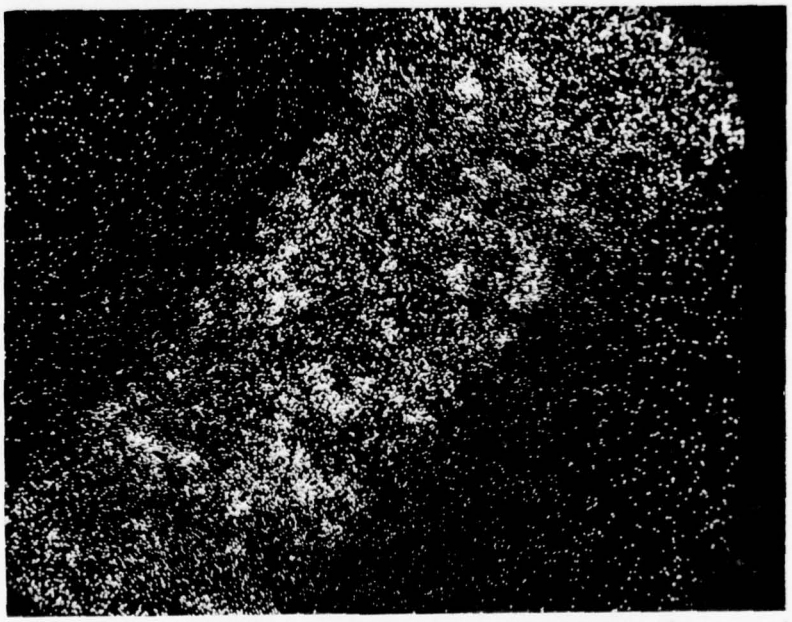

(2) X–RAY (COPPER) SCAN

76-03-33-3

FIG. 28-D

DISTRIBUTION ALONG BAR BY MICROPROBE

X-RAY (COPPER) LINE SCANS AT ENDS AND MIDDLE

Cu

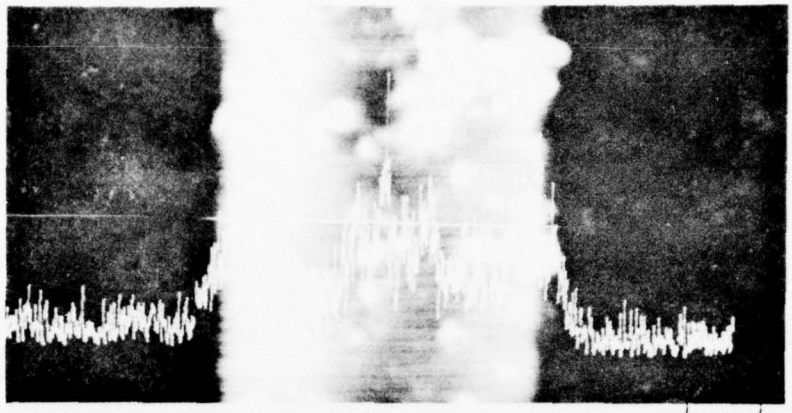

ANODE

2μ

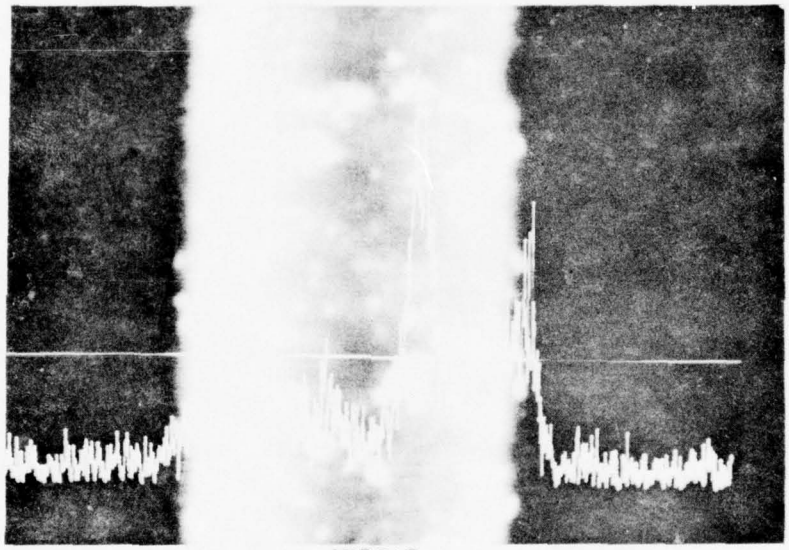

MIDDLE

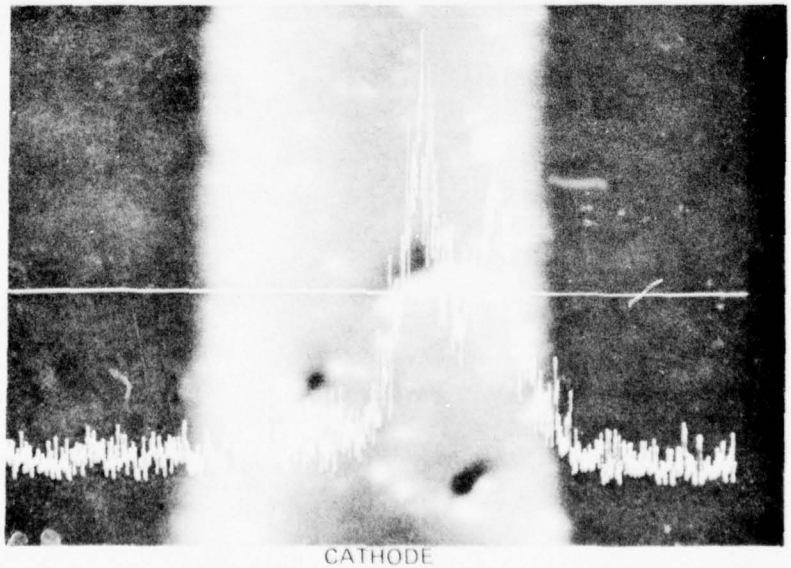

CATHODE

76-03-33-4

FIG. 29–A

DISTRIBUTION ALONG BAR BY MICROPROBE

LONGITUDINAL X–RAY LINE SCANS (Cu & Al) AT EDGES & CENTER

$J = 7 \times 10^6$ amps/cm^2 – 275° 41 hrs

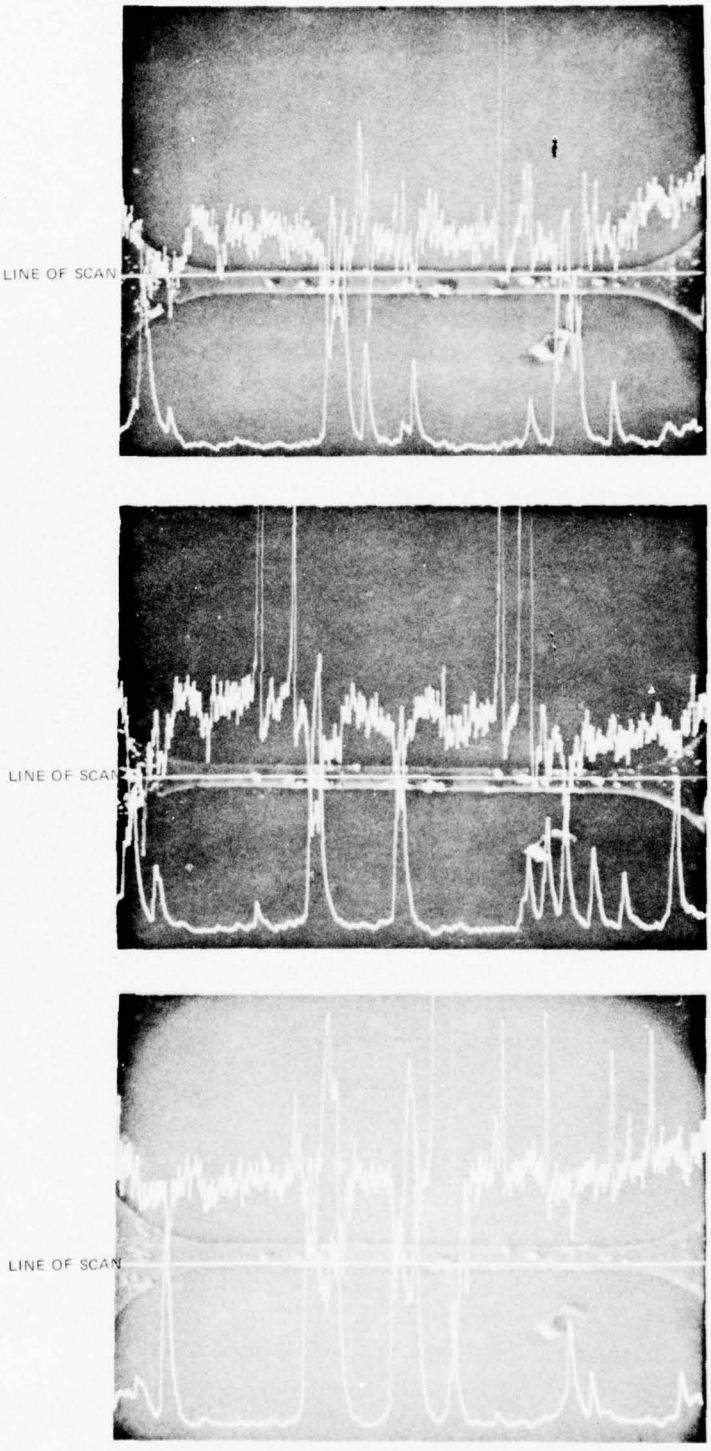

FIG. 29-B

DISTRIBUTION ALONG BAR BY MICROPROBE

TRANSVERSE X-RAY LINE SCANS (Cu & Al) AT SIX POINTS (SEE FIG-C)

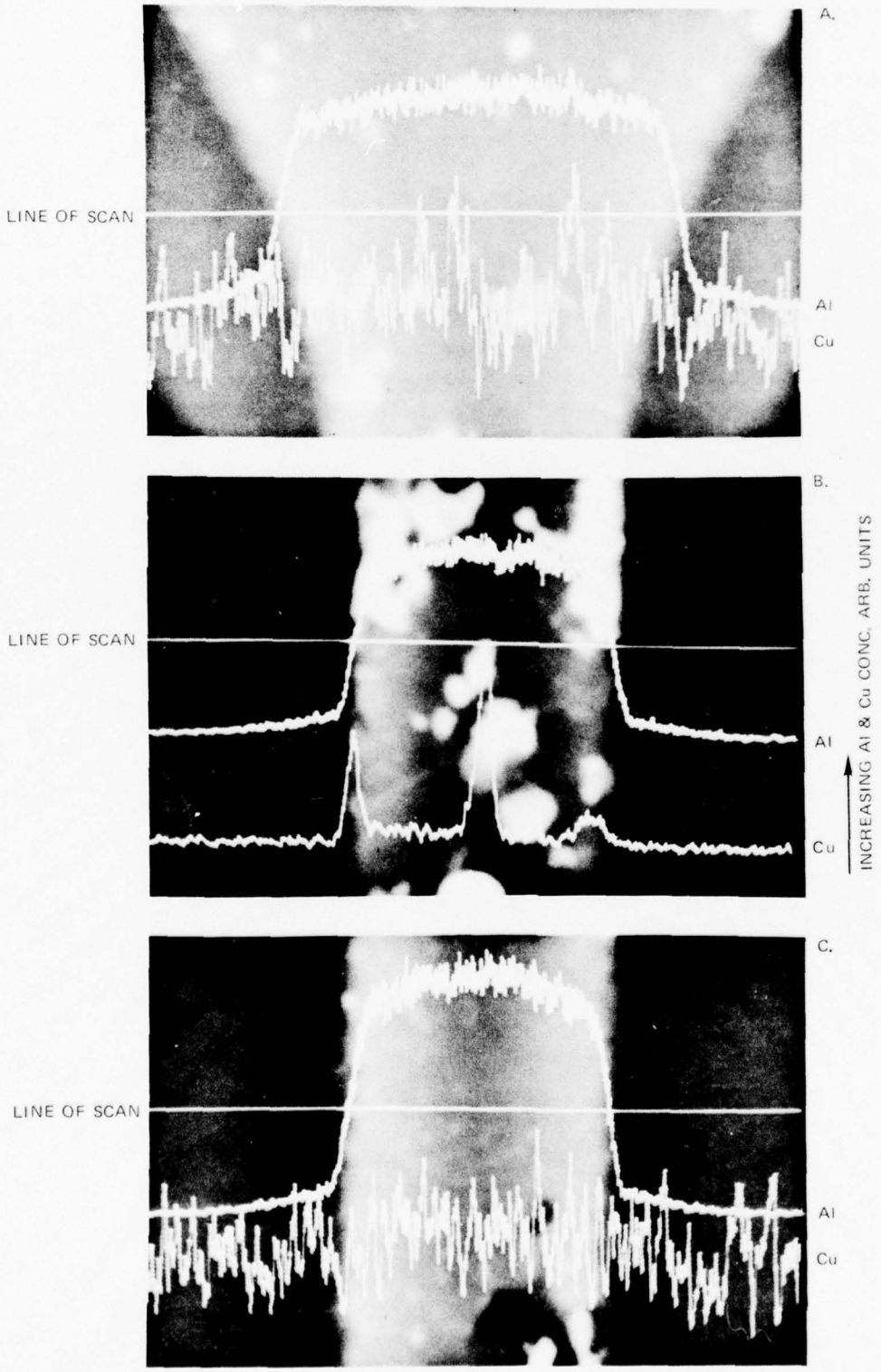

CONTINUED

FIG. 29-B(CONT'

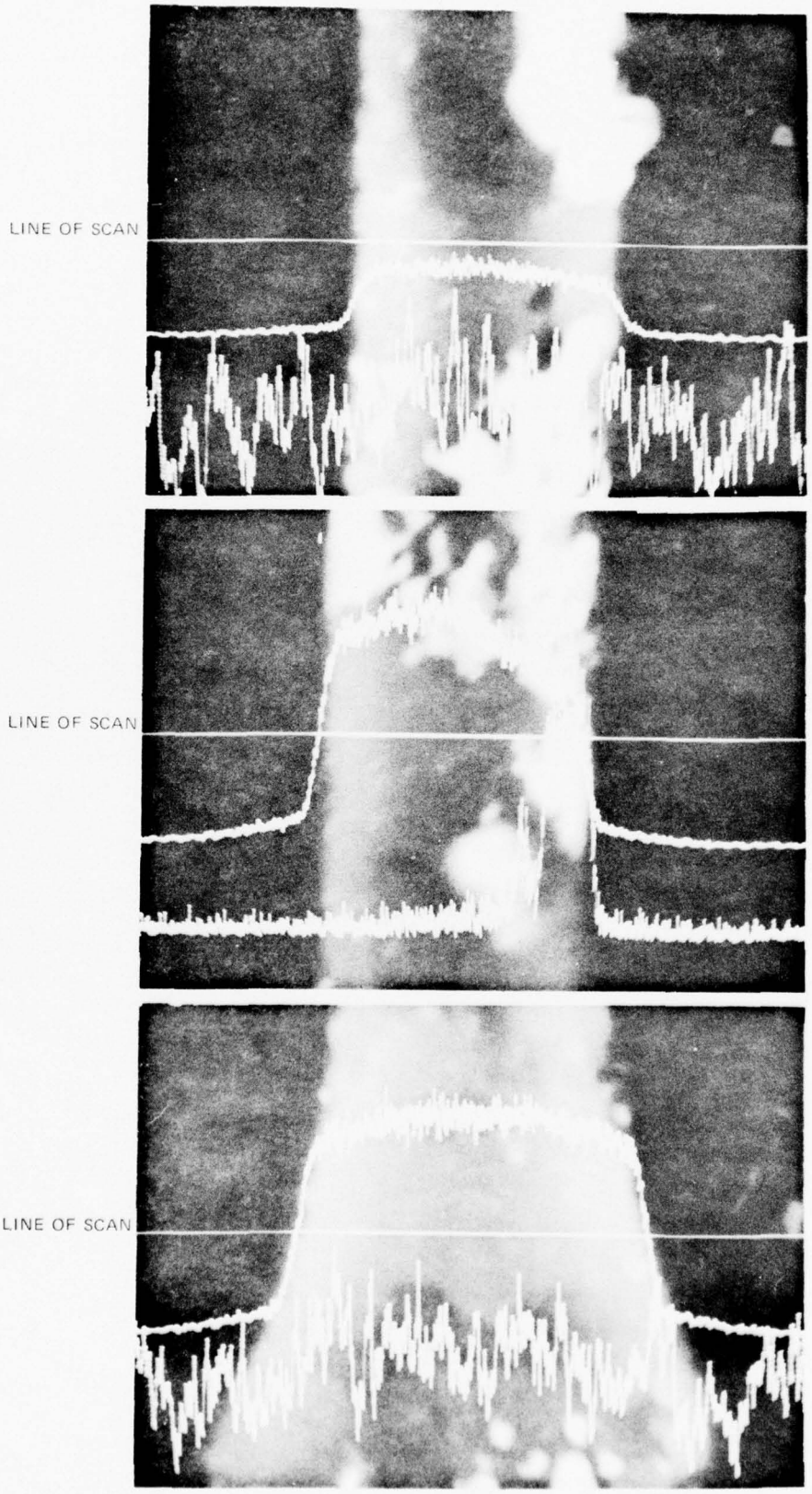

CONTINUED

LOCATION OF TRANSVERSE SCANS

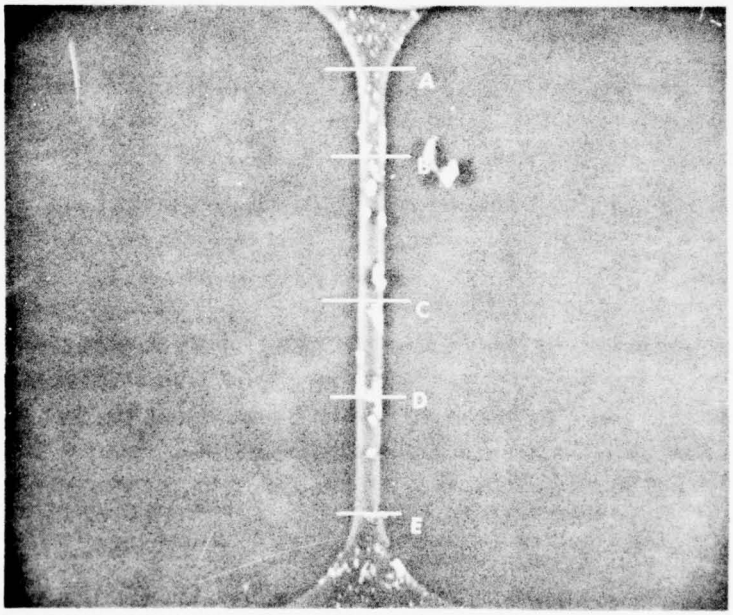

CATHODE

FIG. 29-B(CONT')

LINE SCANS ON ADJACENT BAR

J = 0 amps/cm^2 275^{o}c 436 hrs.

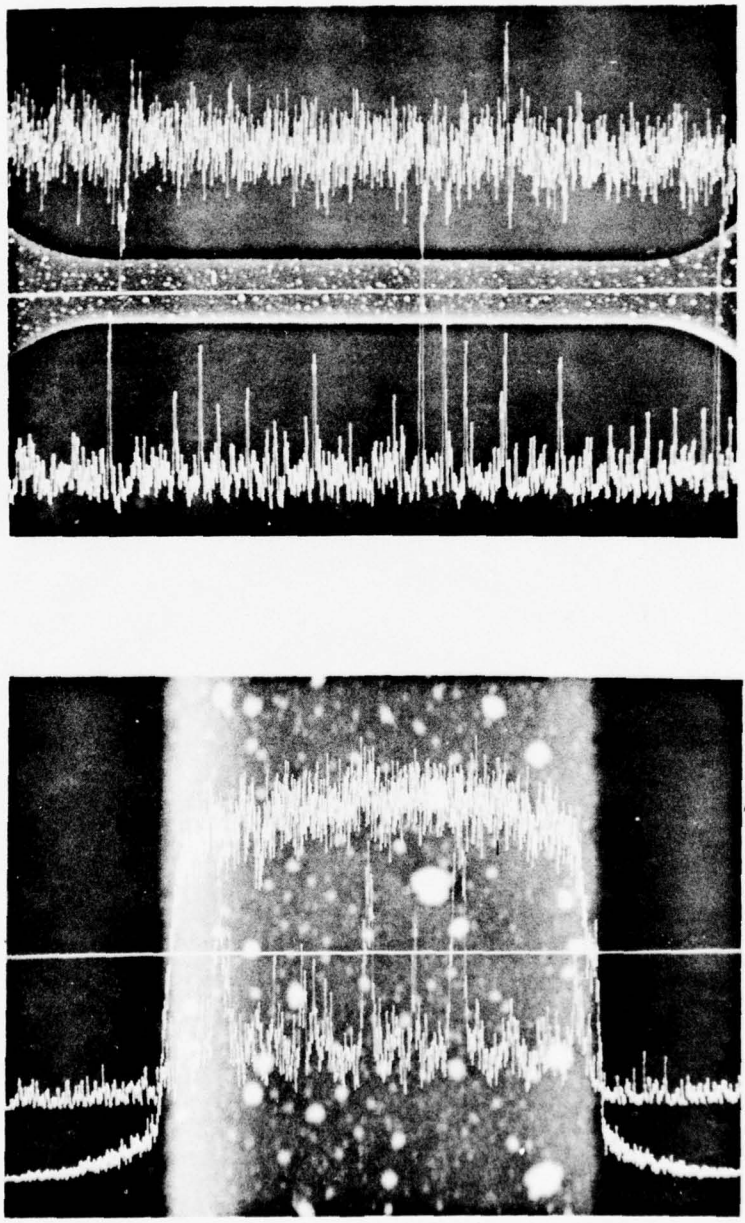

76-04-309-2

FIG. 30

UNSTRESSED TEST BAR–TWELVE PERCENT COPPER–DISTRIBUTION BY MICROPROBE

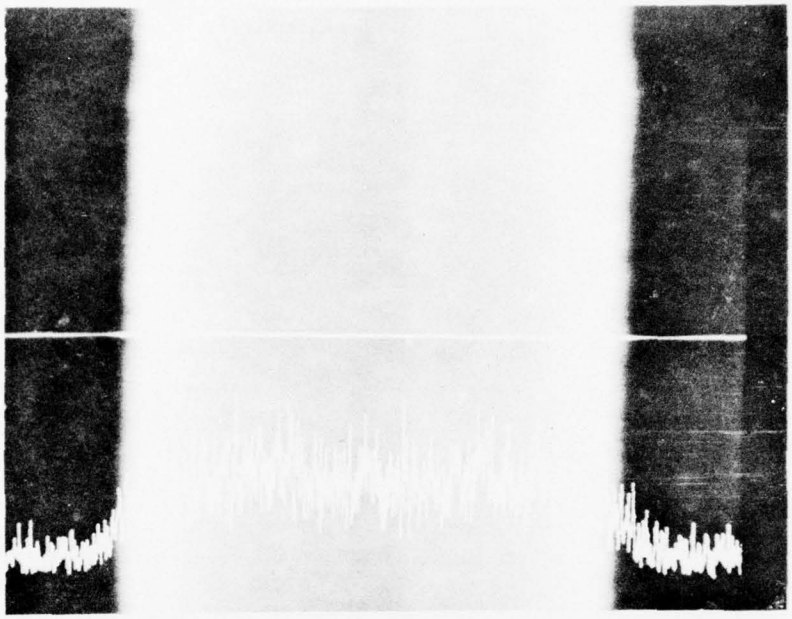

(1) BACKSCATTER PLUS X–RAY (COPPER)

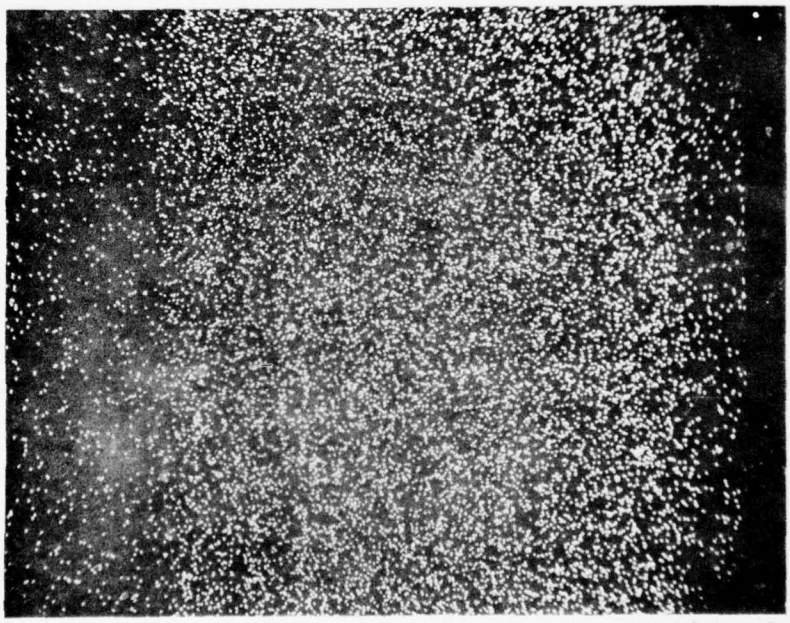

(2) X–RAY (COPPER) SCAN

76–03–33–16

FIG. 31–A

SCRATCH ENHANCED MIGRATION IN TWELVE PERCENT COPPER BAR

TIME TO FAILURE – 3 HRS, 250°, 3×10^6 amps/cm^2

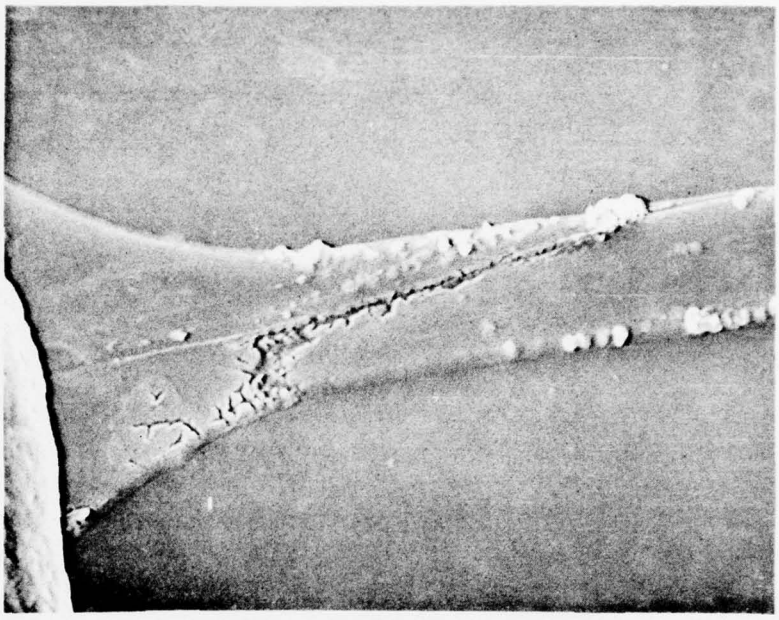

5μ

CATHODE

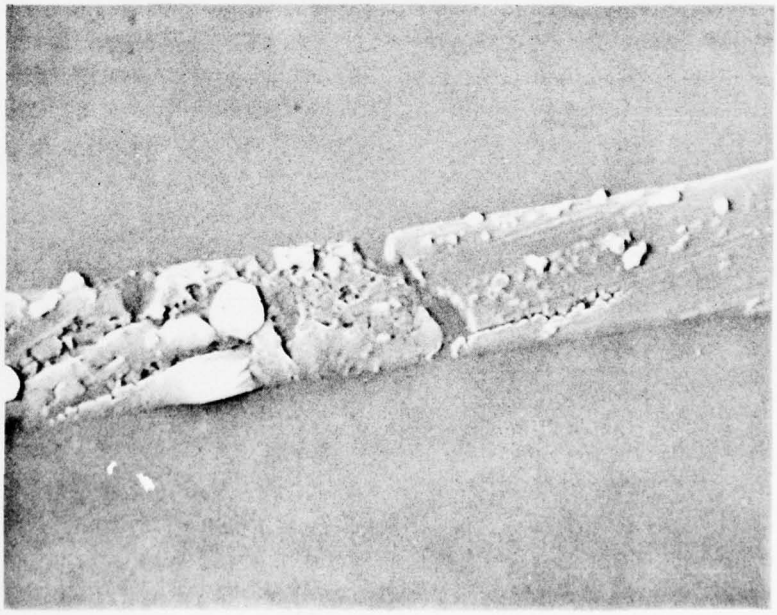

5μ

ANODE

76-03-33-12

FIG. 31-B

COPPER DISTRIBUTION BY MICROPROBE

(1) BACKSCATTER MODE (ATOMIC NUMBER CONTRAST)

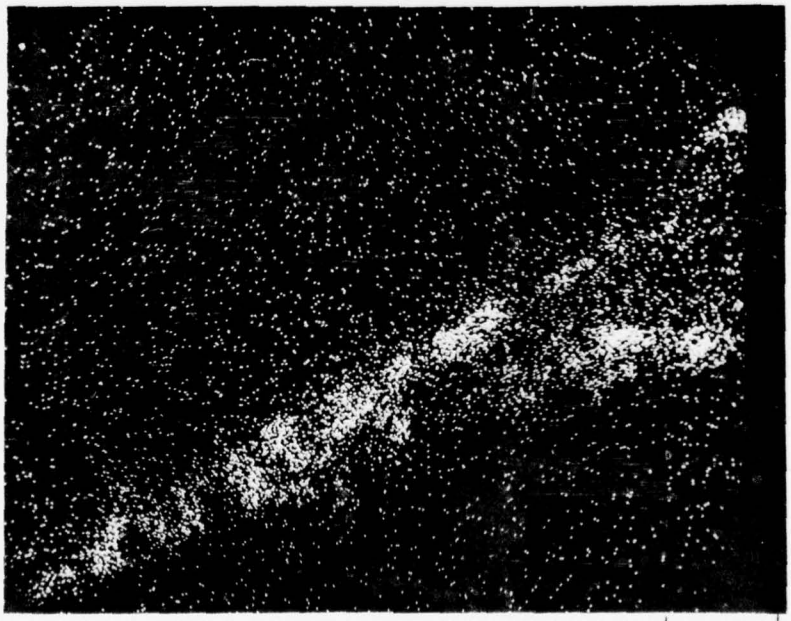

(2) X-RAY (COPPER) SCAN

76-03-33-13

FIG. 32-A

FAILED TEST BAR 12% COPPER

93 MIN, 250°C, 6×10^6 AMPS/CM^2

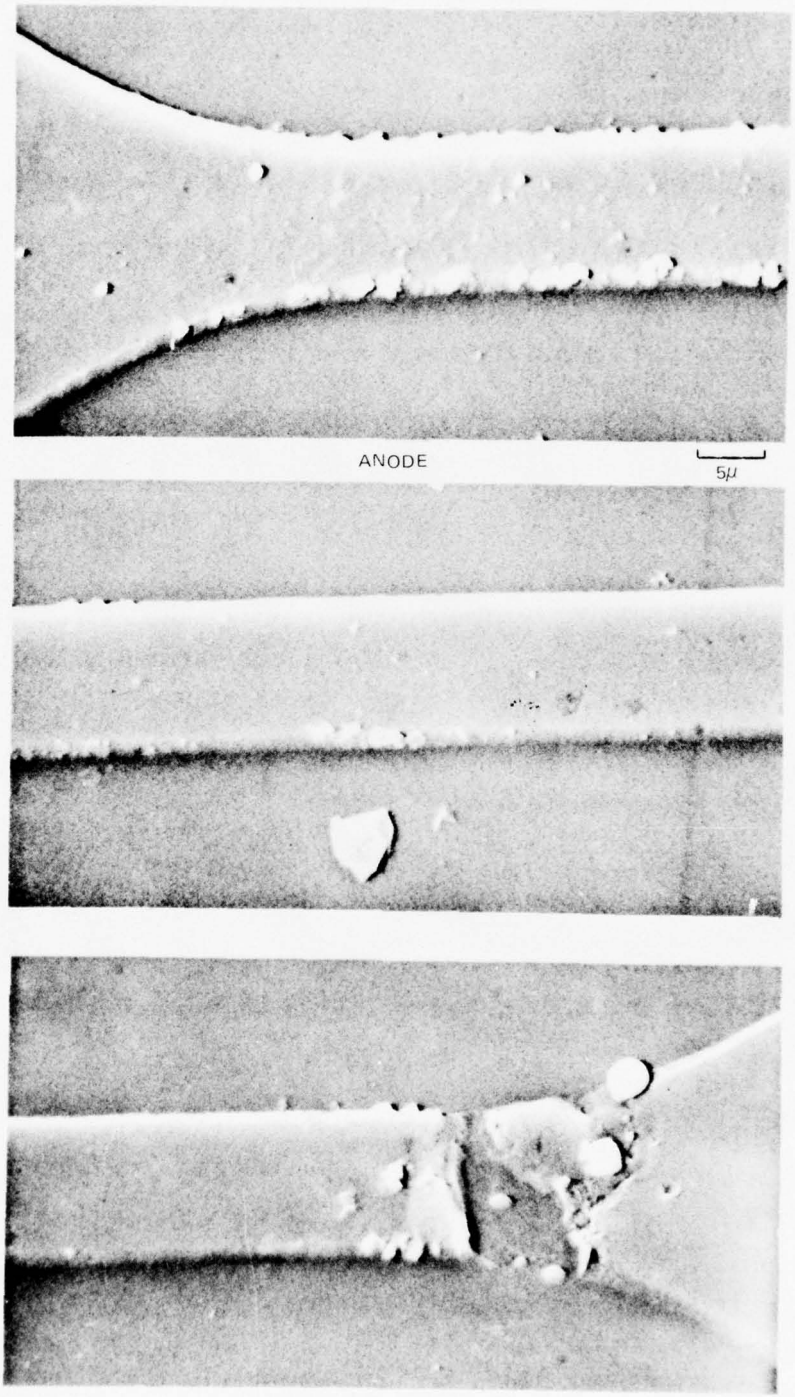

ANODE

5μ

CATHODE

FIG. 32-B

X-RAY LINE SCANS ACROSS ENDS

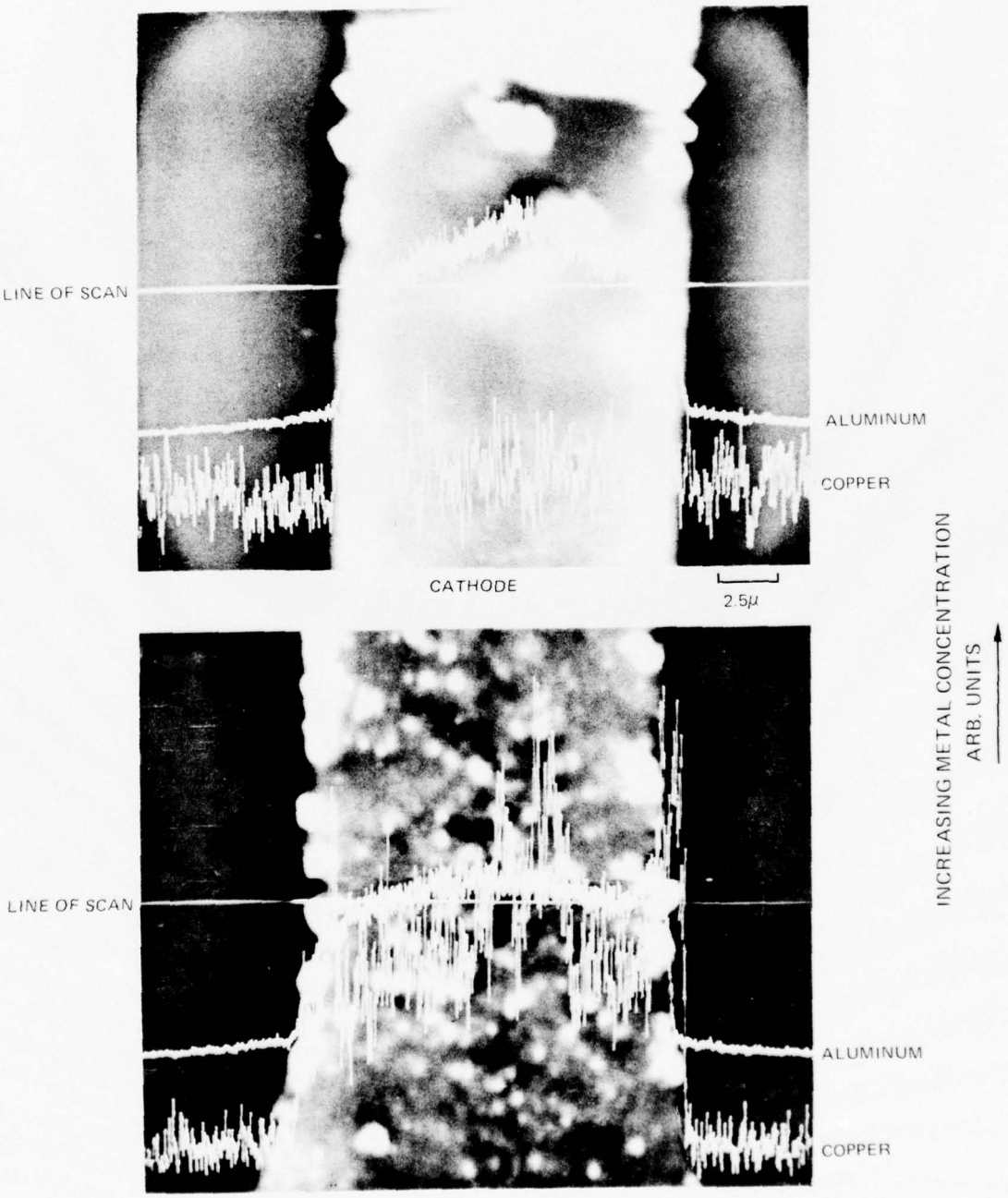

76-03-111-2

FIG. 32-C

LONGITUDINAL X-RAY SCANS

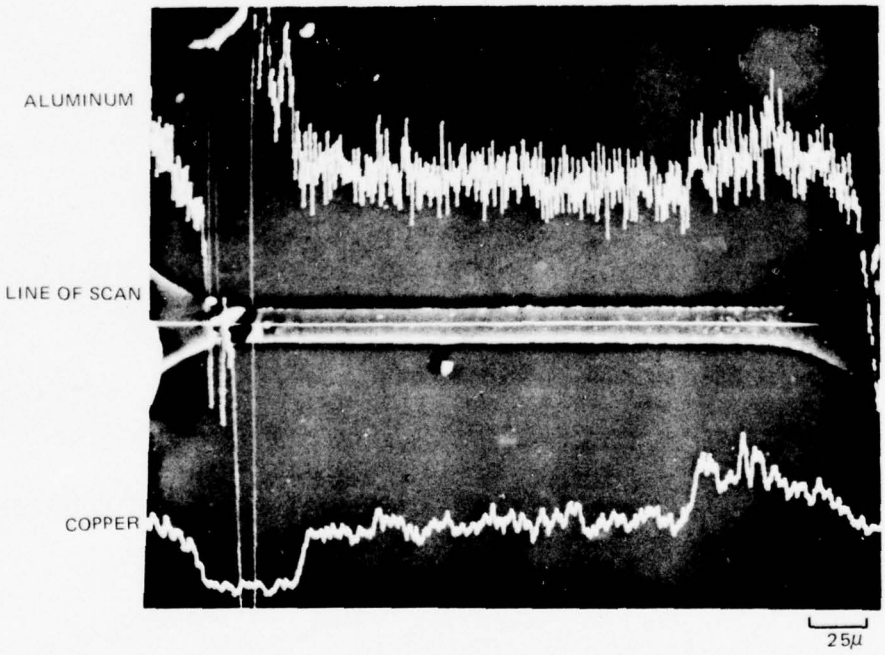

76-03-111-3

FAILED TEST BAR – TWELVE PERCENT COPPER

216 HRS, 250°C, 3×10^6 amps/cm^2

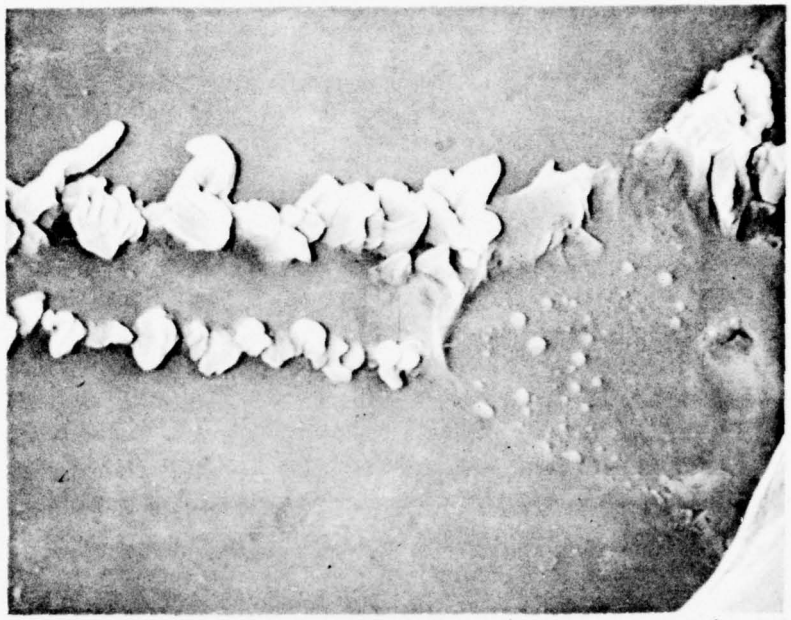

5μ

CATHODE

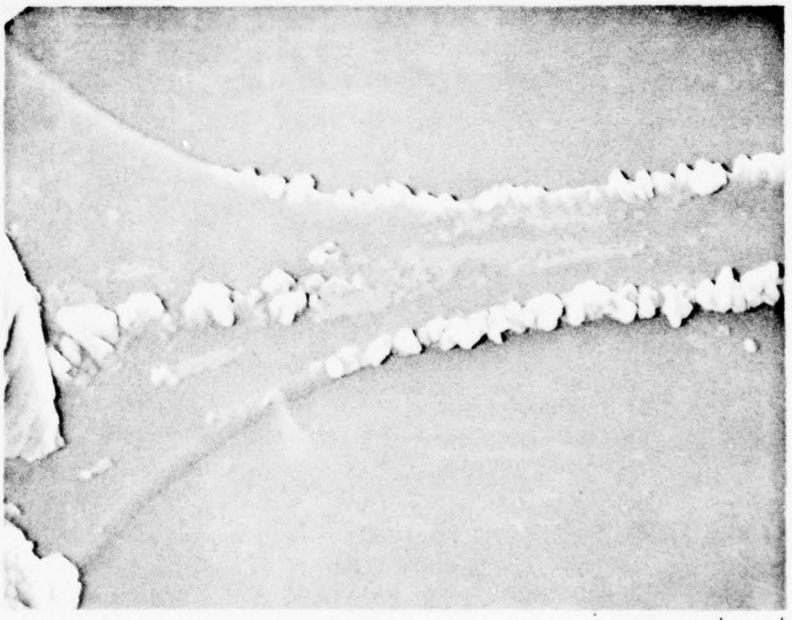

2μ

ANODE

76-03-33-5

ANODE DISTRIBUTION BY MICROPROBE

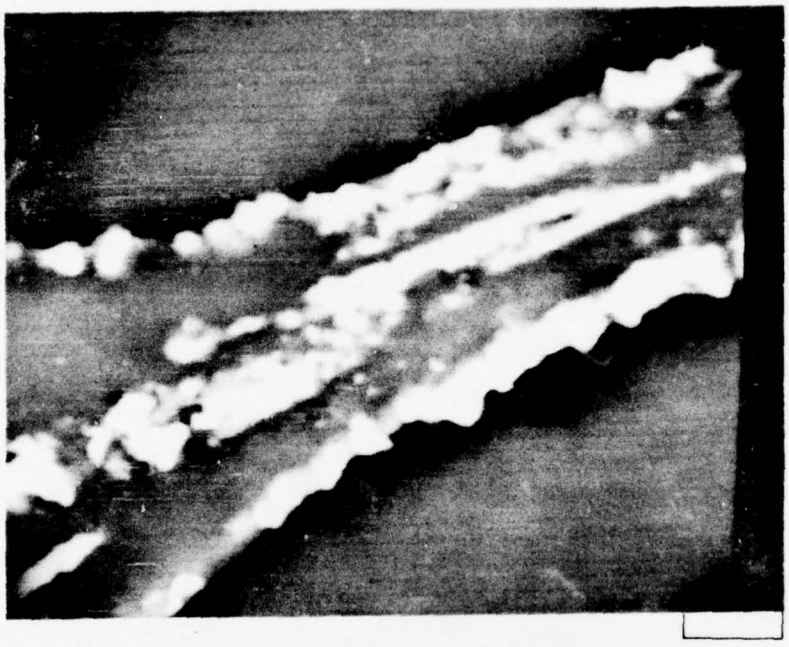

(1) BACKSCATTER (ATOMIC NUMBER CONTRAST)

(2) X-RAY (COPPER) SCAN

76-03-33-6

DISTRIBUTION BY MICROPROBE IN CENTER OF BAR

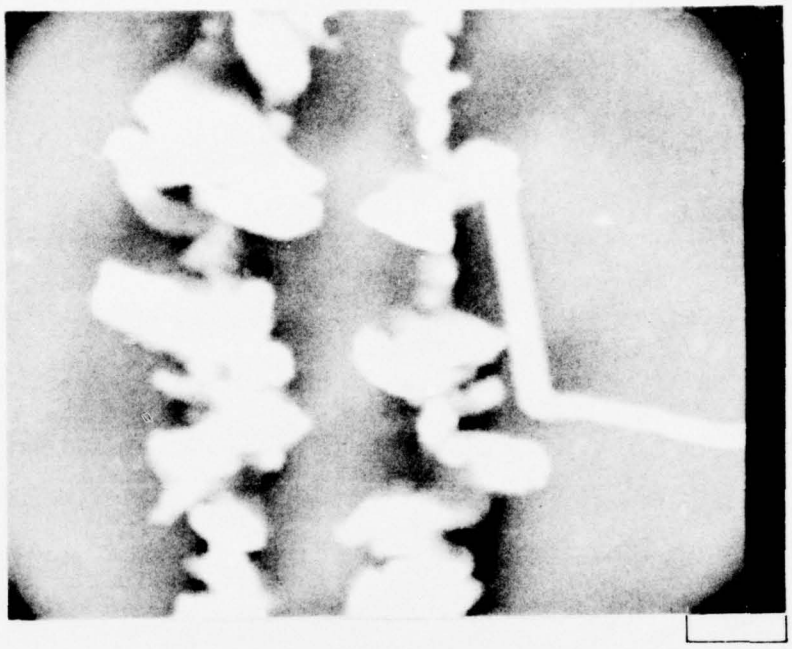

(1) BACKSCATTER (ATOMIC NUMBER CONTRAST)

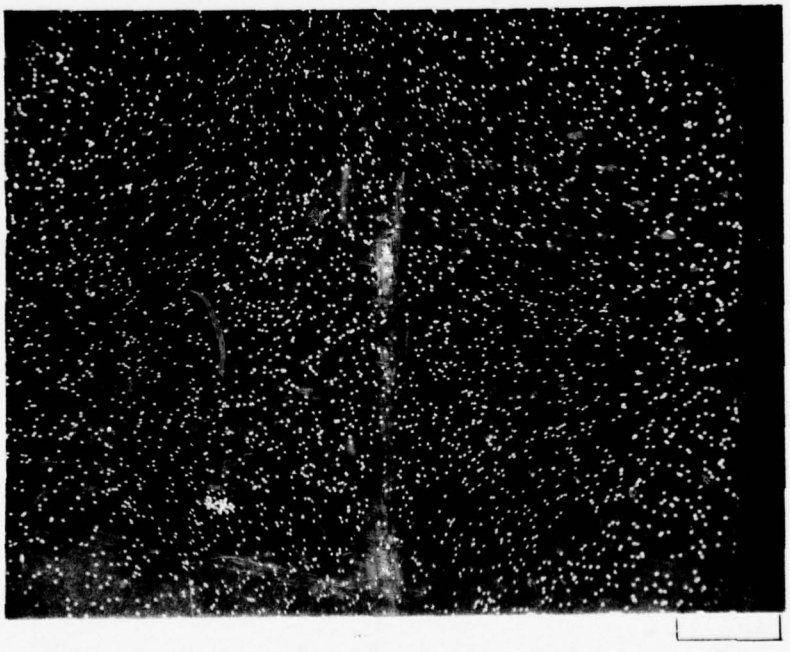

(2) X-RAY (COPPER) SCAN

76-03-33-7

FIG. 33–D

MIDDLE OF BAR

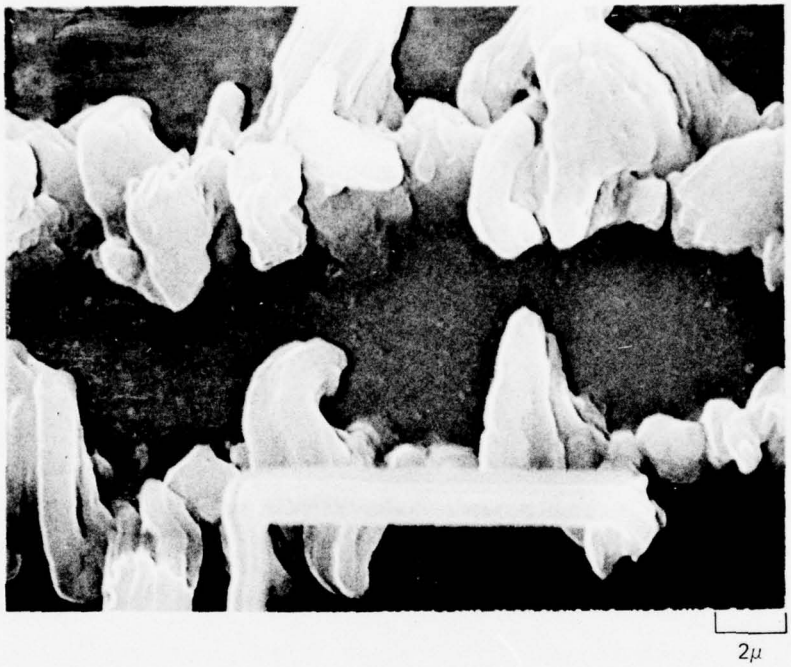

(1) TOPOGRAPHY

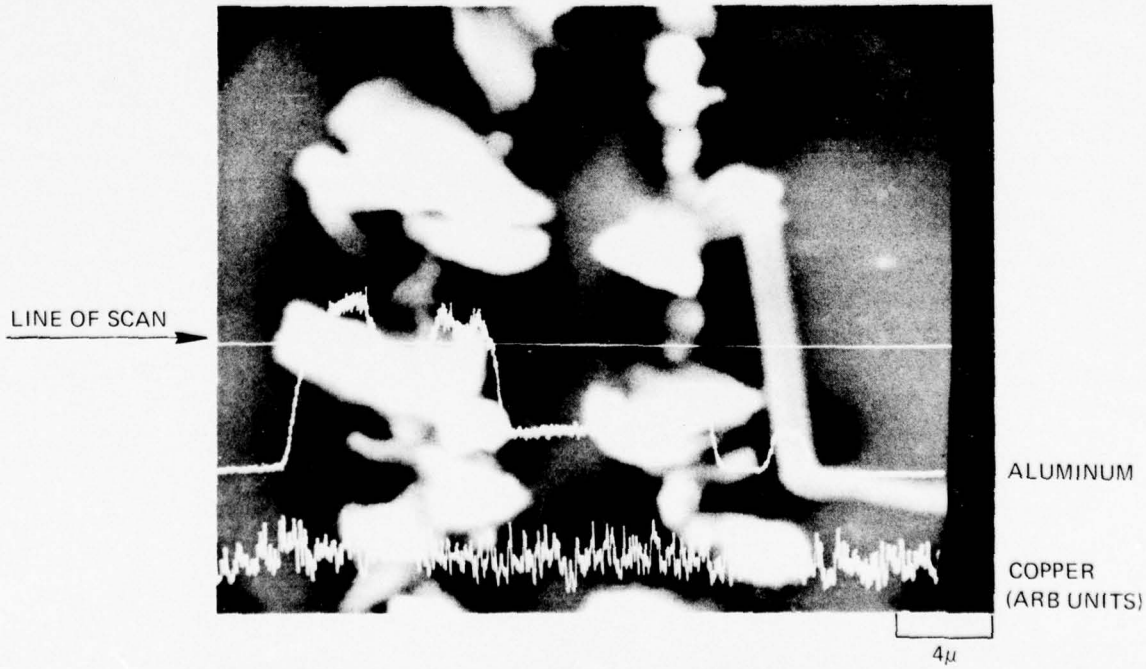

(2) BACKSCATTER PLUS X–RAY (ALUMINUM AND COPPER) LINE SCANS

76–03–33–8

DISTRIBUTION BY MICROPROBE IN ADJACENT BAR

SAME PACKAGE – NO CURRENT STRESS

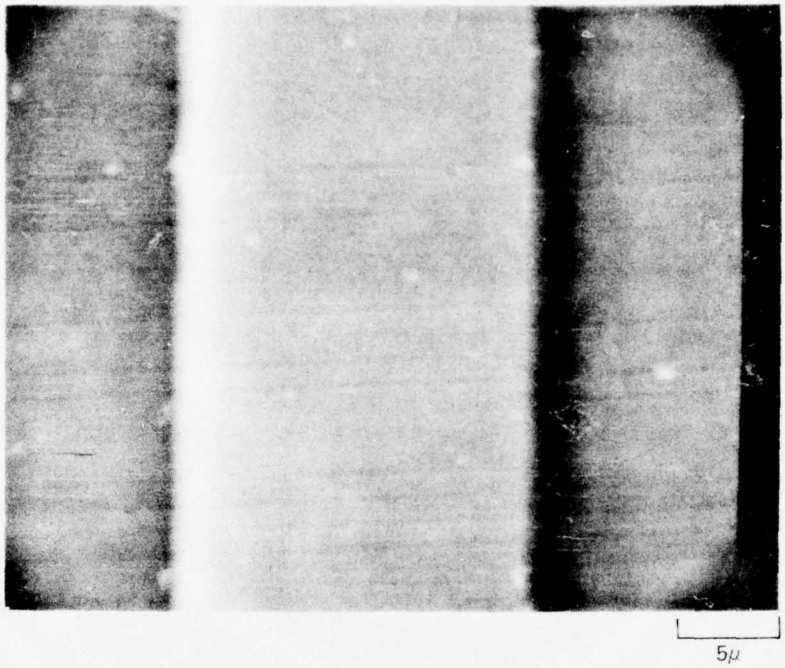

(1) BACKSCATTER (ATOMIC NUMBER CONSTRAST)

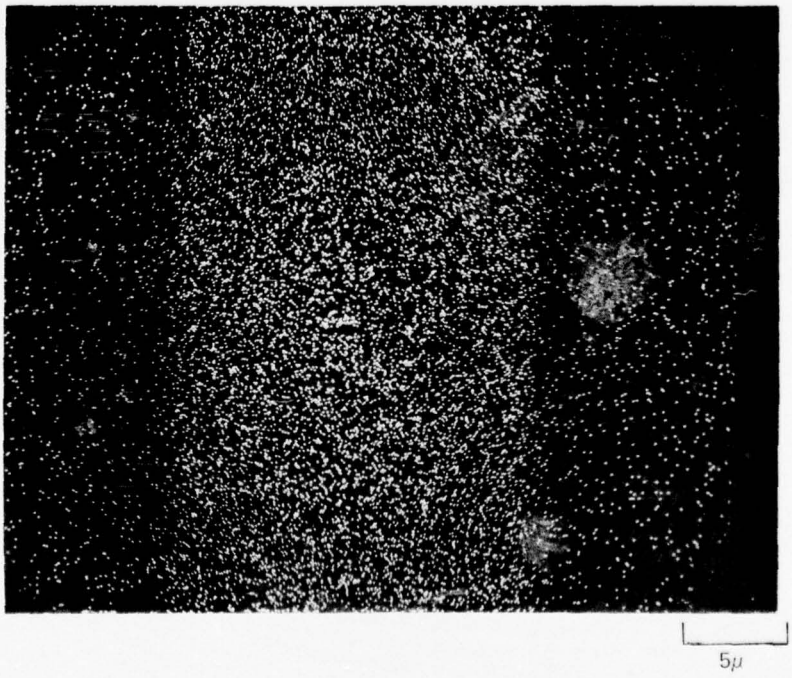

(2) X–RAY (COPPER) SCAN

76-03-33-9

FIG. 34

MICROPROBE X-RAY LINE SCANS ON UNSTRESSED 8% Cu FILM

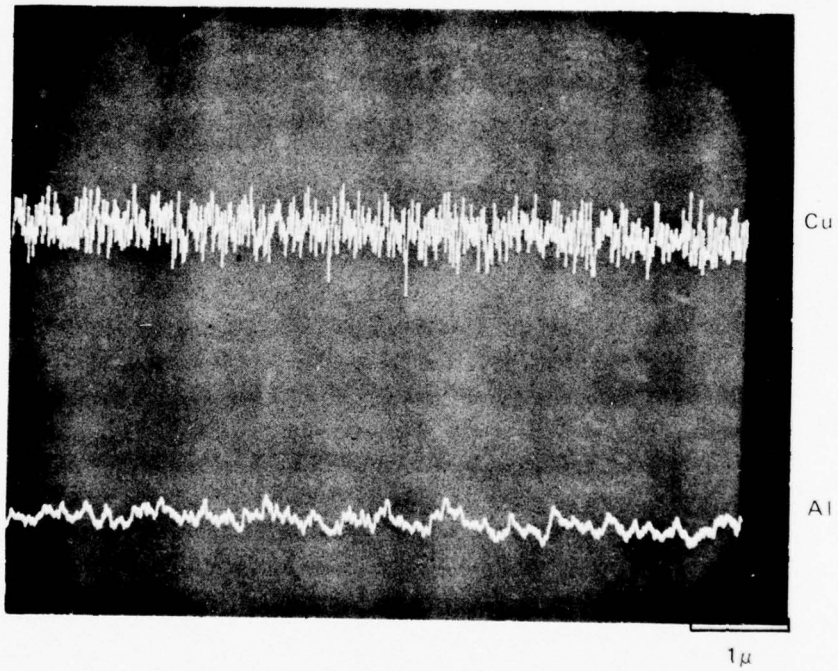

FIG. 35

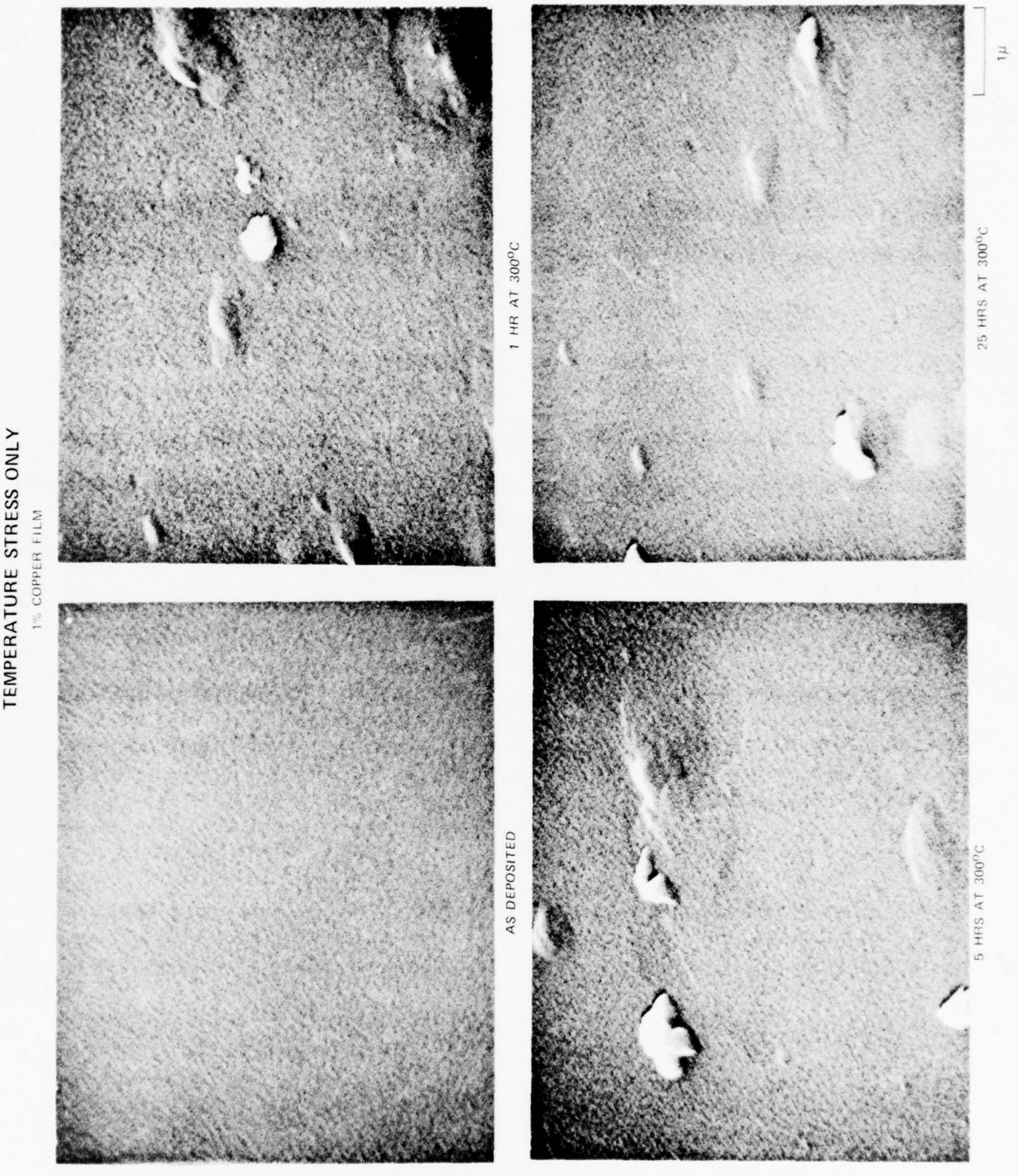
TEMPERATURE STRESS ONLY
1% COPPER FILM
AS DEPOSITED
1 HR AT 300°C
5 HRS AT 300°C
25 HRS AT 300°C
1μ
76-05-26-3

FIG. 36

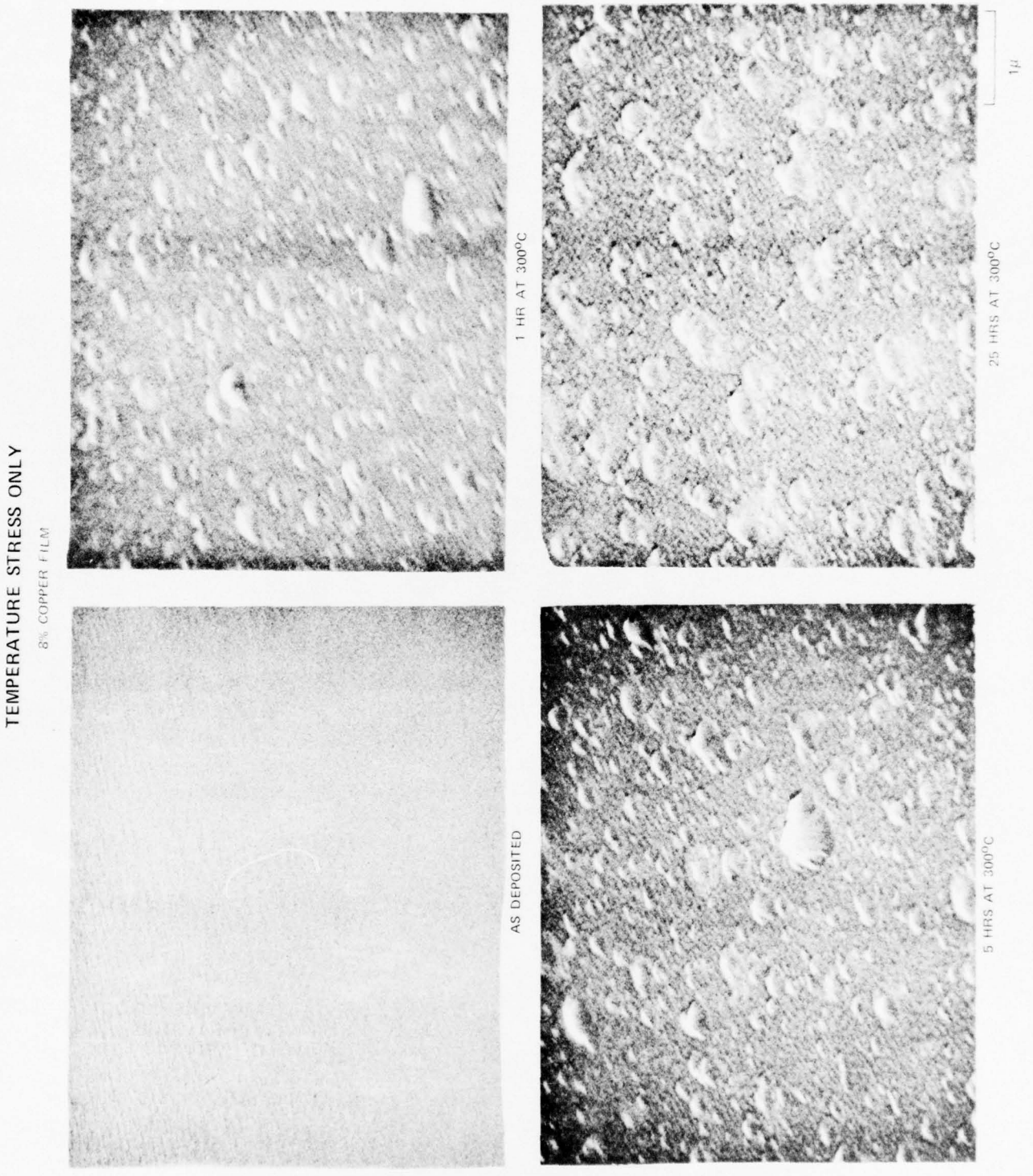
TEMPERATURE STRESS ONLY
8% COPPER FILM
AS DEPOSITED
1 HR AT 300°C
5 HRS AT 300°C
25 HRS AT 300°C
1μ
76-05-26-4

FIG. 37

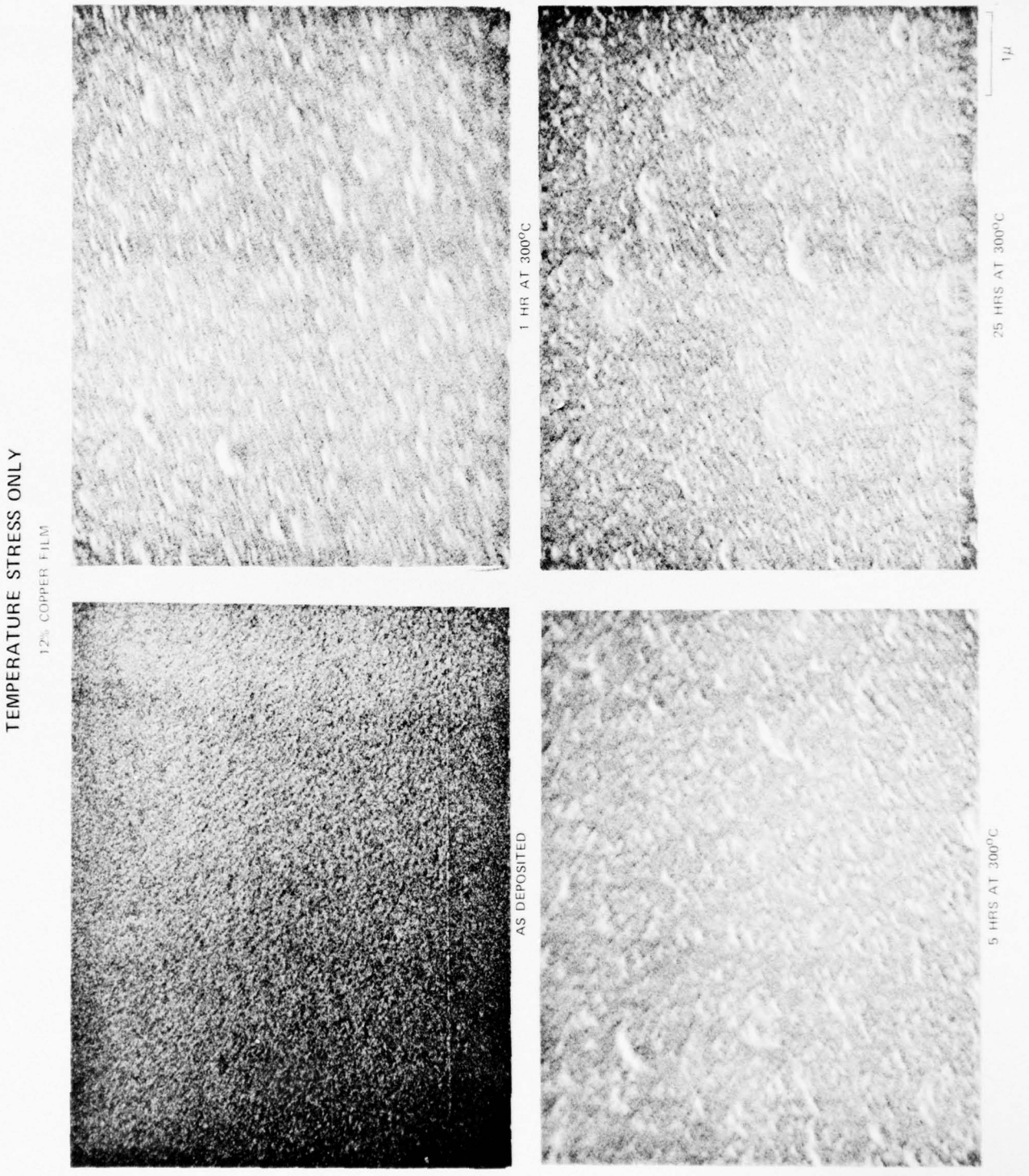
TEMPERATURE STRESS ONLY
12% COPPER FILM
AS DEPOSITED
1 HR AT 300°C
5 HRS AT 300°C
25 HRS AT 300°C
1μ
76-05-26-5

FIG. 38

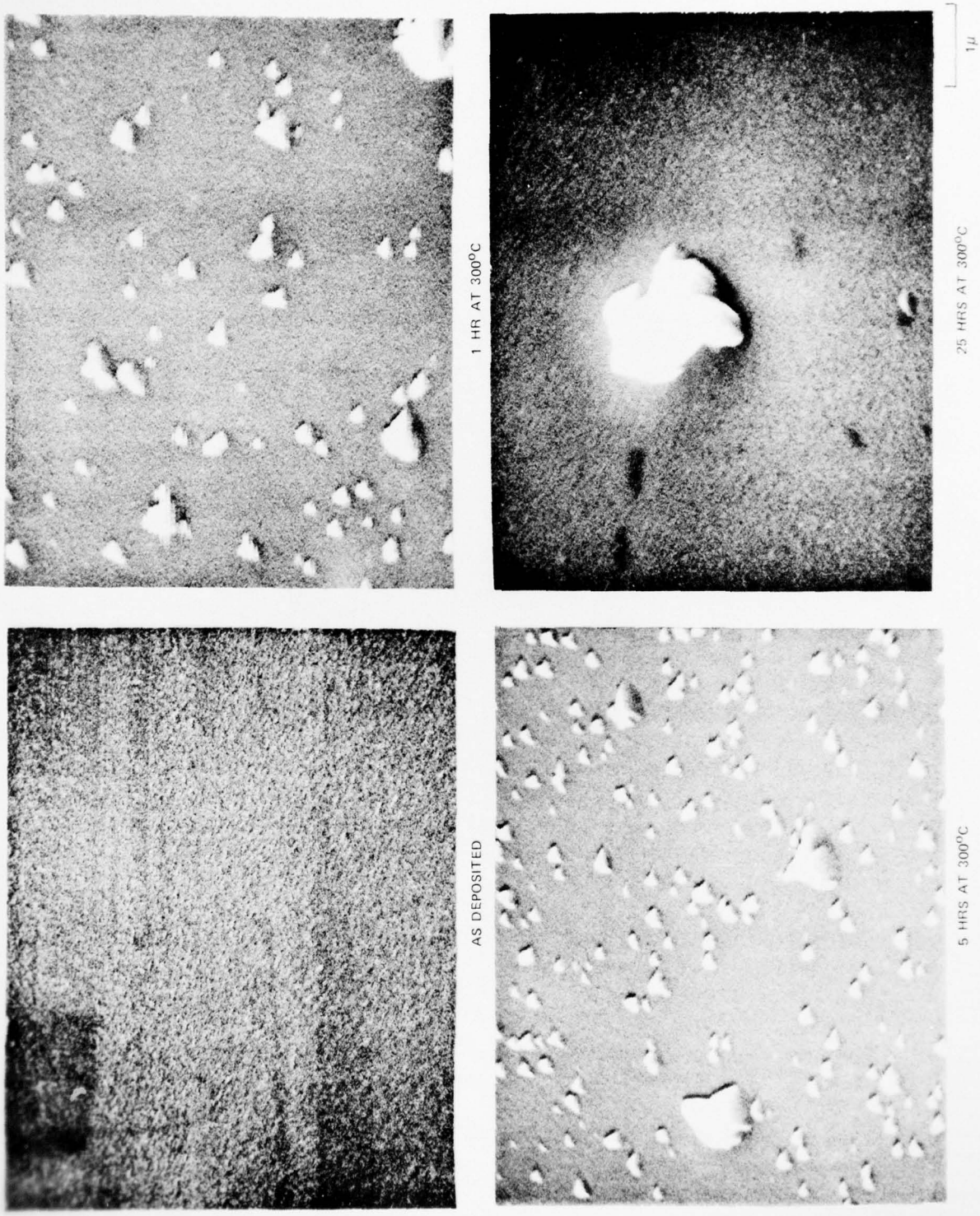
TEMPERATURE STRESS ONLY
12% COPPER FILM FROM REPLACEMENT TARGET
AS DEPOSITED
1 HR AT 300°C
5 HRS AT 300°C
25 HRS AT 300°C
1μ
76-05-26-2

FIG. 39A

LONGITUDINAL X-RAY LINE SCANS
DETECTOR-SAMPLE MISALIGNMENT EFFECT

APPARENT CONCENTRATION VARIATION DUE TO
SAMPLE-DETECTOR ALIGNMENT

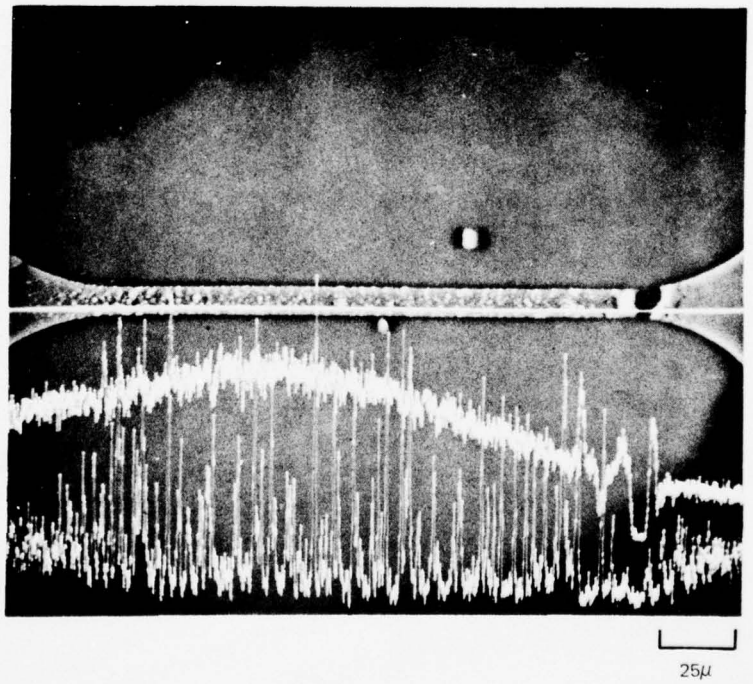

SEE FIG. 22C

76-05-235-2

FIG. 39B

LONGITUDINAL X–RAY LINE SCANS

DETECTOR–SAMPLE MISALIGNMENT EFFECT

APPARENT CONCENTRATION VARIATION DUE TO
SAMPLE–DETECTOR ALIGNMENT

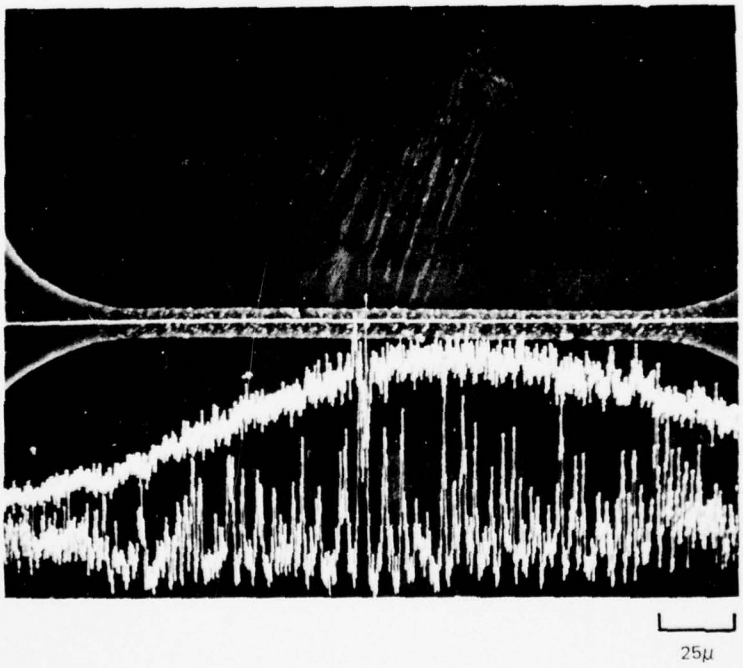

SEE FIG 24C

76–05–190–1

LONGITUDINAL X-RAY LINE SCANS

DETECTOR-SAMPLE MISALIGNMENT EFFECT

APPARENT CONCENTRATION VARIATION DUE TO
SAMPLE-DETECTOR ALIGNMENT

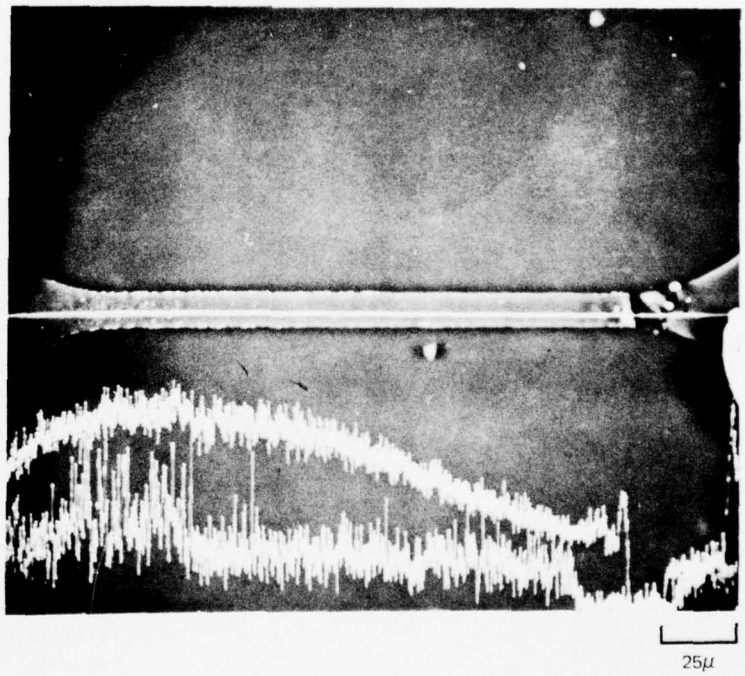

SEE FIG. 32C

4.2 Beryllium Oxide Deposition

Statement of the Problem and Discussion

Thermal management is one of the most important problems in modern solid state electronics device technology. High speed, high power devices rise in temperature to self destruction unless good heat transfer is provided. Eutectic or solder bonding of the device to a metal package is usually accepted as one of the best means for cooling a device short of resorting to heat pipes or to the use of Type II-A diamond.

A major shortcoming of eutectic or solder bonding is in the formation of voids and pockets of oxide in the interface region. These voids and oxide pockets are regions of low thermal conductivity. A device located in the semiconductor above such a low conductivity region will experience a high temperature excursion and degrade at a much faster rate than its design figure. The voids and oxide pockets cause increased thermal path length between device and the heat sink. Elaborate die bonding techniques have evolved to eliminate such low thermal conductivity regions. Vacuum bonding is one such approach.

An alternative approach is to provide a good thermal conductor in intimate contact with the device and move the voids and oxide pockets formed during die bonding further from the device. Sputtering of "thick" thin films of beryllium oxide directly to the back of a device slice offers one means of removing the low conductivity pockets to an acceptable distance from the device. A thick layer of BeO adds a "spreading thermal" conductivity term in parallel with the spreading conductivity of the semiconductor. To zeroth order, a film of BeO with a thermal conductivity approximately 2.5 times that of silicon can double the heat removal rate if it is deposited to a thickness about 0.4 times the silicon thickness. BeO only 0.2 times GaAs thickness would approximately double the "spreading conductivity".

This part of the program had the goals of finding rf sputtering conditions which could be used to deposit 0.001 inch to 0.005 inch thick layers of beryllium oxide on semiconductor device materials without damage to devices. The primary limitation would be to achieve acceptably high deposition rates and thick enough layers without exceeding a substrate temperature in excess of 500 °C.

Constitutive or nonthermal stresses have been observed at extremely high levels for sputtered beryllium oxide. The origins of these stresses are poorly understood but are generally accepted to be related to "quenching" of bond strains in non-equilibrium states. These molecular level forces are translated into macroscopic stresses and strains. Impurities are also often cited as causes of these stress-strain accumulations.

One of the first problems attacked under this program was directed toward the elimination of the built-in or constitutive stresses in beryllium oxide. Pressure, temperature, gas composition and deposition rate were the variables which were available for control.

4.2.1 Equipment and Experimental Procedures

Initially, the rf sputtering was done at a total pressure of ten millitorr with various mixtures of argon and oxygen. Temperature was controlled by wetting the back of the substrates with gallium and attaching them to a controlled temperature block in the chamber. The gallium was for improvement of heat transfer between the block and substrate.

The gas composition was set by admission of argon first to the appropriate pressure and then admission of oxygen until the pressure increased to the desired total. These adjustments were made manually with standard Whitey needle valves whose settings were not changed during the course of the deposition. In some cases, the total pressure changed by ten to twenty percent during the deposition. The pressure was monitored by a Bendix GP 210 C Pirani gauge.

Thickness of a deposit was measured by placing a mechanical mask (usually a silicon chip) on the substrate and measuring the step in the beryllium oxide film. The step height was determined using a Taylor-Hobson Talysurf which has a 10^{-4} inch diameter stylus coupled to a chart recorder. Displacements in stylus height as small as 5.0 nanometers can be measured as the substrate surface is traversed.

Provision for sputter cleaning both target and substrate was made in the sputtering system design. This required a thin stainless steel shutter which could be pivoted into position between target and substrate to collect material sputtered away during cleaning.

The initial sputtering depositions were preceded by about fifteen minutes of sputter cleaning of the target. Most were done without sputter cleaning of the substrate. A range of oxygen partial pressures - from pure oxygen to about twenty percent oxygen - was investigated at an rf power input of from 300 to 500 watts at several temperatures.

4.2.2 Experimental Results and Discussion

Because the goals of the BeO phase of this program were to find a set of sputtering parameters which would lead to adherent stress-free thick films of BeO on silicon or oxidized silicon, detailed documentation of the effects of various parameters on deposition rate, stress and adhesion were not made. The approach taken was to change parameter values in large steps and make crude evaluations of the films produced. It was felt that the greatest likelihood for achieving these goals lay in this direction.

Notably poor reproducibility of results characterized the depositions from a sintered beryllium oxide target. Analysis of the target and the deposited films did reveal strong variations in the generally low contamination levels. It is postulated that a strongly variable particle size distribution existed throughout this target. Rates of deposition were of the order of 8000 Å/hr but could vary up to ±50 percent from this value. Stress levels appeared to vary by several orders of magnitude and were compressive in nature. Surface texture was generally rough. Films deposited at higher temperatures (~ 500°C) exhibited rougher surfaces than those deposited at the lower temperatures. Up to 35 micrometers of beryllium oxide were deposited in approximately 48 hours from the BeO target. It was very rough and showed some stress cracking.

The use of BeO as a target material was finally abandoned because of the lack of reproducibility. Reactive sputtering, though usually much slower, was then investigated as a way of depositing beryllium oxide. A pure beryllium target was installed and the same sputtering apparatus already described was used for the reactive sputtering portion of the program.

Again the partial pressure of oxygen and the temperature were varied but the higher power input (500 W) only was used to keep the rate of deposition as high as possible. These first series of runs had a disappointing sameness of results as for films sputtered from the BeO target. Stresses were evident and the films were rough and discolored.

Contamination was again suspected but analysis of the films failed to identify significant quantities of anything but beryllium oxide. The stress levels appeared to be almost completely insensitive to changes in sputtering parameters while the deposition rate showed modest sensitivity to power level and oxygen content.

Observation of optical patterns on the bottom of the shutter facing the substrate which seemed to match patterns in the deposits suggested contamination of the substrate by emission of trace contaminants from the shutter onto the substrate during sputter cleaning. It was not water cooled and had ample time to increase in temperature and outgas. It may have also been off ground potential and sputtering at a very slow rate.

In the next set of deposits made, the use of the shutter and the sputter cleaning step were eliminated and the stress level dropped to a very low level. It was possible to deposit films about five micrometers in thickness without the poor adhesion and stress cracking observed earlier. The brown-to-gray discoloration and the roughness were still visible, however.

Another series of depositions was made as a function of oxygen pressure, substrate holder temperature, and at two power levels. Because of the very low

deposition rates already experienced, it was not reasonable to work below 350 watts. This series was done with similar parameter values as had been used earlier without success. Three conclusions could be drawn from the results of this series. Best oxygen-argon ratio seemed to be centered about 65-35. Several depositions were made at 60-40 and 70-30 as well to confirm this observation.

Secondly, higher total pressure seemed to favor smoother less discolored films. Twenty- to twenty-five millitorr appeared to be the best total pressure for the depositions. Higher pressure could not be readily used without major system modifications, i. e., reducing cathode-to-ground shield spacing, to maintain the glow discharge. This improvement at higher pressures could be associated with two effects.

Electron emission from the target and bombardment of the substrate causes direct heating of the substrate and may cause some structural damage in the film. Increasing the pressure increases the likelihood of electron scattering and energy loss to the ambient gas before the substrate is reached.

The other likely effect is that the higher oxygen pressure is affecting the reaction rate of beryllium with oxygen on the substrate to form the film. One possible mechanism for reactive sputtering of oxides is the sputtering of metal from the target and direct deposition as the element on the substrate where it reacts with oxygen from the ambient. That this increase in oxygen content is not the significant effect may be inferred from the poorer films resulting from increasing oxygen content at lower pressures.

Making depositions at lower substrate holder temperatures also seemed to improve the film texture and color. Several films were then deposited in thicknesses up to twenty micrometers. The surface texture of these films were degraded during the very long depositions required. They were examined by the Scanning Electron Microscope and exhibited a classic "columnar" growth. The diameter of the "columns" or vertically oriented grains was less than one micrometer (Figs. 40 through 42). The surface roughness appears from these photos to be of the order of a few thousand Angstroms, probably good enough to accept a metallization layer thick enough for bonding.

A more serious problem is evidenced, however, in Figs. 43 and 44. A crack about 0.10 micrometers wide appears in the film. There are many of these cracks near the edges of the silicon substrates. Some of the cracks do not appear at the surface but irregularities in the surface are evident both with the SEM and optical microscopy, which suggest crack formation and then subsequent covering.

In some cases, the thicker films requiring longer deposition times, the cracks spread across the entire substrate. The number per unit area changed from edge to

FIG. 40

BERYLLIUM OXIDE FILM – SURFACE AND EDGE ON SILICON SUBSTRATE

$T = 60^{o}C$; W_{rf} = 500 watts; P_{GAS} = 20 μ; 65% O_2

THICKNESS = 20 μ

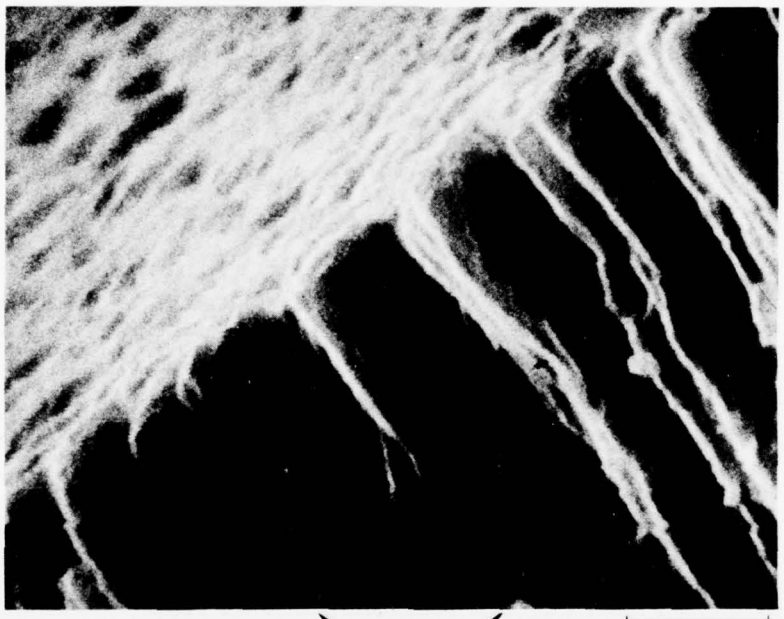

SEM MICROGRAPH

76-03-247-5

FIG. 41

BERYLLIUM OXIDE FILM – SURFACE AND EDGE

SILICON SUBSTRATE

$T = 60^{\circ}C$; $W_{rf} = 500$ watts; $P_{GAS} = 20\ \mu$; 65% O_2

THICKNESS = 20 μ

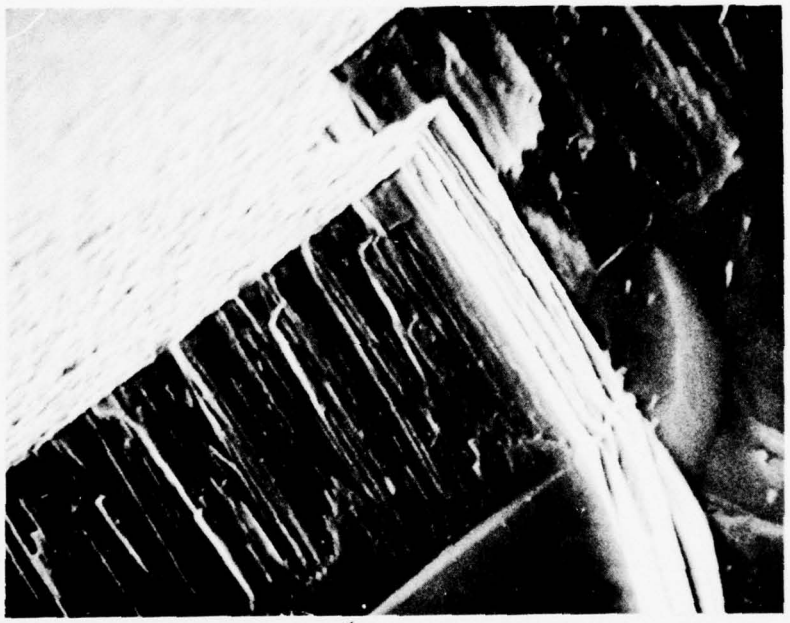

SEM MICROGRAPH

76–03–247–4

FIG. 42

BERYLLIUM OXIDE FILM–SURFACE AND EDGE

SEM MICROGRAPH

$T = 60^{o}C$, $P_W = 500$ watts; PRESSURE = 20 μ

THICKNESS = 20 μ

ON SILICON SUBSTRATE

76–03–247–2

FIG. 43

BERYLLIUM OXIDE FILM—THERMAL STRESS CRACK ON SILICON SUBSTRATE

$T = 60^{\circ}C$; $W_{rf} = 500$ watts; $P_{GAS} \approx 20\ \mu$; 65% O_2

THICKNESS = 20 μ

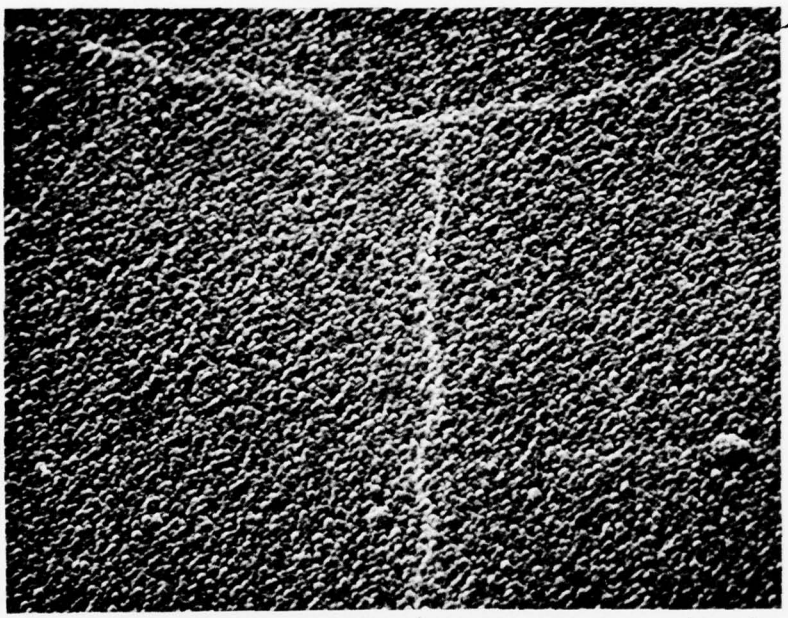

SEM MICROGRAPH

76-03-247-8

BERYLLIUM OXIDE FILM – THERMAL STRESS CRACK ON SILICON SUBSTRATE

$T = 100^{\circ}C$; $W_{rf} = 500$ watts; $P_{GAS} = 28\mu$; 65% O_2

THICKNESS = 20 μ

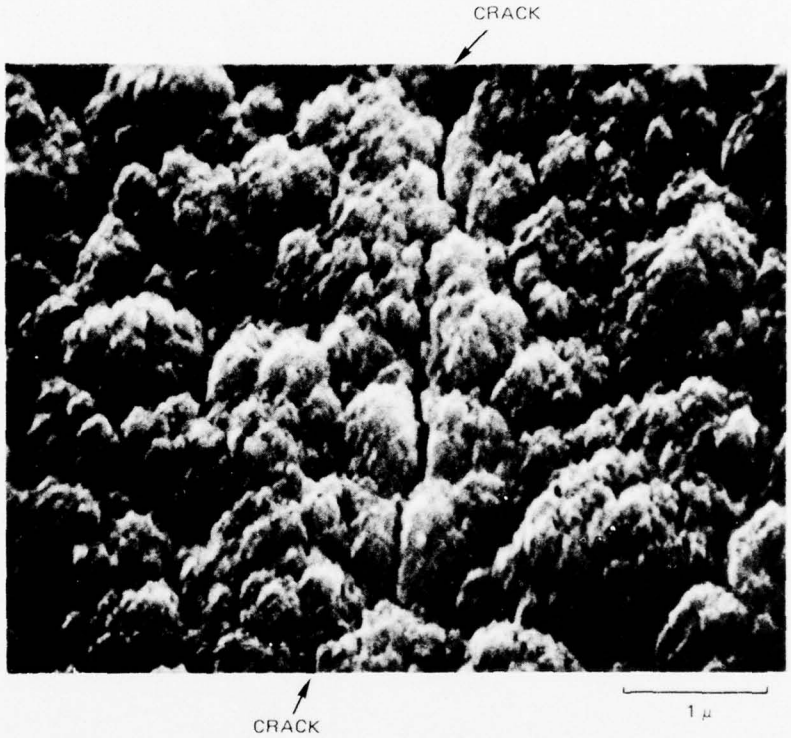

SEM MICROGRAPH

76-03-247-10

center. These did not appear to be the same type of cracks resulting from the structural or constitutional stresses observed earlier in the program. Peeling of the films did not result from this type of stress.

The above observations suggested that thermal stresses were generated. The substrate edges were poorly heat sunk with the holder design used - perhaps 0.125 inch of the outer edge was not in contact with the holder and depended on lateral conduction through the substrate to the gallium contacted portion of the substrate holder interface. It was this region which showed the first cracks in the films. Progressively longer deposition times were seen to be associated with a larger band of cracks around the outside edge of the substrate.

Gallium arsenide has a larger coefficient of thermal expansion than does silicon - it nearly matches that of beryllium oxide. A deposition was made on a gallium arsenide single crystal substrate with no attempt to heat sink with gallium. Under these conditions and 500 watts input power, the temperature of the gallium arsenide would rise to about 500 °C. This deposition would be expected to produce the same problems on gallium arsenide as on silicon except for thermal stresses. Indeed, no cracks were observed in the film on gallium arsenide while the film on silicon exhibited the same pattern seen in earlier depositions (Figs. 45 through 48).

Evidently, the thermal stresses in the films deposited on silicon were due to de-wetting of the gallium from the substrate. The normal affinity of gallium for oxygen and the enhanced reactivity of the oxygen in the glow discharge apparently caused much faster oxidation of gallium than room air. A progressive oxidation of the gallium from the edge of the substrate and proceeding toward the center was responsible for a loss of wetting and a gradual increase in temperature of the substrate as the deposition progressed. Whether there was a volume change associated with the gallium oxide formation and thus a "prying-up" of the substrate from the edges or whether the gallium oxide was sufficiently volatile to be transported out of the interface region leaving a gap was not clear.

A deposition was made using Apiezon N vacuum grease as the heat sink medium. All other conditions remained the same. The results were similar to the cases where gallium had been used for the heat sink medium - cracks in the film. In this case, the heat sink medium disappeared completely, due no doubt, to the volatility of the oxidation products from the grease.

Another heat sinking approach used a metal film - chromium overlaid with copper - on the back of the substrate to give better wetting. Again, oxidation of the gallium occurred and at a somewhat higher rate than when used alone. Apparently, the presence of the copper enhances the oxidation of the gallium by the plasma.

AD-A032 441 UNITED TECHNOLOGIES RESEARCH CENTER EAST HARTFORD CONN F/G 20/12
IMPROVEMENT OF ELECTRONICS RELIABILITY BY RF SPUTTERING TECHNIQ--ETC(U)
MAY 76 D H GRANTHAM, J L SWINDAL N00019-75-C-0465
UNCLASSIFIED UTRC-R76-922139-4 NL

2 OF 2
ADA032441

END

DATE
FILMED
1 - 77

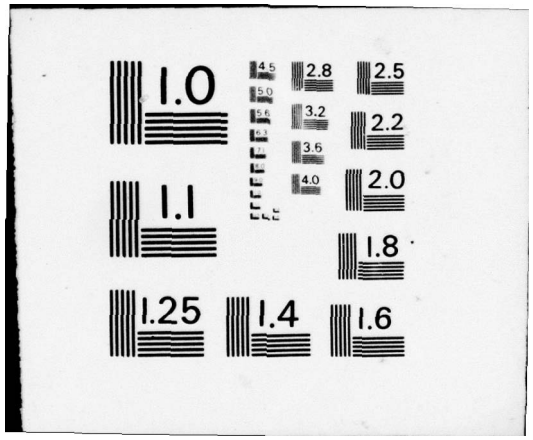
1.0
1.1
1.25
1.4
1.6
1.8
2.0
2.2
2.5
2.8
3.2
3.6
4.0
4.5
5.0
5.6

FIG. 45

BERYLLIUM OXIDE FILM – ON GaAs

TEMP = 100°C; W_{rf} = 500 watts; P_{GAS} = 20 μ; 65% O_2

THICKNESS = 20 μ

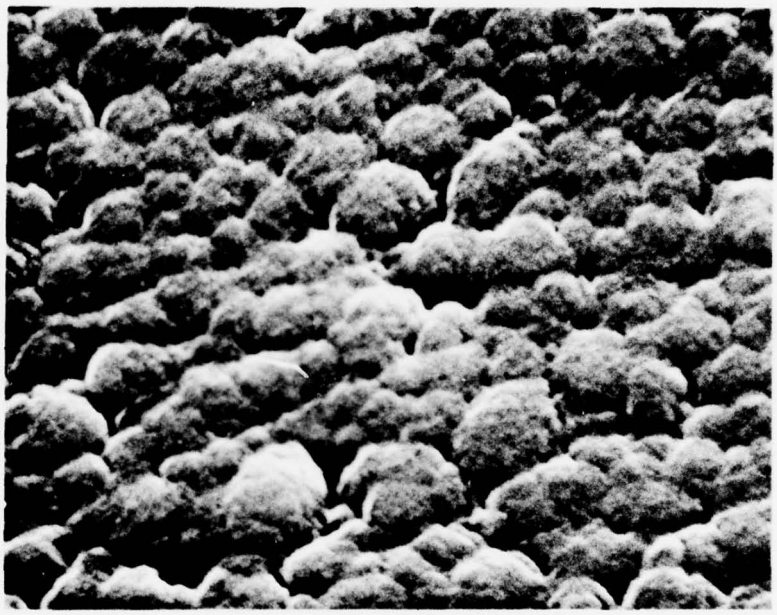

SEM MICROGRAPH

76-03-247-6

BERYLLIUM OXIDE FILM – GaAs

TEMP = 100°C; W_{rf} = 350 watts; P_{GAS} = 25 μ; 65% O_2

THICKNESS = 5.6 μ

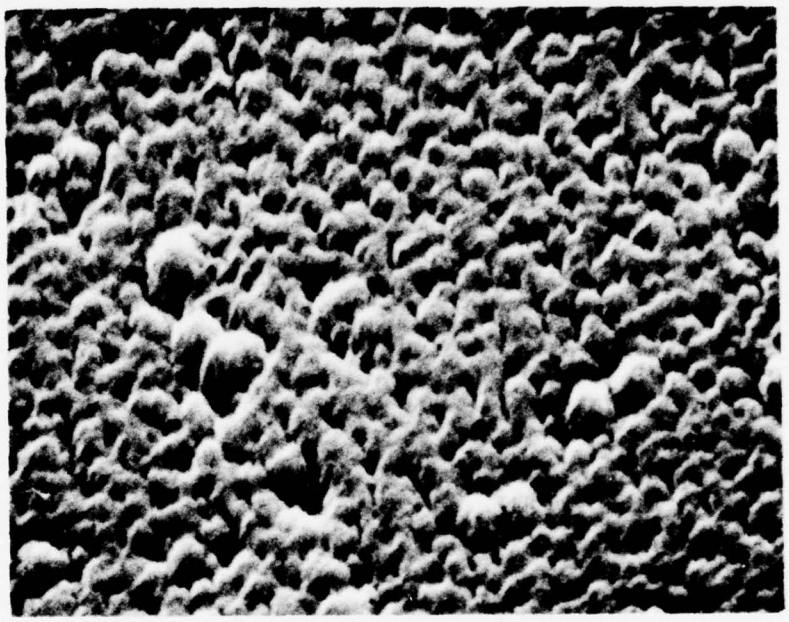

SEM MICROGRAPH

1 μ

76-03-247-1

BERYLLIUM OXIDE FILM – ON GaAs

$T = 100^{0}C$; $W_{rf} = 500$ watts; $P_{GAS} = 20\ \mu$; 65% O_2

THICKNESS = 20 μ

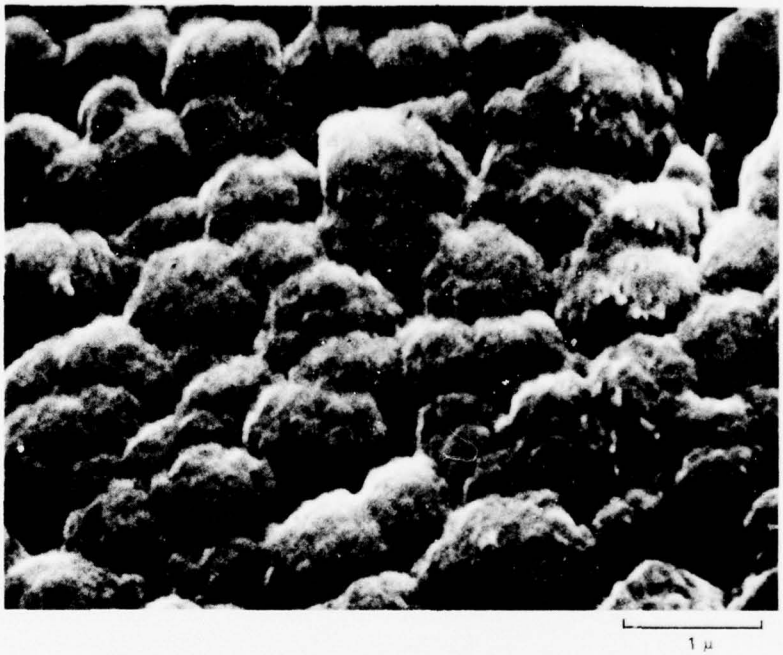

SEM MICROGRAPH

76–03–247–7

BERYLLIUM OXIDE FILM – ON GaAs

$T = 100^{O}C$; $W_{rf} = 500$ watts; $P_{GAS} = 20\ \mu$; 65% O_2

THICKNESS = 5 μ

SEM MICROGRAPH

76-03-247-9

TABLE V

BeO Sputtering - Parametric Effects

Power Watts	Pressure Millitorr	% Oxygen	Substrate Temp.	Deposition Time (Hrs)	Film Thickness μ
500	9	65	150	6	2.1
'	10	70	150	8	2.8
'	10	65	150	15	5.2
'	10	70	150	15	5.6
'	11	65	150	14.7	6.0
'	10	65	100	15.3	5.6
'	20	65	100	13.5	4.3
'	20	65	100	14.4	4.9
'	25	65	100	13.2	4.8
'	20	65	100	13.6	4.2
'	20	65	100	53.0	19.5
'	10	60	200	5.0	1.6
'	10	60	200	5.5	2.0
'	10	80	200	6.0	2.6
'	10	80	200	5.0	2.2
	10	80	200	4.8	1.35
350	13	65	100	15.1	4.64
'	20	65	100	12.3	3.24
'	25	65	100	14.3	5.6
'	5	100	350	8.0	2.0

A hot filament electron source was used in two configurations in an attempt to increase the rate by enhancing the plasma density in the glow discharge. In one, the filament surrounded the discharge region and in the other, the filament was shorter and opposed to an anode some twelve inches away on the same diameter through the system. The filament surrounding proved to be a poor design and could not be run at significant emission currents. The filament-anode opposed configuration was stable and could support about 0.5 ampere of emission.

The electron emission supported mode required an increase in target-to-substrate spacing (to 1.375 in.) in order to accomodate all the fixturing. This normally means a reduction in deposition rate. However, the electron emission enhancement was sufficient to offset the reduction due to increased spacing. Approximately 0.4 micrometer/hour was the rate observed at 500 watts rf input. At 1000 watts rf input power, the rate increased to 0.8 micrometers/hour. In all of these depositions, indium was used for heat sinking. Rates could be increased by increasing the rf power to the cathode while the temperature remained fixed at 125 °C. Insufficient time remained in the program to verify the efficacy of this solution for depositions over long periods but no obvious problems were evident.

5.0 SUGGESTIONS FOR FUTURE WORK

5.1 Multilevel Interconnect Technology

The data collected for this report only "scratches the surface" for the use of aluminum based metal alloys for interconnects. The metallurgists have investigated extensively, literally dozens of binary as well as multicomponent systems based on aluminum. Many have been seen to be resistant to creep and fatigue. High values of hardness have been found to be characteristic of some of these alloys. Aluminum has been strengthened by small additions of iron to form a dispersed intermetallic phase. These alloys maintain reasonably good electrical conductivity at the same time as their strength increases. Because of the similarity between creep and fatigue behavior and the processes associated with electromigration, these alloy systems developed already for their improved mechanical properties should be evaluated in film form for their electromigration susceptibility. The sputtering process is uniquely suited for deposition of these multicomponent materials without changing composition. Just as sputtered copper in aluminum was seen from the data in this report to cause marked reduction in electromigration susceptibility over pure aluminum, other metal additions in sputtered films can be expected to show the same kind of improvement. More data on sputtered aluminum-metal films is necessary.

The relative importance of film thickness ratio to surface area has not been unequivocally established. A series of films with varying surface area but constant cross-section should be evaluated for electromigration susceptibility. That the overcoating of the metal film with silicon dioxide increases the life under high current density strongly suggests a surface migration effect inhibited by sputtered coatings.

Beryllium as a new metal interconnect material should be investigated for electromigration susceptibility. Some work has been done within UTRC and at other laboratories which already answers some of the questions regarding adhesion and deposition rates. Compatibility with silicon dioxide poses no apparent problems.

5.2 Beryllium Oxide Deposition

1) Use of indium for the heat sinking medium. Initial work showed this to be effective. Indium melts at 150 °C and is very ductile so that cooling to 125 °C for the deposition should not introduce undue stresses in the substrate. A metal film backing would most likely be required for good wetting. Some oxidation might occur at the edges of the substrate but diffusion of oxygen through the solid products should be slow. Long deposition times should be made to confirm the viability of this technique.

2) Enhance the deposition rate by use of a stronger magnetic field or by use of a supported discharge produced from a thermiionic electron emitter. The diffusion and reaction of the oxygen with the heat sink material might proceed slowly enough that a thick film could be deposited before de-wetting becomes significant.

3) Use of a shaped magnetic field to direct secondary electrons away from the substrate. This technique has been demonstrated in this laboratory but uniformity in film thickness has proven to be a severe problem.

4) Interruption of the film deposition process after a few hours and re-wetting of the substrate and holder with gallium. This could be a time consuming and tedious procedure.

5) Develop an S-gun or similar configuration suitable for rf sputtering. In the dc-mode, the substrate is placed outside the volume between the target and anode so that electron and ion bombardment of the substrate is virtually eliminated.

6) A hollow cathode approach might prove to give a much lower heat flux to the substrates.

The brittle nature of beryllium oxide and the tendency to develop columnar growths may not be problems which can be readily overcome. Bias sputtering may break up the columnar growths but it will also slow deposition rate. Doping of the beryllium oxide by addition of some other oxide (silicon dioxide or magnesium oxide for example) may be effective in retarding the development of columnar growths. For example, calcium oxide and thorium oxide have been used to prevent a phase change in zirconium oxide at elevated temperatures.

APPENDIX I

WEIBULL ANALYSIS OF TEST DATA

When we analyze data we put it in order. The data may be placed in alphabetical groups, numerical ranks, or in some other order. We then examine the groups to see if there are simple or systematic relationships in order corresponding to the observed output. It may be possible to describe these relationships with a line on a graph, or with a few symbols. If we can establish and describe the relationships we can say the analysis has added to the meaning and usefulness of the original data.

Data points from tests or measurements can be plotted to show the frequency distribution with a selected independent variable, such as weight, length, or time. This histogram will show how many times each value of the variable is likely to occur. We may find we have an exponential distribution, or the familiar "normal" distribution, or something else. If the distribution curve were known, then we could define mathematically the product reliability, quality, or conformity. A very useful distribution curve was suggested by Waloddi Weibull in 1950. The analysis entails the plotting of data points on a specially prepared graph paper now called Weibull probability paper. A few simple measurements then directly provide the shape and position

parameters of the distribution curve. The scales on the Weibull probability paper are laid out to display the three parameters that define the distribution curve:

β , the Weibull Slope

η , the characteristic life

t_o , the starting point of the curve.

Direct measurements on the paper can be made to determine a product's reliability.

This system of analysis is based on a mathematical model known as the Weibull equation:

$$F(t) = 1 - e^{-\left(\frac{X}{\eta}\right)^{\beta}} \qquad (1)$$

where:

$F(t)$ = Cumulative probability of failure (the area under the distribution from t_o to t).

β = Weibull slope

η = Characteristic life

t = Random variable (time, stress, size, cycles, etc.)

t_o = Origin of the distribution

The probability density function f(t) is equal to $\frac{d\,F(t)}{dt}$, the ordinate of the frequency distribution.

$$f(t) = \frac{\beta\,(t - t_o)^{\beta - 1}}{\eta^{\beta}}\; e^{-\left(\frac{t - t_o}{\eta}\right)^{\beta}} \qquad (2)$$

Some of the possible distributions of f(t) are shown in Figure 1.

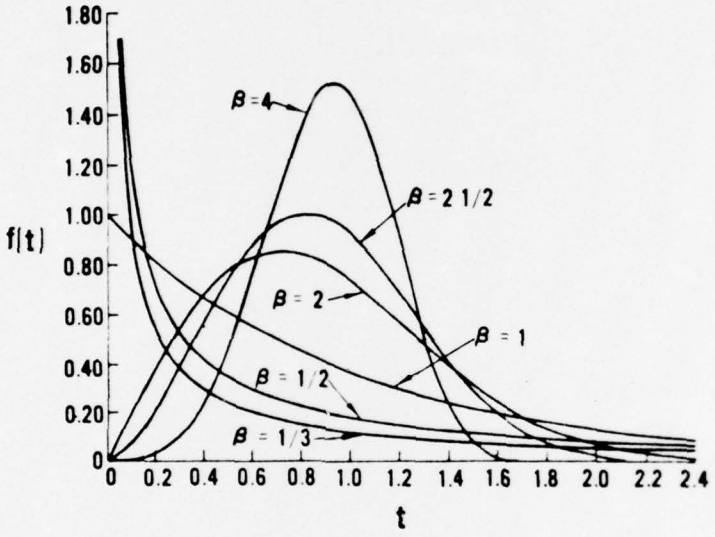

Figure 1 Possible Distributions of f (t).

DERIVATION OF THE RELIABILITY EQUATION

The flexible form of the Weibull equation can be understood by studying a rigorous, but general, mathematical model.

$$\text{Reliability } (R) = \frac{N}{N_o} = \frac{N_o - r}{N_o} = 1 - \frac{r}{N_o}$$

Where N_o is the number of units tested, r is the number failed and N is the number surviving.

In Figure 1 the unit cannot fail between 0 and t_o, hence R = 1.00; we

can say the product is 100% reliable before time t_o.

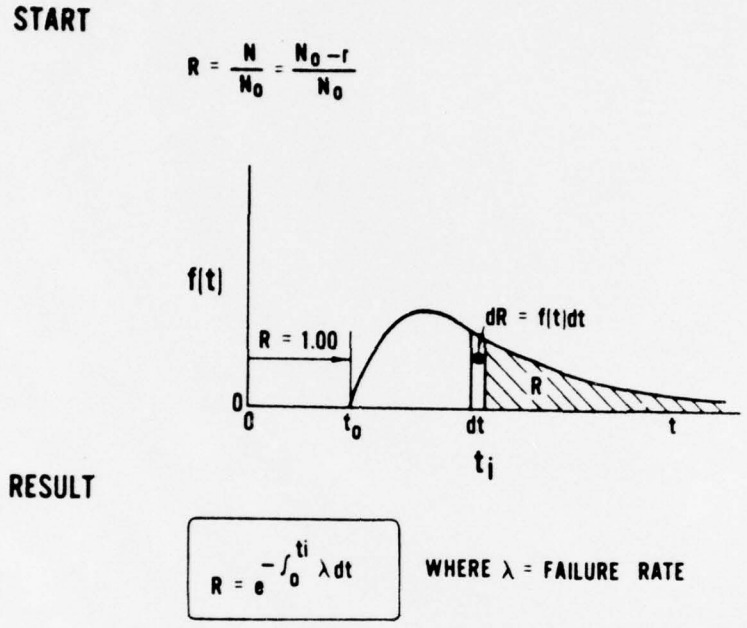

Figure 2 Picture of any Distribution.

Taking the derivative of $R = 1 - \frac{r}{N_o}$ with respect to time

$$\frac{dR}{dt} = \frac{d}{dt}\left(1 - \frac{r}{N_o}\right) = \frac{1}{N_o}\frac{dr}{dt}$$

$$\frac{dr}{dt} = -N_o\frac{dR}{dt}$$

Dividing by N to get the rate of failure per unit still being tested:

$$\frac{1}{N}\frac{dr}{dt} = -\frac{N_o}{N}\frac{dR}{dt} = -\frac{1}{R}\frac{dR}{dt}$$

The rate of failure is referred to by a Greek symbol λ, called the instantaneous failure rate or the hazard rate.

$$\frac{1}{N} \quad \frac{dr}{dt} = \lambda$$

By substitution

$$\lambda = - \frac{1}{R} \quad \frac{dR}{dt}$$

$$\frac{1}{R} \quad \frac{dR}{dt} = - \lambda$$

$$\frac{dR}{R} = - \lambda \ dt$$

$$\int_1^{R_{t_i}} \frac{dR}{R} = - \int_o^{t_i} \lambda \ dt \qquad \text{when } t_o = 0,\ R = 1.00 \text{ and when } t = t_i,\ R = R_{t_i}$$

Integrating R

$$\ln R_i = - \int_o^{t_i} \lambda \ dt$$

$$R_{t_i} = e^{- \int_o^{t_i} \lambda \ dt} \qquad (4)$$

Equation (4) is a mathematical expression for the reliability of any failure mode at time t_i, but only useful if we know the equation for λ as a function of t. If λ is a constant, not a function of time, the $R_{t_i} = e^{- \int_o^{ti} \lambda \ dt} = e^{- \lambda t_i}$. This is the well known exponential expression for reliability. Weibull noticed that a great variety of data distributions seemed to fit an expression of the form $R_{t_i} = e^{- \left(\frac{t_i - t_o}{\eta} \right)^{\beta}}$ where $\left(\frac{t_i - t_o}{\eta} \right)^{\beta} \approx \int_o^{t_i} \lambda \ dt$ This is the Weibull model. His approximation of expression (4) has three parameters.

1. β describes shape of the distribution or the (slope on Weibull probability paper).
2. t_o = starting point or origin of the distribution
3. η = characteristic life

*NOTE: β and η must be greater than 0.

Figure (3) shows a distribution curve with a Weibull slope of 2 and two different characteristic lives. These distributions would appear as two parallel lines on Weibull probability paper with the line containing the greater η lying on the right. In these cases failure can begin to occur at $t_o = 0$. Be aware that some products like car batteries can fail before they are installed, and others, like a work-hardening material, can fail only some time after testing starts.

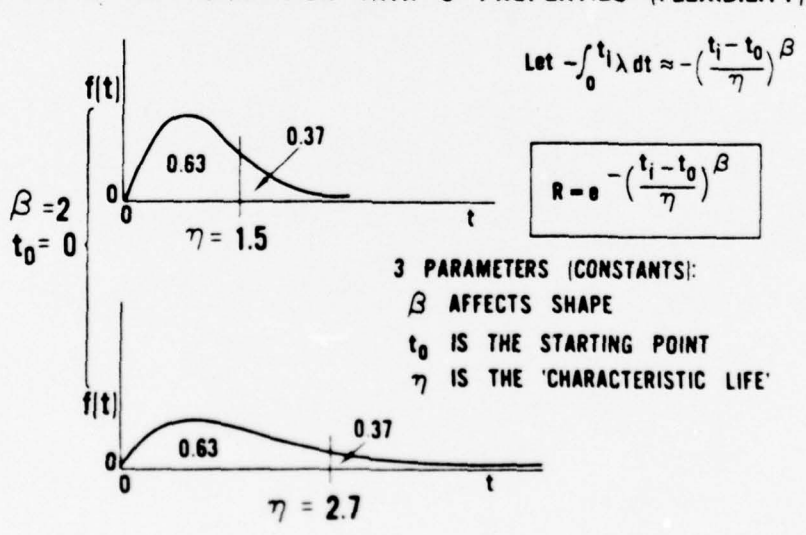

Figure 3 Effect of Characteristic Life on Distribution.

An interesting result occurs in the Weibull equation when $t_i - t_o = \eta$

$$R = e^{-\left(\frac{\eta}{\eta}\right)^{\beta}}$$

$$R = e^{-(1)^{\beta}}$$

$$R = e^{-1} = 0.37$$

The reliability is always 0.37 at the characteristic life. This is true for any value of β since 1 taken to any power is still equal to 1.

When test data is plotted on Weibull probability paper the three parameters can be estimated without involved mathematical calculations.

The basis for the design of Weibull probability paper is as follows:

$$R = e^{-\left(\frac{t_i - t_o}{\eta}\right)^{\beta}} \qquad \text{Let } t_o = 0$$

$$R = e^{-\left(\frac{t_i}{\eta}\right)^{\beta}}$$

$$\frac{1}{R} = e^{\left(\frac{t_i}{\eta}\right)^{\beta}}$$

$$\ln \frac{1}{R} = \left(\frac{t_i}{\eta}\right)^{\beta}$$

$$\ln \ln \frac{1}{R} = \beta \ln t_i - \beta \ln \eta \qquad (5)$$

$$y = A x + B$$

This last equation is in the form of a straight line where A and B are constants. Notice that the line's slope $A = \beta$. Using Weibull probability paper, the Weibull distribution will be represented by a straight line. Changes in the slope β correspond to changes in the shape of the Weibull distribution. On Weibull probability paper the slope of the

fitted straight line can be directly measured. From algebra we remember that the slope is $\frac{y_1-y_o}{x_1-x_o}$. By superimposing a sheet of regular transparent graph paper over the Weibull paper we can easily determine the slope.* Figure 4A shows that by moving 1 unit on the t axis and measuring the change in F, the slope is $\frac{2}{1}$ or 2. Figure (4B) shows the same method but with a slope of $\frac{5}{1}$ or 5. The corresponding failure distributions are shown above 4A and 4B

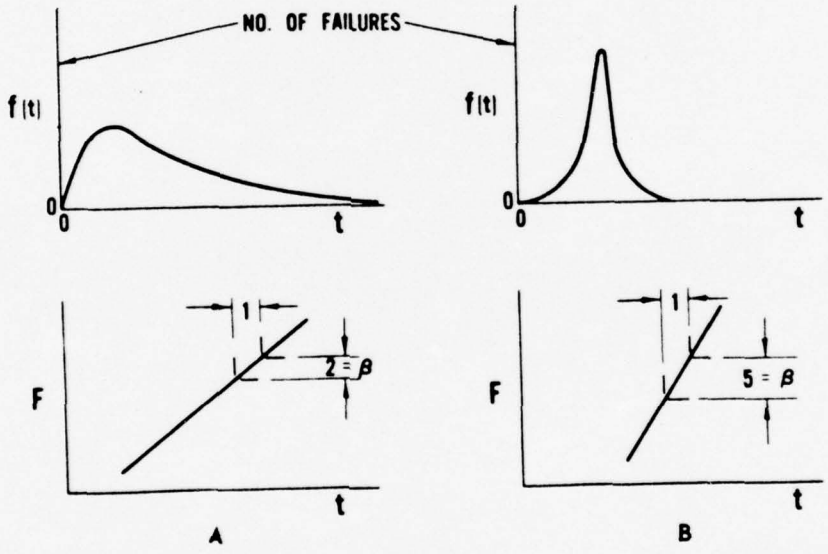

Figure 4 **Effect of Weibull Slope on the Distribution Curve.**

Characteristic failure distribution curves, defined by values of β are shown in Figure 5 For any value of β less than or equal to 1.0 the frequency distribution of failures is a curve which starts at a high frequency at t = 0 and approaches zero as t approaches infinity. Two

* This superimposition will only work when a β of 1 makes a 45° angle with the abscissa.

examples are shown with $\beta = 0.5$ and $\beta = 1.0$. When $\beta = 1$ we have the "exponential-life" distribution.

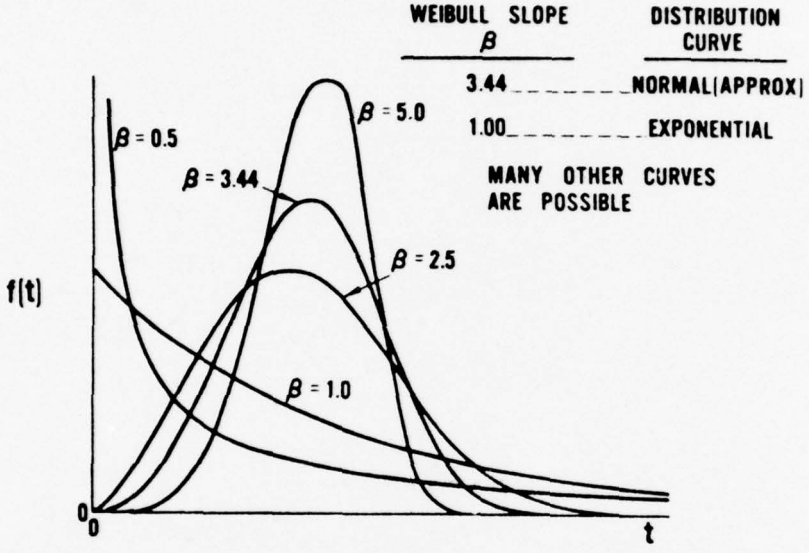

Figure 5 Characteristic Failure Distribution Curves.

When β is greater than 1.0, the origin of the distribution curve starts at a frequency of zero failures. For values of β slightly greater than 1.0, the frequency distribution is highly skewed with a long tail to the right. The distribution becomes essentially symetrical as β approaches 3.44 and becomes more sharply peaked with reverse skewness as β increases beyond 3.44. When $\beta \approx 3.44$ the values of the mean and the median of the distribution are equal and in this special case we have nearly a one-parameter normal distribution.

The two parameters β and η respectively identify the shape of the distribution and the point where 63% of the population will have failed. For other analytical studies, such as the t-test, F-test, etc., we must determine the average time to failure ($\bar{t}$) and variance (s^2). The general formula for each is given below.

$$\bar{t} = \eta \, \Gamma \left(1 + \frac{1}{\beta}\right)$$

$$s^2 = \eta^2 \Gamma \left(1 + \frac{2}{\beta}\right) - \eta^2 \left[\Gamma\left(1 + \frac{1}{\beta}\right)\right]^2$$

Previously we said that when $\beta \approx 3.44$, the median and mean are equal and the Weibull distribution closely approximates a normal distribution. To show this we replace t by $\bar{t}$ in equation 1 and calculate $F(\bar{t})$ for various values of β

$$F(\bar{t}) = 1 - e^{-\left(\frac{\bar{t}}{\eta}\right)^{\beta}}$$

or

$$F(\bar{t}) = 1 - e^{-\left[\Gamma\left(1 + \frac{1}{\beta}\right)\right]^{\beta}}$$

Figure 6 is a graph of $F(\bar{t})$ for various Weibull slopes. When $0 < \beta < 3.44$ the median is greater than the mean and the reverse is true when $\beta > 3.44$.

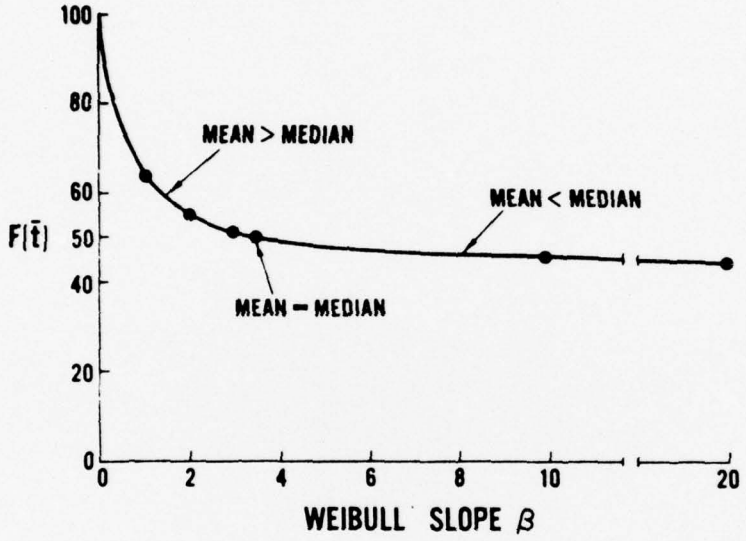

Figure 6 Failure Probabilities with Varying Weibull Slope.

ACKNOWLEDGEMENT:

The material in this section (Appendix) is an excerpt from Pratt and Whitney Aircraft Division of United Aircraft Corporation, document PWA 3001, Introduction to Weibull Analysis by R. A. Mitchell, January 6, 1967.

MEDIAN RANKS

RANK ORDER	SAMPLE SIZE 1	2	3	4	5	6	7	8	9	10
1	50.0	29.2	20.6	15.9	12.9	10.9	9.4	8.3	7.4	6.6
2		70.7	50.0	38.5	31.3	26.4	22.8	20.1	17.9	16.2
3			79.3	61.4	50.0	42.1	36.4	32.0	28.6	25.8
4				84.0	68.6	57.8	50.0	44.0	39.3	35.5
5					87.0	73.5	63.5	55.9	50.0	45.1
6						89.0	77.1	67.9	60.6	54.8
7							90.5	79.8	71.3	64.4
8								91.7	82.0	74.1
9									92.5	83.7
10										93.3

MEDIAN RANKS

RANK ORDER	SAMPLE SIZE 11	12	13	14	15	16	17	18	19	20
1	6.1	5.6	5.1	4.8	4.5	4.2	3.9	3.7	3.5	3.4
2	14.7	13.5	12.5	11.7	10.9	10.2	9.6	9.1	8.6	8.2
3	23.5	21.6	20.0	18.6	17.4	16.3	15.4	14.5	13.8	13.1
4	32.3	29.7	27.5	25.6	23.9	22.4	21.1	20.0	18.9	18.0
5	41.1	37.8	35.0	32.5	30.4	28.5	26.9	25.4	24.1	22.9
6	50.0	45.9	42.5	39.5	36.9	34.7	32.7	30.9	29.3	27.8
7	58.8	54.0	50.0	46.5	43.4	40.8	38.4	36.3	34.4	32.7
8	67.6	62.1	57.4	53.4	50.0	46.9	44.2	41.8	39.6	37.7
9	76.4	70.2	64.9	60.4	56.5	53.0	50.0	47.2	44.8	42.6
10	85.2	78.3	72.4	67.4	63.0	59.1	55.7	52.7	50.0	47.5
11	93.8	86.4	79.9	74.3	69.5	65.2	61.5	58.1	55.1	52.4
12		94.3	87.4	81.3	76.0	71.4	67.2	63.6	60.3	57.3
13			94.8	88.2	82.5	77.5	73.0	69.0	65.5	62.2
14				95.1	89.0	83.6	78.8	74.5	70.6	67.2
15					95.4	89.7	84.5	79.9	75.8	72.1
16						95.7	90.3	85.4	81.0	77.0
17							96.0	90.8	86.1	81.9
18								96.2	91.3	86.8
19									96.4	91.7
20										96.5

DISTRIBUTION LIST

Government	Copies
Advisory Group on Electron Devices 201 Varick Street, 9th Floor Attn: Secretary New York, New York 10014	1
Air Force Avionics Laboratory Attn: Mr. Jim Skalski (AFAL/TEA) Wright-Patterson Air Force Base, Ohio 45433	1
Air Force Avionics Laboratory Attn: Mr. H. H. Stienbergen (AFAL/TEA) Wright-Patterson Air Force Base, Ohio 45433	1
Air Force Avionics Laboratory Attn: AFAL/TEA (Maj. J. DeCaire) Wright-Patterson Air Force Base, Ohio 45433	1
Air Force Cambridge Research Laboratory L. G. Hanscom Field Bedford, Massachusetts 01730	1
Air Force Materials Laboratory Attn: AFML/LTE (Mr. Gene Miller) Wright-Patterson Air Force Base, Ohio 45433	1
Office of the Chief of Naval Operations Deputy Chief of Naval Operations (Development) Technical Analysis and Advisory Group (Code NOP-077D) Washington, D.C. 20350	1
Chief, Data Processing Branch Federal Aviation Administration 800 Independence Avenue, S.W. Washington, D.C. 20553	1
Defense Documentation Center for Scientific and Technical Information (DDC) Bldg. No. 5, Cameron Station Alexandria, Virginia 22314	14
To be forwarded via: Commander, Naval Air Systems Command Attn: Code AIR-954 Washington, D.C. 20361	
Harry Diamond Laboratories Attn: Branch 920 (Mr. A. J. Baba) Washington, D.C. 20438	1

	Copies
Mr. David Harratz, USAECOM Fort Monmouth, New Jersey 07703	1
Intelligence and Electronic Warfare Laboratory Rome Air Development Center, Griffis Air Force Base Attn: Mr. James Previte Rome, New York 13442	1
NASA, Marshall Space Flight Center Huntsville, Alabama 35812	1
National Aeronautics and Space Administration Manned Space Flight Center Houston, Texas 77058	1
Director, National Security Agency Attn: TDL, Dianne Haslup Fort George G. Meade, Maryland 20755	1
Commander, Naval Air Development Center Attn: Code AEHA (Mr. H. Naubriet) Johnsville, Pennsylvania 18974	1
Commander, Naval Air Development Center Attn: Mr. E. Ressler Johnsville, Pennsylvania 18974	1
Commander, Naval Air Systems Command Attn: AIR-360 (F. Lueking) Washington, D.C. 20361	1
Commander, Naval Air Systems Command Attn: AIR-954 Washington, D.C. 20361	2
Commander, Naval Air Systems Command Attn: AIR-52022 (C. D. Caposell/A. S. Glista/S. M. Linder) Washington, D.C. 20361	3
National Bureau of Standards Bldg. 225, Room A-331 Attn: Mr. Leedy Washington, D.C. 20234	1
Naval Avionics Facility Attn: Mr. Dale Tague 21st and Arlington Ave. Indianapolis, Indiana 46218	1
Commander, Naval Electronics Laboratory Center Attn: Code 4800 San Diego, California 92152	1

	Copies
Naval Electronics Systems Command Attn: Code ELEX-05143 (C. R. Suman) Washington, D.C. 20360	1
Naval Electronics Systems Command Attn: Code 033 (L. Sumney/J. Merz) Washington, D.C. 20360	2
Naval Surface Weapons Center/White Oak Laboratories Attn: Code WR34 (Dan Gordon) Silver Spring, Maryland 20910	1
Superintendent, Naval Post Graduate School Attn: T. Houlihan Monterey, California 93940	1
Director, Naval Research Laboratory Attn: Mr. George Abraham Washington, D.C. 20390	1
Commander, Naval Sea Systems Command Attn: Technical Library Washington, D.C. 20360	1
Commander, Naval Weapons Center Attn: Mr. Henry Blasic China Lake, California 93557	1
Mr. Dan Reed, USAMICOM Huntsville, Alabama 35812	1
Office of the Secretary of Defense Director of Defense Research and Engineering The Pentagon (Rm. 3D1079) Electronics & Physical Sciences Washington, D.C. 20301	1
Rome Air Development Center Attn: Mr. J. Brauer Griffis Air Force Base, New York 13440	1
Strategic Systems Project Office Department of the Navy Attn: Code SP-23 (Mr. David Gold) Washington, D.C. 20360	
Director, Naval Research Laboratory Attn: Code 5210 (Dr. John Davey) Washington, D.C. 20390	1

Industries/Universities

American Lava Corporation 1
Cherokee Blvd. and Manufacturers Rd.
Attn: Technical Library
Chattanooga, Tennessee 37405

American Micro-Systems, Inc. 1
3800 Homestead Road
Santa Clara, California 95051

Ampex Corporation 1
401 Broadway
Attn: H.A. Ferrier
Redwood City, California 94063

Autonetics Division 1
North American Rockwell Corporation
P.O. Box 4173, 3370 Miraloma Avenue
Attn: Dr. G. Pulliam
Anaheim, California 92803

D. H. Baldwin Company 1
1801 Gilbert Avenue
Attn: Mr. J. W. Brean
Cincinnati, Ohio 45202

Bell Telephone Laboratories, Inc. 1
Mountain Avenue
Attn: Mr. W. Boyle
Murray Hill, New Jersey 07971

Bell Telephone Laboratories, Inc. 1
Whippany Road
Attn: Technical Reports Center (Rm. 2A-160)
Whippany, New Jersey 07981

The Boeing Company 1
P.O. Box 3999
Attn: J. Pogson
Seattle, Washington, 98124

The Boeing Company 1
Aerospace Division
Attn: Mr. James M. Bartlemay
Seattle, Washington 98124

The Bunker-Ramo Corp. 1
Electronic Systems Group
Government Systems Group
Attn: H. L. Parks
31717 LaTienda Drive
Westlake Village, California 91361

	Copies
Burroughs Corporation Defense, Space and Special Systems Group Central Avenue Attn: Mr. Robert L. Davis Paoli, Pennsylvania 19301	1
Mr. Frank P. Caiti Manager, System Design Electronic Control Systems GM Technical Center Warren, Michigan 48090	1
University of California Department of Engineering Attn: Dr. G. Estrin Los Angeles, California 90024	1
Components Corporation Attn: Jerry B. Minter Denville, New Jersey 07834	1
Conrac Corporation P.O. Box 32 Attn: Mr. John Lawton, Jr. Caldwell, New Jersey 07006	1
Cornell University School of Electrical Engineering Phillips Hall Attn: J. Frey Ithaca, New York 14850	1
Corning Glass Works Technical Information Center Sullivan Park Attn: R. R. Barber Corning, New York 14830	1
Delco Electronics Division of General Motors 7927 S. Howell Avenue Attn: Technical Library Oak Creek, Wisconsin 53154	1
Department of Electrical Engineering University of Minnesota Attn: Larry L. Kinney Minneapolis, Minnesota 55455	1
Fairchild Semiconductor R^2 Advanced Development Engineering 4001 Junipero Sierra Blvd. Attn: C. J. Dell'Oca Palo Alto, California 94301	1

	Copies
Fairchild Semiconductor Research and Development Laboratory 4001 Junipero Sierra Boulevard Attn: J. M. Early Palo Alto, California 94301	1
Garrett Corporation 1625 Eye Street, N.W. Washington, D.C. 20006 Attn: Pat Stone	1
Fairchild Semiconductor Research and Development Laboratory 4001 Miranda Avenue Attn: Dr. H. Sello Palo Alto, California 94304	1
General Electric Company Electronics Park Attn: Eldon D. Fox Syracuse, New York 13201	1
General Electric Company Electronics Park Attn: C. S. Kim Syracuse, New York 13201	1
General Electric Company Mail Drop 211 French Road Attn: R. C. May Utica, New York 13502	1
Grumman Aerospace Corporation Attn: R. Hong Bethpage, Long Island, New York 11714	1
Harris Semiconductor P.O. Box 883 Attn: Mr. A. L. Rivoli Melbourne, Florida 32901	1
Honeywell, Inc. Aerospace Division 13350 U.S. 19 Attn: Thomas Crutcher St. Petersburg, Florida 33733	1
Honeywell Inc. Systems and Research Center Research Dept. 2345 Walnut Street Attn: Technical Library Roseville, Minnesota 55113	1

	Copies
The Johns Hopkins University Applied Physics Laboratory Attn: Dr. C. Feldman Silver Spring, Maryland 29010	1
Hughes Aircraft Company 500 Superior Avenue Attn: Mr. George Wolfe, Jr. Newport Beach, California 92660	1
Hughes Aircraft Company Data Systems Division Attn: Dr. D. Calhoun Culver City, California 90230	1
Hughes Research Laboratory 3011 Malibu Canyon Road Attn: Dr. G. Brewer Malibu, California 90265	1
Teledyne Controls 200 North Aviation Blvd. El Segundo, California 90425 Attn: M. Jasper	1
University of Illinois Digital Computer Laboratory Attn: Dr. W. J. Poppelbaum Urbana, Illinois 61801	1
Inselek Company 743 Alexander Road Attn: Joseph R. Burns Princeton, New Jersey 08540	1
Intel Corporation 365 Middlefield Road P.O. Box 668 Attn: Dr. G. Moore Mountain View, California 94040	1
International Business Machines Federal Systems Division Electronic Systems Center Attn: Mr. C. McNeil Owego, Tioga County, New York 13827	1
Iowa State University Electrical/Ceramics Engineering Department Attn: T. A. Smay Ames, Iowa 50010	1

	Copies
ITT Research Institute 10 West 35th Street Attn: Harold A. Lauffenburger Chicago, Illinois 60616	1
ITT Avionics Division 500 Washington Avenue Attn: Dept. 64511 (Mr. F. L. Koved) Nutley, New Jersey 07110	1
Lawrence Radiation Laboratory P.O. Box 808 Attn: Technical Information Dept., L-3 Livermore, California 94550	1
Litton Systems, Inc. Guidance and Control Systems Division 5500 Canoga Avenue Attn: Dr. H. Abbink, M.S. 5330 Mr. J. Birdsall, M.S. 5330 Woodland Hills, California 91364	1
Lockheed Missiles and Space Company Dept. 81-42, Bldg. 531 P.O. Box 504 Attn: Mr. W. L. Morrison Sunnyvale, California 94088	1
The Magnavox Company Bueter Road Attn: M. E. Seif Fort Wayne, Indiana 46803	1
Massachusetts Institute of Technology Dept. of Aeronautics and Astronautics 68 Albany St. Attn: Mr. G. Ives Cambridge, Massachusetts 02139	1
McDonnell Douglas Corp. P.O. Box 516 Attn: Mr. Kent C. Smith St. Louis, Missouri 63166	1
University of Michigan Electron Physics Laboratory 3505 East Engineering Bldg. Ann Arbor, Michigan 48104 Attn: Ken D. Wise	1
The Mitre Corporation Attn: Library Bedford, Maine 01730	1

	Copies
Montana State University Electrical Engineering Department Attn: D. Rudberg Boseman, Montana	1
Motorola Incorporated Semiconductor Projects Division Mesa ICC 2200 W. Broadway Attn: John Osborne, Mail Drop M504 Mesa, Arizona 85036	1
National Beryllia Corp. Greenwood Avenue Haskell, New Jersey 07420	1
Rockwell International Electronics Research Div. 3370 Miraloma Ave. Anaheim, California 92803 Attn: W. H. Kraemer	1
Northrop Electronics Division 2301 West 120th Street Attn: Mr. M. Jasper Hawthorne, California	1
Radio Corporation of America Astro-Electronics Division P. O. Box 800 Attn: Maurice G. Staton Princeton, New Jersey 08520	1
Radio Corporation of America David Sarnoff Research Center Attn: Mr. J. H. Scott, Jr. Princeton, New Jersey 08540	1
Radio Corporation of A ica Defense Electronic Products Route 202 Attn: D. Hampel Somerville, New Jersey 08876	1
Raytheon Company Missile Systems Division Attn: Dr. R. E. Thun Bedford, Massachusetts	1
Sandia Laboratories P.O. Box 5800 Attn: Technical Library 3141 Albuquerque, New Mexico 87115	1

	Copies
Sanders Associates, Inc. 95 Canal Street Attn: D. B. Newman Nashua, New Hampshire 03060	1
Safeguard Systems Office 1320 Wilson Blvd. Attn: Dr. Richard Merwin Arlington, Virginia 22209	1
Signetics Corporation 811 E. Arques Avenue Sunnyvale, California 94086	1
Siliconix, Inc. 2201 Laurelwood Santa Clara, California 95054	1
Singer-General Precision, Inc. Kearfott Division 1150 McBride Avenue Attn: Mr. L. Laermer Little Falls, New Jersey 07424	1
Sperry Rand Corp. Sperry Rand Research Center Attn: Mr. H. A. Richard Wegener Sudbury, Massachusetts 01776	1
Stanford Research Institute Engineering Sciences Laboratory Attn: Philip J. O'Donnell Menlo Park, California 94025	1
Teledyne Systems Company 19601 Nordhoff St. Attn: Earl Kanter Northridge, California 91324	1
Texas Instruments Incorporated P. O. Box 5012 Attn: D. J. Manus, M.S. 72 Dallas, Texas 75222	1
Texas Instruments Incorporated P. O. Box 66027 Attn: Bob R. Evans, M.S. 649 Houston, Texas 77006	1
Texas Instruments Inc. Central Research Laboratories P. O. Box 5936 Attn: Dr. John M. Pankratz, M.S. 105 Dallas, Texas 75222	1

	Copies
TRW Systems, Inc. System Group One Space Park Attn: Dr. B. Dunbridge Redondo Beach, California 90278	1
Tyco Laboratories, Inc. 16 Hickory Attn: Dr. A. I. Mlavsky Bear Hill, Waltham, Massachusetts 02100	1
United Aircraft Corporation United Aircraft Research Laboratories Attn: Dr. A. J. Demaria East Hartford, Connecticut 06108	1
UNIVAC Federal Systems Division Univac Park Attn: Mr. W. D. Miller St. Paul, Minnesota 55116	1
Western Electric Corporation Defense Activities Division 83 Maiden Lane Attn: Information Center (4th Floor) New York, New York 10038	1
Westinghouse Electric Corporation Aerospace Division Friendship International Airport P. O. Box 746 Attn: Dr. Paul M. Pan Baltimore, Maryland 21203	1
Westinghouse Electric Corporation Westinghouse Research Laboratory Bulah Road, Churchill Borough Attn: Dr. D. Muss Pittsburg, Pennsylvania 15235	1
Youngstown State University 410 Wick Avenue Attn: Dr. M. Siman Youngstown, Ohio	1
Autonetics Division Rockwell International 3370 Miraloma Ave. Attn: Dr. James J. Licari Anaheim, California 92803	1
Hamilton Standard Windsor Locks, Connecticut 06096 Attn: H. C. Fishman	1

SECURITY CLASSIFICATION OF THIS PAGE (When Data Entered)

APPROVED FOR PUBLIC RELEASE: DISTRIBUTION UNLIMITED

REPORT DOCUMENTATION PAGE

READ INSTRUCTIONS BEFORE COMPLETING FORM

1. REPORT NUMBER: R76-922139-4
2. GOVT ACCESSION NO.:
3. RECIPIENT'S CATALOG NUMBER:

4. TITLE (and Subtitle): IMPROVEMENT OF ELECTRONICS RELIABILITY BY R F SPUTTERING TECHNIQUES.

5. TYPE OF REPORT & PERIOD COVERED: Final Report. 1 May 1975 — 1 May 1976

6. PERFORMING ORG. REPORT NUMBER:

7. AUTHOR(s): D. H. Grantham, J. L. Swindal

8. CONTRACT OR GRANT NUMBER(s): N00019-75-C-0465 NEW

9. PERFORMING ORGANIZATION NAME AND ADDRESS: United Technologies Research Center, East Hartford, Conn. 06108

10. PROGRAM ELEMENT, PROJECT, TASK AREA & WORK UNIT NUMBERS: 6276N

11. CONTROLLING OFFICE NAME AND ADDRESS: Naval Air Systems Command

12. REPORT DATE: May 1976

13. NUMBER OF PAGES: 118p.

14. MONITORING AGENCY NAME & ADDRESS (if different from Controlling Office):

15. SECURITY CLASS. (of this report): Unclassified

15a. DECLASSIFICATION/DOWNGRADING SCHEDULE:

16. DISTRIBUTION STATEMENT (of this Report)

Distribution limited to U.S. Government agencies only; test and evaluation Dec. 1974. Other requests for this document must be referred to the Commander, Naval Air Systems Command, Code: AIR 52022, Washington D.C. 20361.

17. DISTRIBUTION STATEMENT (of the abstract entered in Block 20, if different from Report)

UTRC-R76-922139-4

APPROVED FOR PUBLIC RELEASE: DISTRIBUTION UNLIMITED

18. SUPPLEMENTARY NOTES

19. KEY WORDS (Continue on reverse side if necessary and identify by block number)

R. F. Sputtering, Thin Film, Interconnection, Electromigration, Berylium oxide, Reactive Sputtering

20. ABSTRACT (Continue on reverse side if necessary and identify by block number)

Electromigration in rf sputtered films of aluminum-copper alloys was documented. Copper content was 1%, 8%, and 12% nominally. At less than 200°C and current densities of less than 3 million amps/cm^2 the films with 1% copper exhibited significantly longer life than the films with higher copper content.

Beryllium oxide was sputtered from a BeO target and reactively from a beryllium target. Constitutive stresses were reduced until the films deposited

DD FORM 1 JAN 73 1473 EDITION OF 1 NOV 65 IS OBSOLETE S/N 0102-014-6601

UNCLASSIFIED

SECURITY CLASSIFICATION OF THIS PAGE (When Data Entered)

409252 LB

BLOCK 20. ABSTRACT

on silicon were dominated by thermal stresses. Heat-sinking with gallium proved to be extremely difficult in the presence of the activated oxygen species introduced during sputtering. Films approximately 0.001 inch thick were deposited on Ga As substrates without thermal stress cracking. Columnar growth of the beryllium oxide was observed in all cases.